Microfluidic cell-chip for an *in vitro* hepatic disease model

Sofia Alves Bernardo Pirata Relvas

Dissertation to obtain the Master of Science Degree in

Biomedical Engineering

Supervisor(s): Prof. Dr. João Pedro Estrela Rodrigues Conde
and Prof. Dr. Joana Paiva Gomes Miranda

Examination Committee

Chairperson: Prof. Dr. João Miguel Raposo Sanches

Supervisor: Prof. Dr. João Pedro Estrela Rodrigues Conde

Members of the Committee: Prof. Dr. Tiago Paulo Gonçalves Fernandes
and Prof. Dr. Rui Eduardo Mota Castro

November 2021

Preface

The work presented in this thesis was performed at the INESC-MN, Instituto de Engenharia de Sistemas e Computadores - Microsistemas e Microtecnologias, University of Lisbon (Lisbon, Portugal), and at iMed.ULisboa, Instituto de Investigação do Medicamento, University of Lisbon (Lisbon, Portugal), during the period March-October 2021, under the supervision of Dr. João Pedro Conde and Dr. Joana Miranda, respectively.

Declaration

I declare that this document is an original work of my own authorship and that it fulfills all the requirements of the Code of Conduct and Good Practices of the Universidade de Lisboa.

Acknowledgments

First, I would like to express my gratitude to Prof. João Pedro Conde for accepting me as a master thesis student at INESC-MN and for giving me the opportunity to work on this exciting and challenging project. I always felt supported, guided, and motivated under his supervision, and for that I am grateful. I also wish to thank Prof. Joana Miranda for welcoming me to iMed.ULisboa, Faculty of Farmacy, and for her support and advice.

At INESC-MN, I would like to thank Pedro Monteiro for the friendship, incredible mentorship provided throughout my thesis, advice during troubleshooting, and for always being ready to help in the experiments at the Faculty of Farmacy. I also want to thank the other PhD students and the master students from the INESC-MN group for the support, friendship, and for all the conversations and funny moments in the office that lighten up the thesis writing.

At iMed.ULisboa, I would like to thank Joana Rodrigues for the friendship, for always being available to answer my questions, for passing me her knowledge, inspiring me to investigate more about this topic, for all the suggestions to improve my work, for always being so motivational, and, most importantly, for being so patient with me.

I would like to thank TFIST-Tuna Feminina do Instituto Superior Técnico for being a family for me during all these years at IST, for providing me with so many incredible moments full of music and friendship, and for teaching me that Técnico is not always about studying. I am proud to say that I am part of this amazing group! I want to give a special mention to ‘atum’ because it was always a safe spot for me and home for the most unforgettable moments.

I also want to thank the amazing friends that I have made throughout this journey at IST, namely Rafael Silva, for always being so supportive, Rita Silvério and Beatriz Correia, for the hugs, trips, and motivation, Mariana Gomes and Mariana Martins, for all the funny moments, conversations and support, Ana Rita Abreu, for driving me home so many times, Inês Ribeiro, for being so caring, Ana Sofia Amorim, for always be able to have lunch with me (at 12h), Eunice Gonçalves, Raquel Silva and Maria Catarina Baptista, for still missing me after I left biological engineering. I also want to thank my childhood friends, Aíssa Baldé and Marta Costa, and my high school friends, Beatriz Mónica, Mónica Pingo, and Daniela Martins, for always being there for me, even if we followed different paths.

I would like to thank my family, especially my mother, father, and sister, for always believing in me, and for pushing me forward to pursue my dreams. I also want to thank Mel for being the best company ever. Finally, but not least important, I wish to thank my cousin Martim because without him I would have never thought about being a biomedical engineer.

Resumo

Sabe-se que os hepatócitos e as células de Kupffer (KCs) estão envolvidas na resistência à insulina (IR). No entanto, ainda é necessário investigar o efeito das KCs no fenótipo patológico dos hepatócitos, tendo em vista a conceção de novas terapias. Para isso, é necessário desenvolver modelos hepáticos *in vitro* fidedignos. Dispositivos de microfluídica têm um enorme potencial para produzir esse tipo de modelos, proporcionado uma melhor mimetização do ambiente hepático do que as culturas macroscópicas. Nesta tese, um dispositivo microfluídico para estudar as interações entre hepatócitos e KCs no contexto da IR foi desenhado e fabricado. Como o dispositivo é complexo, aqui apenas focámos na adaptação e caracterização dos hepatócitos no mesmo. Células tipo-hepatócitos (HLCs) derivadas de células estaminais demostraram ser uma alternativa promissora para o desenvolvimento de modelos hepáticos *in vitro*, por isso, foram escolhidas para este trabalho.

Um dispositivo de duas camadas foi fabricado com sucesso. De modo a adaptar completamente as HLCs ao dispositivo foram realizadas otimizações. As HLCs foram mantidas por mais do que uma semana dentro do dipositivo, tendo apresentado uma morfologia poligonal típica dos hepatócitos durante todo o tempo em cultura. Para demostrar que o chip pode providenciar a criação de modelos hepáticos off-the-shelf, a adaptação de HLCs congeladas no chip foi também avaliada. Tanto HLCs frescas como congeladas cultivadas no dispositivo demostraram maior produção de ureia comparativamente com as HLCs cultivadas em placas, o que prova o potencial das culturas em microescala.

Em suma, o trabalho aqui realizado constitui o primeiro passo para o desenvolvimento de um modelo hepático *in vitro* que integra hepatócitos e KCs para ser usado em estudos de modelação de doenças e testes de medicamentos.

Palavras-chave: Dispositivo de microfluídica, Fígado, Células tipo-hepatócito.

Abstract

It is known that hepatocytes and Kupffer cells (KCs) are involved in insulin resistance (IR) disease. However, the impact of KCs on hepatocyte's pathological phenotype still needs to be further investigated with the view to achieving new therapies. To do that, more physiologically relevant hepatic *in vitro* models are required. Microfluidic devices have an enormous potential to develop these types of models, mimicking better the liver environment than macroscopic cultures. In this thesis, a microfluidic device to study the interactions between hepatocytes and KCs was designed and fabricated. As the device is complex, we only focused on adapting and characterizing hepatocytes in it. Stem cell-derived hepatocyte-like cells (HLCs) were employed in this work since they were demonstrated to be a promising alternative for the development of hepatic models.

A two-layer hepatocyte-chip was successfully fabricated. Optimizations were firstly performed with the view of fully adapting the HLCs culture into their chamber. The maintenance of HLCs for more than one week into the chip was accomplished, having presented hepatocyte's typical polygonal morphology. To demonstrate that the chip can provide off-the-shelf models, the adaptation of cryopreserved HLCs was accessed. Fresh and cryopreserved HLCs demonstrated higher urea production compared with HLCs cultured in regular plates, proving the potential of microscale cultures.

In conclusion, the work here accomplished constitutes the first step towards the development of an *in vitro* hepatic model intended to integrate both hepatocytes and KCs to be used in disease modeling and drug testing studies.

Keywords: Microfluidic device, Liver, Hepatocyte-like cells.

Index

List of Figures

Figure 10 - Fluidic layer and control layer master molds. The fluidic layer master mold (a) is constituted by the chambers, 100 µm height, and the channels, 35 µm height. The control layer master mold (b) is constituted by the valves with 50 µm of height. The silicon is represented in black, the SU8-50 in grey, and the AZ40XT-11D in white.

Figure 11- Final steps to create the hepatocyte-chip structure for perfusion experiments. (a) represents the fluidic layer PDMS after being removed from the mold. (b) shows the structure after being drilled. In this device, it was added two more access holes, one above the top dispenser (inlet) and, the other, below the bottom dispenser (outlet). Additionally, another two holes were drilled above/below the new ones to ensure the independence of the cell's chamber. And (c) shows the structure sealed against the PS of a Petri dish.

Figure 12- Final steps to create the hepatocyte-chip structure for recirculation experiments. In (a) it is represented the drilled control layer PDMS sealed against the fluidic layer PDMS, (b) shows the structure after the fluidic layer be drilled, and (c) shows the final structure after the sealing against the Petri dish's PS.

Figure 13- Fluidic layer dimensions of the final hepatocyte-chip in millimeters (mm). In image (a) it is being represented an overview of the main dimensions of the fluidic part of the device. In (b) it is possible to visualize a detailed representation of the cell's chamber including some particular dimensions and the given access hole's nomenclature. Image (c) represents specific dimensions of the culture medium chamber.

Figure 14- Control layer dimensions of the final hepatocyte-chip in millimeters (mm). In image (a) it is being represented the disposition of the pneumatic valves and pump throughout the fluidic layer design, and the numbers attributed to each. In (b) it is possible to visualize a detailed representation of each valve conformation and pump, as well as some of their dimensions.

Figure 15- Hepatocyte-like cells differentiation protocol. The HLCs differentiation is constituted by three main steps after cell expansion: endoderm commitment and foregut induction, hepatoblast formation and differentiation and, HLCs maturation. Throughout these steps, the culture medium composition is changed in order to achieve the correct hepatocyte phenotype. BM is composed of IMDM with 1% of Pen-strep and 0.01% of Anfo.

Figure 16- Steps followed during perfusion experiments. Six main steps had to be considered during these assays: device submersion in water and UV exposure, coating with collagen, cell's insertion, and adhesion in the chip, then, on day 0, Diff supplemented with FBS and 5-AZA is flowed, on day 1, the medium is changed to Diff without the FBS and 5-AZA, and, on day 4, the medium is changed Physiol.

Figure 17- Scheme of the final perfusion set-up. The culture medium was being flowed using a syringe pump with a constant flow rate of 0.2 µL/min, at the same time, the cell's supernatant was being collected through an Eppendorf placed in the far end of the outlet tube. The hepatocyte-chip was inside the incubator to maintenance the typical cell's environment.

Figure 18- Scheme representing the components used for single valves and pump control.

Figure 19- Simplified scheme of devices A and B used to optimize the culture surface. Device A has a culture surface area of 10 mm x 10 mm and device B has a surface of, approximately, 12 mm x 4 mm in a diamond-like shape. The middle chamber access holes

were used to insert the coating and the HLCs, two of the others were used to perfuse the culture medium, the rest was closed with metallic plugs.

Figure 20- Cell's aspect, from day 0 to day 2, when cultured on PS (MD 1) and PDMS (MD 2) surfaces inside microfluidic devices. (a) and (b) show the cell's dispersion after being inoculated in the devices (day 0). (c) and (d) show cell adhesion in PS and PDMS, respectively, one day after the cell's insertion (day 1). (e) shows HLCs on their second day (day 2) in the device sealed against PS. Scale bar = 100 µm.

Figure 21- Cell's behavior when seeded on a PS culture surface coated with type I collage diluted with PBS (MD 1) and with acetic acid (MD 2). (a) and (b) show the cell's dispersion after being inoculated in the devices (day 0). HLCs, after one day of inoculation (day 1), on a surface coated using PBS (c) and acetic acid (d) are also presented. Scale bar = 100 µm.

Figure 22- Collagen fibers throughout the final hepatocyte's chamber. In the images, it is shown three different parts of the final chamber where it can be distinguished several collagen fibers after performing the two coatings. Scale bar = 200 µm.

Figure 23- Hepatocyte's chamber filled with trypan blue solution. Trypan blue solution was inserted through the top inlet (above the top dispenser), as shown in the image, but also through the center inlet.

Figure 24- Comparison between cell dispersion in the chambers without (a) and with (c) the addition of the side channels. (b) and (d) represent the cell's disposition in one of the sides of the designed chambers (a) and (c), respectively. Scale bar = 200 µm.

Figure 25- Push-down valve with the dimensions used in the final Hepatocyte-chip (a) and Push-up valve (b). In each type is represented the three main valve components: control layer, fluidic layer, and the membrane in between. In the final hepatocyte-chip, the control layer valve has a width of 300 µm and a height of 35 µm, and the fluidic channel has the same width as the valve and a height of 50 µm.

Figure 26- Optimized inoculation steps. Cell's insertion in the chamber is constituted by four steps: (a) radially dispersion of cells through inlet **a** with a flow rate of 5 µm/min during 2 min; (b) side's dispersion through inlet **a** with a flow rate of 10 µm/min during 2 min; (c) dispersion through inlet **a** towards the chamber corners with a flow rate of 10 µm/min during 2 min; (d) cell's insertion through inlets **b**, **c**, **d**, and **e** with a flow rate of 10 µm/min during 1 min in each.

Figure 27- Differences in cell confluency in a device where the last inoculation step was not included (a) and in one where that step was performed (b). The images show the cells on their day 0 (day of cell's insertion) right after spending 1 hour in the incubator to promote adhesion. Scale bar = 200 µm.

Figure 28- Maintenance of HLCs inside the designed cell chamber for 17 days. In each image, it is represented the cell's aspect in different zones of the chamber in some days (0, 1, 4, 7, 10, 14, and 17) after inoculation. Scale bar = 200 µm.

Figure 29- Urea production 4 and 7 days after the inoculation of HLCs into the microfluidic device and plates. Undifferentiated hnMSCs are the negative control. HepG2 and hpHep are positive controls. *, **, *** Significantly differs among the controls with $p < 0.05$,

$p < 0.01$ and $p < 0.001$, respectively. Abbreviations: hnMSCs (human neonatal mesenchymal stem cells), hpHep (human primary hepatocytes), MD (microfluidic device).

Figure 30- Urea production 4 and 7 days after inoculation of cryopreserved HLCs into the microfluidic device and plates. Undifferentiated hnMSCs are the negative control. HepG2 and hpHep are positive controls. *, **, *** Significantly differs among the controls with $p < 0.05$, $p < 0.01$ and $p < 0.001$, respectively. Abbreviations: hnMSCs (human neonatal mesenchymal stem cells), hpHep (human primary hepatocytes), MD (microfluidic device).

Figure 31- Comparison between freshly differentiated and thawed HLCs on plate and microfluidic device cultures. (a) and (b) are freshly differentiated HLCs cultures on plate and device, respectively. (c) and (d) are thawed HLCs cultures on plate and device, respectively. Scale bar = 100 µm (a and c), 200 µm (b and d).

Figure 32- Valve operation with the increase of air pressure. The valve channel is above and the fluidic layer channel is underneath. The air pressure inside the valve channel is increasing from (a) to (c). In (a) the valve is not being actuated. In (c) the valve is being actuated with 400 Pa (maximum regulator pressure) and the fluidic channel is completely closed. And, in (b) the valve is being actuated by an intermediate pressure. Scale bar = 300 µm.

Figure 33- Sequence of steps used to operate the pneumatic pump. This sequence was done in loop. A time interval divided each step. Abbreviations: 1 (valve actuated; fluidic channel closed), 0 (valve non-actuated; fluidic channel open).

List of Tables

List of Abbreviations

2D	Two-dimensional
3D	Three-dimensional
5-AZA	5-azacytidine
Al	Aluminum
Anfo	Amphotericin B
APTS	3-Aminopropyltriethoxysilane
ATP	Adenosine triphosphate
BM	Basal medium
BSA	Bovine serum albumin
Caco-2	Human colorectal adenocarcinoma cells
CK-18	Cytokeratin 18
Dexa	Dexamethasone
DI water	Deionized water
Diff	Differentiation medium
DMEM	Dulbecco's modified Eagle's medium
DMSO	Dimethyl sulfoxide
DWL	Direct Write Lithography System
ECM	External cell matrix
EGF	Epidermal growth factor
ESCs	Embryonic stem cells
FBS	Fetal bovine serum
FFAs	Free fatty acids
FGF	Fibroblast growth factor
HGF	Hepatocyte growth factor
HHEX	Hematopoietic-expressed homeobox protein
HK-2	Human kidney-2 cells
HLCs	Hepatocyte-like cells
hnMSCs-UCM	Human neonatal umbilical cord tissue
hpHep	Primary human hepatocytes
HUVECs	Human umbilical vein endothelial cells
IMDM	Iscove's modified Dulbecco's medium
IPA	Isopropanol
iPSCs	Induced pluripotent stem cells
IR	Insulin resistance
ITS	Insulin-transferrin-selenium
KCs	Kupffer cells
L0-2	Liver-2 cells
MD	Microfluidic device

MEMS	Microelectromechanical systems
MSCs	Mesenchymal stem cells
NAFLD	Nonalcoholic fatty liver disease
NEAA	Non-essential amino acids
NTA	Nicotinamide
OoC	Organ-on-a-chip
OSM	Oncostatin M
PBS	Phosphate-buffered saline
PDMS	Polydimethylsiloxane
Pen-strep	Penicillin-streptomycin
PGMEA	Propylene glycol ether acetate
Physiol	Physiological medium
PMMA	Polymethyl methacrylate
PP	Periportal
PS	Polystyrene
PSCs	Pluripotent stem cells
PV	Perivenous
qPCR	Quantitative polymerase chain reaction
ROS	Reactive oxygen species
SCs	Stem cells
Si	Silicon
T2DM	Type II diabetes mellitus
TAGs	Triacylglycerides
TMAH	Tetramethyl ammonium hydroxide
TNF-α	Tumor necrosis factor
UV	Ultraviolet
VLDL	Very-low density lipoproteins
α-MEM	Minimum essential medium Eagle with alfa modification
$\boldsymbol{L}$	Linear dimension
$\boldsymbol{Re}$	Reynolds number
$\boldsymbol{p}$	Fluid pressure
$\boldsymbol{v}$	Fluid velocity
$\boldsymbol{\mu}$	Dynamic viscosity
$\boldsymbol{\rho}$	Fluid density

I. Introduction

I.1. Motivation

Liver-associated diseases account for about 2 million deaths per year worldwide [1]. Obesity is one of the risk factors that contribute to the prevalence of liver diseases. According to the World Health Organization, 1.9 billion adults are overweighted and 650 million of those are diagnosed as obese [2]. Obesity, together with insulin resistance (IR), is the main cause of type II diabetes mellitus (T2DM) which constitutes the most common type of diabetes [3]. Obesity and T2DM are included in the most common mortality causes, which have reached epidemic proportions in the western populations during the last decade [4, 5]. Those conditions together can trigger non-alcoholic fatty liver disease (NAFLD), the most frequent form of chronic liver disease and it is forecasted to rise along the years [1, 6]. Currently, the treatments for these liver diseases include weight management by alterations in the patient lifestyle, bariatric surgery, and regulation of the blood glucose concentration through pharmacological treatments [7]. These treatments are inefficient because they are incapable of stopping the rising numbers of these conditions [7]. Therefore, it is urgent to find new therapies to combat the growing prevalence of hepatic diseases in our nowadays society. Also, it is still necessary to understand the mechanisms that lead to liver diseases development to produce new solutions. Therefore, it is essential to create trustworthy *in vitro* human hepatic models that can mimic the human liver architecture and functions to investigate the mechanisms that trigger liver diseases and to test new therapies.

Microfluidic technologies applied to cell culture can bring huge advantages regarding the creation of reliable liver models. These platforms can provide tight control of the fluid flow, and the physiological levels (e.g.: trophic factors produced by cells) are easily achieved since the cell-to-medium ratio is low and close to the human. Moreover, these devices can be designed in a fit-for-purpose manner in order to simulate the desired biological environment [8, 9]. In microfluidic cultures, different cell types can interact with each other, leading to more realistic cultures that better mimic liver and body mechanisms [10]. Indeed, microfluidic devices, besides allowing the integration of different hepatic cells involved in the disease progression, are also able to co-culture liver cells with cells that belong to other organs, which is of particular interest in the case of the referred liver conditions since they are mainly associated with the adipose tissue and the skeletal muscle. Microfluidic chips can have features such as valves, and pumps embedded inside which can lead to controlled and automatized cell cultures, constituting a great advantage in comparison with macroscale cultures. These devices have, thus, an enormous potential to accurately create *in vitro* human liver models which can be employed in disease modeling or toxicology studies.

I.2. Overview of liver structure and functions

The liver is a large organ that is located in the upper-right part of the abdominal cavity, beneath the diaphragm and is placed above the stomach [11, 12]. It weighs approximately 1.5 kg, representing 2% of the adult weight, and is considered the second major organ of the human body [13, 14].

Blood is supplied to the liver by two main sources: the portal venule (75% of the blood), which contains blood rich in nutrients, and the portal arteriole (25% of the blood), where oxygenated blood flows [11, 14]. Macroscopically, the liver is divided into two main lobes, the right and the left [15]. However, it can also be distinguished by further two lobes, the caudate and the quadrate, that are situated between the main ones [15]. At the microscopic level, the liver is organized into hexagonal-shaped lobules (**Figure 1**), that constitute its functional unit [14]. Each lobule has in its constitution the central vein that is located in the middle part of the hexagon [15]. In the corners, there are three branches collectively known as the portal triad, they are the portal venule, the portal arteriole (also called hepatic artery), and the bile duct [14, 15]. The foundations of the lobules are composed of the major liver cell type, the hepatocytes, which are parenchymal cells and represent 60% of the total number of hepatic cells and 80% of the total liver volume [14, 16, 17].

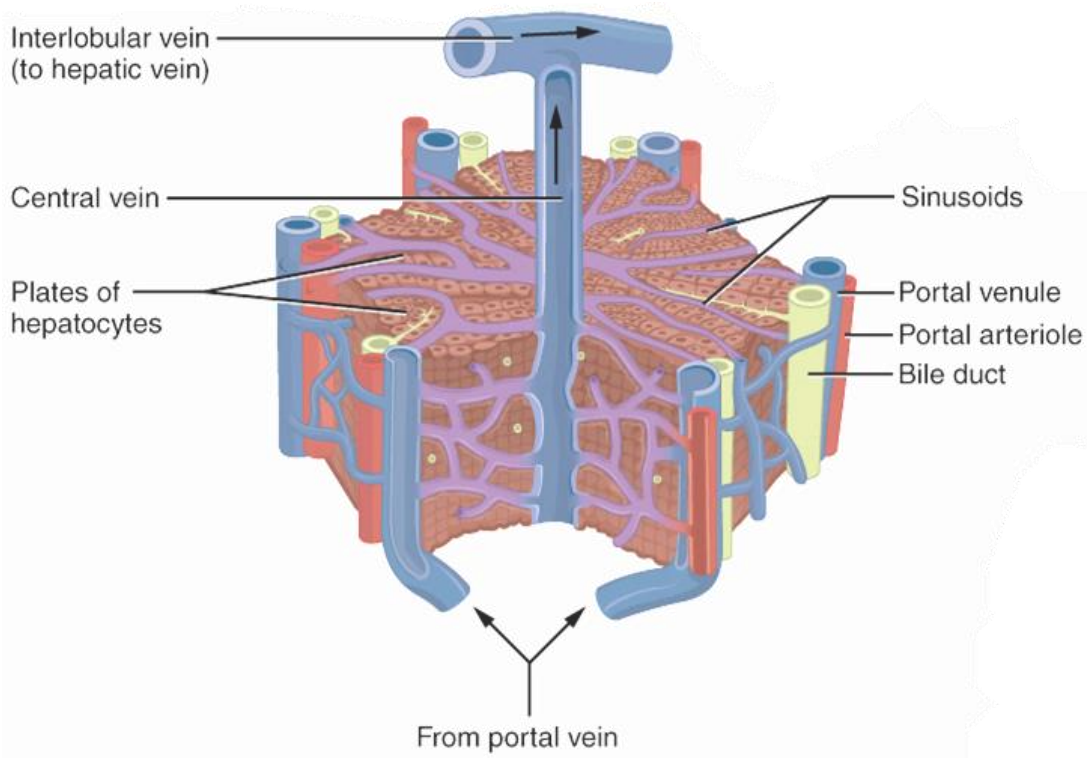

Figure 1- Hepatic lobule. The hexagonal-shaped hepatic lobule is constituted by parenchymal cells and contains, in the middle, the central vein, in each edge, the portal triad (portal venule, portal arteriole, and bile duct), sinusoid branches, and bile ducts throughout the inner part. Adapted from Anatomy & Physiology from OpenStax website [18].

Hepatocytes are subjected to two types of flow, the blood flow in its basolateral membrane and a bile flow in its apical membrane (**Figure 2**), conferring to these cells the particularity of being highly polarized [19]. In this manner, hepatocytes are characterized by different proteins, namely transporters, and lipids in the basolateral-sinusoidal and the apical-canalicular domains [19]. Between the sinusoids and the hepatocyte's basolateral membrane, there is the space of Disse, which is composed of an extracellular matrix that offers support and structure to the hepatocytes [14]. The space of Disse also contains hepatocyte's microvilli that have the important role of communicating with the blood supply [14]. Also inside the lobule, bile canaliculi are formed by the hepatocyte's apical membranes, which facilitate the bile flow towards the bile duct [14]. The two blood supplies of the lobule (portal venule and portal arteriole) drain blood to the central vein through the sinusoids, which will further lead to the hepatic vein [14]. While the bile is leaving the liver through the bile duct, the blood that flows in the portal venule and portal arteriole is entering to deliver nutrients and oxygen to hepatocytes, respectively [14]. Therefore, hepatocyte's domains give these cells the ability to perform both sinusoidal collections of nutrients and oxygen, and secretion of, for instance, several blood proteins and, canalicular bile secretion [19].

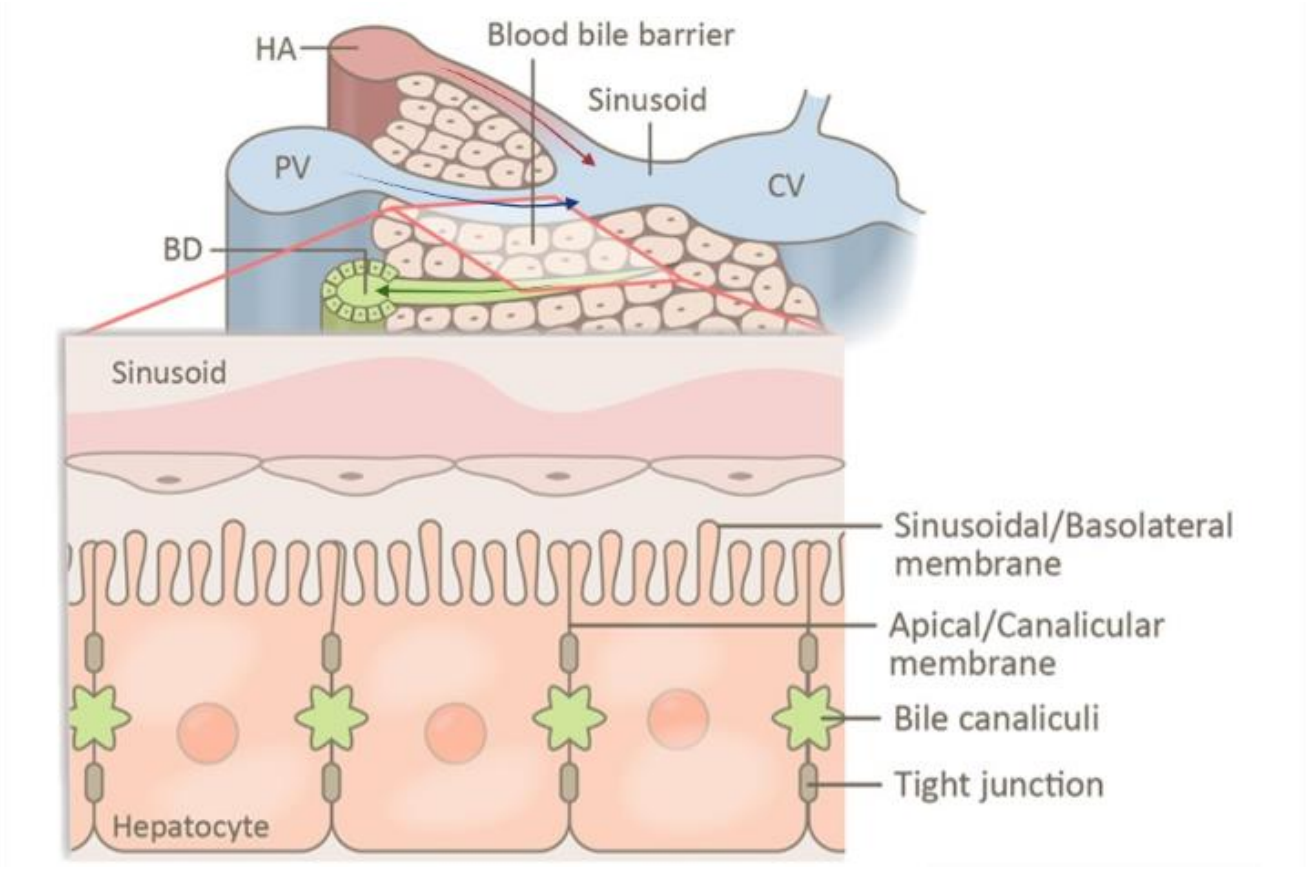

Figure 2- Representation of the hepatocyte's sinusoidal-basolateral and apical-canalicular membranes. Bile canaliculi are placed in the apical membrane and the sinusoids contact with the basolateral membrane through the space of Disse, forming a blood bile barrier. Tight junctions in the apical hepatocyte domain prevent the mixing between blood and bile. Adapted from Sundd & Monga, 2019 [20]. Abbreviations: HA (Hepatic artery), PV (Portal venule), BD (Bile duct), CV (Central vein).

Besides hepatocytes, the liver is also composed of non-parenchymal cells namely cholangiocytes, macrophages, sinusoidal endothelial cells, and stellate cells, which also have important functions [7]. Cholangiocytes are the epithelial cells that form the bile ducts [21]. They are involved in the modification of the bile that is derived from hepatocytes, a process that is regulated through intracellular cascades of hormones, peptides, and other molecules [21]. Sinusoidal endothelial cells line the blood vessels forming a barrier between the sinusoid and the space of Disse, having a crucial role in the maintenance of the metabolic and immune homeostasis [22]. Kupffer cells (KCs) are the liver macrophages that are localized in the inner side of the sinusoids adherent to the endothelial cells [23]. These cells, which constitute around 80-90% of all the macrophages in the body and 12% of the total hepatic cell's number, protect the liver from bacterial infections and toxic agents [7, 23, 24]. Finally, the stellate (or Ito) cells, located in the space of Disse, constitute a vitamin A reservoir and produce the liver extracellular matrix, namely collagen fibers [14, 25].

The liver is the main organ that governs the energy metabolism in our body [26]. It is involved, namely, in the protein, carbohydrate, and lipid metabolisms [26]. The blood that comes from the digestive tract through the portal vein is filtered by the liver which captures the nutrients, such as glucose, amino acids, and fatty acids, and uses them in several metabolic pathways [27]. By them, the liver maintains the blood glucose levels by being involved in the realizing and storage of this molecule that comes both from the diet and its inner production [26]. Plus, it is responsible for oxidizing glucose whenever energy is wanted. This organ also degrades lipids, namely fatty acids, according to the energy demand, but also stores them in other tissues [28]. Additionally, the liver synthesizes ketone bodies through the excess of fatty acids, which are an important intervenient in muscle and brain energy generation during starvation [26]. The liver is the major handler of protein metabolism as it produces blood proteins, like albumin, that will have an important role in the transport of substances, such as fatty acids, steroids, amino acids, vitamins, and drugs, to other organs, and in the maintenance of the osmotic pressure, clotting factors, and also immunoglobins in the blood [26, 28]. Moreover, the liver is involved in the urea metabolism because uptakes amino acids, such as alanine and glutamine, from peripheral tissues (muscles and kidneys), and degrade their nitrogen group to create urea, which will be then discarded in the urine [26, 28]. Furthermore, it metabolizes drugs into nontoxic substances that can be easily used by the body [11, 27]. So, has the function of detoxifying toxic metabolites, xenobiotics, and medicines [26]. Liver parenchymal cells are also involved in the production of bile that is important for processing digestion and aborting lipids in the intestine [16].

The liver is, thus, a unique organ. It functions as a buffer in our organism since it maintains energy homeostasis, and a filter because it removes all the blood toxins that come from the stomach [27, 28]. In this way, complications like nonalcoholic fatty liver disease (NAFLD), insulin resistance, and diabetes, which alter liver functions, can be overwhelming since no other organ is capable of compensating it [26, 27].

I.2.1. Homeostatic metabolic pathways

In homeostasis, the main metabolic pathways involved in the liver are tightly controlled by two pancreatic hormones, insulin and glucagon, which are both linked with blood glucose regulation [27, 31]. After each meal, the carbohydrates are digested by enzymes into glucose molecules, increasing their concentration in the blood [26]. Glucose is seen as the main energy source of our body, especially to the brain which only depends on it to provide the "fuel" to allow its physiological functions [32]. It is, thus, one of the most important molecules. In human beings, the levels of glucose in the blood are kept constant between the range of 4 to 7 mM, hence mechanisms to maintain those concentrations are required [33]. The liver is the main organ that ensures the control of blood glucose concentrations.

Insulin is an anabolic hormone synthesized and secreted by the β-cells in response to an increase of glucose (beyond 3.3 mM) and amino acids in the bloodstream that occurs after ingesting a meal [31]. This hormone stimulates the decrease of glucose concentration in the circulation [31]. To do this, insulin starts by increasing the uptake of glucose by the peripheral tissues, then, promotes glucose storing in the liver through the synthesis of glycogen, and finally, inhibits glucagon secretion [31]. Glucagon is a catabolic hormone produced by the α-cells and is characterized by having the opposite effects of insulin [31]. This hormone stimulates the increase of glucose in the blood, during fasting, by inducing its hepatic synthesis [31]. Both glucagon and insulin have a fundamental role in keeping the basal blood glucose concentrations within the normal ranges [31].

In this way, it is possible to distinguish two metabolic stages, the fed and fasted state (**Figure 3**), which activate different metabolic pathways in the hepatocytes accordingly to the insulin-glucagon ratio [26]. In physiological conditions, the metabolic pathways stimulated in the fed state by insulin are inhibited in the fasted state by glucagon, and vice-versa.

Under feeding conditions, the high glucose concentrations cause insulin secretion which elicits the glucose catabolism in hepatocytes through glycolysis and oxidative phosphorylation, generating energy in the form of ATP [27, 34]. The excess of glucose in the blood is also used to produce glycogen through glycogenesis, and fatty acids through the lipogenesis pathway [26, 27]. The fatty acids can be transformed into triacylglycerides (TAGs) that are then transported in lipidic droplets, namely very-low density lipoproteins (VLDL) to adipocytes for storage purposes, providing supplementary substrates to generate energy [26]. Fatty acids can also be converted to phospholipids which will become part of the membranes, providing structure and integrity to cells and organelles [26]. Besides, in this state, insulin is involved in the promotion of amino acid synthesis which can be metabolized into proteins or other bioactive molecules [27].

On the other hand, during the fasted state, the low blood glucose concentrations trigger glucagon release and, consequently, the activation of glycogenolysis in the hepatocytes, which consists of glycogen degradation to obtain glucose molecules [26]. When all the glycogen stores are depleted, gluconeogenesis is activated, and glucose is synthesized using lactate, glycerol, and amino acids that come from the muscle and then released into the blood stream [26, 27]. β-oxidation in the mitochondria is increased, which allows the obtainment of ATP energy through the catabolism of fatty acids that comes

from the adipose tissue [27]. During prolonged fasting, ketogenesis is stimulated, generating ketone bodies that constitute the main “fuels” for our body during this state and in the presence of a high-fat diet [26, 27].

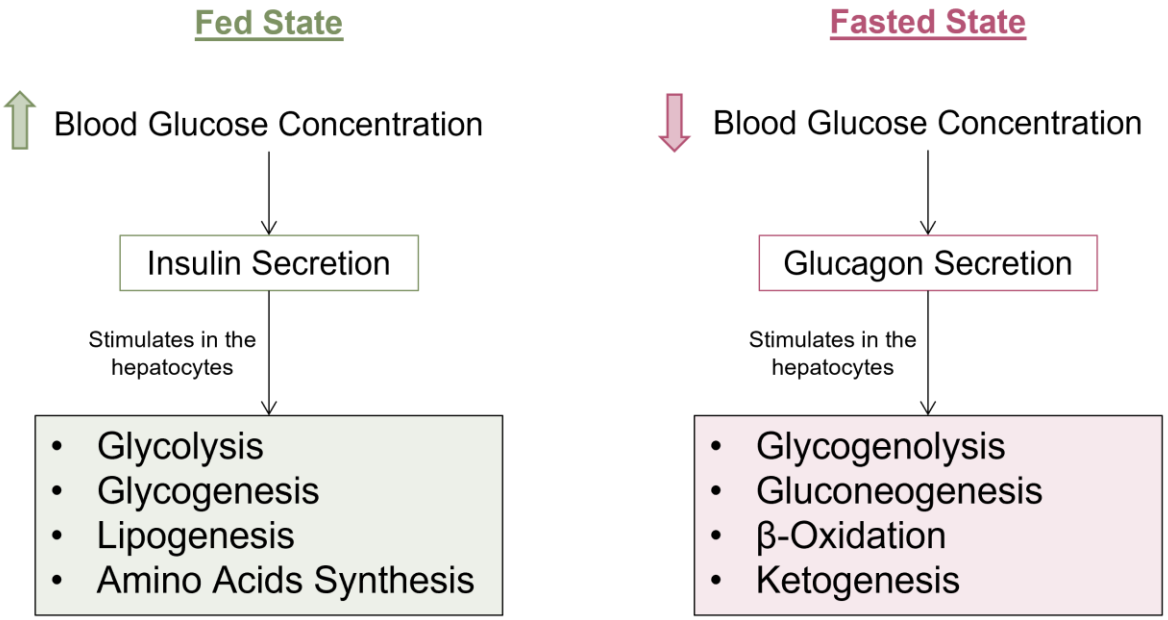

Figure 3- Impact of the fed and fasted states on hepatocyte’s metabolism: carbohydrate, lipid, and protein metabolisms. In the fed state, β-cells secrete insulin which will stimulate anabolic reactions such as: glycolysis, glycogenesis, lipogenesis, and amino acids synthesis in hepatocytes, inhibiting the opposite pathways. On contrary, in the fasted state, α-cells secrete glucagon promoting catabolic reactions as: glycogenolysis, gluconeogenesis, β-oxidation, and ketogenesis in hepatocytes.

I.2.2. Liver’s role in insulin resistance

The liver connects several tissues through the metabolism, including the skeletal muscle and the adipose tissue [27]. This permits the delivery, and also collection, of nutrients and energy to, and from, each system, allowing their co-operation. However, this metabolic interconnection can be altered in case of pathology, as it happens in insulin resistance (IR). IR occurs due to a decrease in both peripheral tissues and hepatocytes’ metabolic response to insulin [35]. Consequently, higher concentrations of this pancreatic hormone are needed to achieve a normal metabolism [35]. Even though the mechanisms that lead to IR are not totally understood, it is known that the liver is the primary driver of this disorder [4].

IR is considered as a subsequent cause of obesity which is highly related to lifestyle factors, such as high-fat diets and sedentarism [35, 36]. It is thought that several factors influenced the rising prevalence of this condition, however, the western diet is considered the major booster since it is highly rich in fat and sugar [37]. These diets lead to augmented visceral fat, which will increase the quantity of free fatty acids (FFAs), cytokines, and pro-inflammatory substances in the portal circulation, activating several inflammatory signaling pathways [38, 39]. The FFAs and cytokines in circulation will trigger lipid accumulation in hepatocytes which will impair the glucose uptake induced by insulin, reducing the hepatocyte's sensitivity to that hormone. Therefore, insulin fails to inhibit hepatic gluconeogenesis and

glycogenolysis (**Figure 4**), which leads to high glucose concentrations in the blood (hyperglycemia), and, consequently, compensatory insulin production and secretion by the pancreas, leading to hyperinsulinemia [36]. However, hyperglycemia and hyperinsulinemia contribute to the maintenance of fatty acids' synthesis (lipogenesis) and, thus, their delivery to the adipocytes inducing lipotoxicity [7, 36]. This lipogenesis stimulation constitutes a paradox, called 'selective hepatic IR', and can be related to liver zonation since the PP (periportal) hepatocytes are responsible for gluconeogenesis, inhibited by insulin, and the PV (perivenous) hepatocytes are associated with lipogenesis, that is still maintained by insulin [40, 41]. The constant stimulation of lipogenesis in the PV hepatocytes leads to oxidative stress in those cells, triggering hepatic steatosis, which constitutes the first stage of non-alcoholic fatty liver disease (NAFLD), one of the most important chronic liver diseases worldwide [42]. Advances in this condition lead to Kupffer cells (KCs) activation to a pro-inflammatory phenotype amplifying the hepatic inflammatory state and further contributing to insulin sensitivity (**Figure 4**) [42]. The constant release of insulin to compensate the demand for glucose uptake to decrease blood glucose concentrations can lead to the deficient function of β-cells [43]. If the pancreas reaches a state where is no longer capable of producing enough insulin to balance the glucose blood concentrations, type 2 diabetes mellitus (T2DM) is triggered [38, 43].

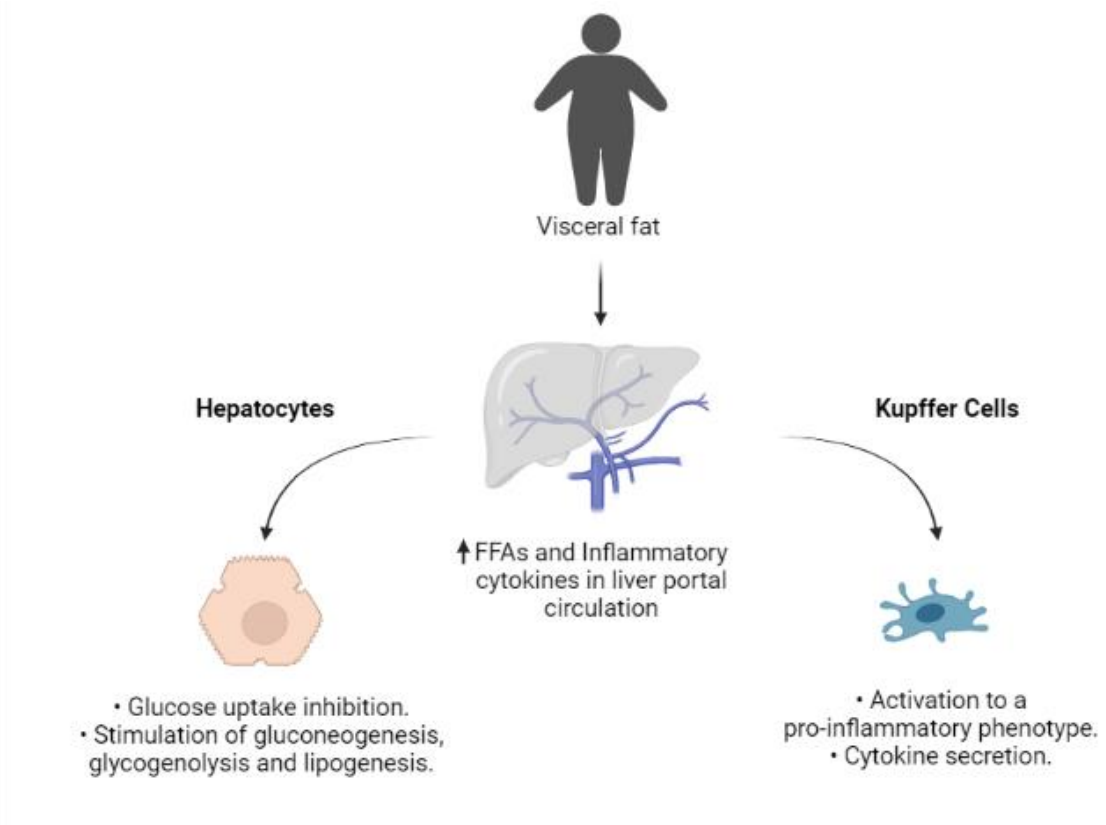

Figure 4- Development of insulin resistance: the effects on hepatocytes and Kupffer cells functions. Abbreviation: FFAs (free fatty acids).

Since the two main liver cells involved in the development of hepatic IR are the hepatocytes and liver macrophages, the KCs, it would be interesting to investigate their role and connection to better

understand the underlying mechanisms of IR with the view to find new therapeutic solutions. However, for that to happen, reliable hepatic models need to be created.

I.3. Deriving hepatocytes to create human *in vitro* hepatic models

In the pharmacology industry, the source of hepatocytes cells should be chosen to develop reliable human *in vitro* models not only to create liver disease models with a view to a treatment discovery but also to use them for toxicological studies. There are different sources by which it is possible to derive hepatocytes. Primary human hepatocytes (hpHep) are directly isolated from the liver tissue, which can be obtained from human liver resections, non-transplanted human livers, or fetal human livers [44, 45]. Therefore, these cells are of difficult access since they can only be obtained from living liver tissues which leads to scarce availability problems [8]. Nevertheless, hpHeps are the "gold standard" when it comes to the creation of relevant *in vitro* human liver cultures since they are the ones that better show the maintenance of the hepatic phenotype *in vitro* [8]. Consequently, hpHep's functionality is very similar to the hepatocytes found in the human liver, which gives them the potential to deliver highly predictive results [46]. However, hpHeps do not proliferate easily *in vitro* because of their highly differentiated stage [47]. In this way, this cell type leads to limitations in the number of cells in culture [8, 47]. Moreover, it was also verified that these hepatocytes lose functions during the culturing time through a process called dedifferentiation, which compromises medium and long-term studies [8, 47]. Hepatocytes from animal origin raise ethical concerns and are not adequate to predict human toxicity due to species differences in the pathways involved in the drug's metabolization [8].

Another option is to use human liver cell lines, such as the Huh7, HepG2, and HepaRG, which are obtained from tumors (e.g. hepatoma) or by genetic manipulation of primary human liver cells [47]. Even though they do not account for population differences like hpHeps, this type of cell is highly available and easy to be maintained in culture [8, 46]. Nevertheless, their proliferation ability is, in most cases, connected with a loss of metabolic and genetic functions [46]. In this way, they present an incomplete phenotype, which represents a crucial drawback when it comes to the creation of a reliable human hepatic model [46].

As an alternative, stem cells (SCs) have a great potential to originate mature hepatocytes in large amounts due to their ability to self-renewal [46, 48]. SCs can be classified according to their differentiation potential as totipotent stem cells (ability to develop an entire organism and extra-embryonic structures), pluripotent stem cells (can be differentiated into almost all types of cells, such as cells derived from the three germ layers), multipotent stem cells (capability to differentiate only into cells from their family, like mesenchymal stem cells), and unipotent stem cells (able to differentiate into a single cell type) [49, 50]. A specific example of pluripotent stem cells (PSCs) is, for instance, embryonic stem cells (ESCs), which are derived from the inner mass of the embryo. Human ESCs present ethical concerns, in this way, they are not usually used [46]. As an alternative, human-induced pluripotent stem cells (hiPSCs) emerged to erase those issues. hiPSCs are referred to as somatic cells that are reprogrammed back to stem cells in order to restore the pluripotency [46, 51]. This type of stem cells shows an interesting capability of generating hepatocytes, better than the liver cell lines [46]. However, the epigenetic memory of iPSCs

may impact the differentiation protocol [46]. Moreover, iPSCs are unstable and their reprogramming efficiency is low [52].

By offering advantages over other SC types, mesenchymal stem cells (MSCs) may be regarded as a promising alternative for the development of *in vitro* platforms for toxicological assessment, disease modeling, and drug screening. Mesenchymal stem cells (MSCs) can be derived from adult or neonatal tissues, such as human bone marrow, human adipose tissue, and human umbilical cord tissue [47, 53]. MSCs from the human neonatal umbilical cord tissue (hnMSCs-UCM) seems to be one of the most advantageous primary sources since they are strongly available, easy to expand *in vitro* and, come from a tissue that would be discarded otherwise [54]. Furthermore, hnMSCs-UCM demonstrated to have the capability to commit with the endoderm linage by showing the present hepatic markers (e.g.: CK-18, albumin, and α-fetoprotein) that facilitate the derivation into hepatocytes [47]. Indeed, it has been reported in the literature that hnMSCs-UCM can be differentiated into hepatocyte-like cells (HLCs) by the mimicking of the liver embryogenesis [46]. For instance, Campard *et al.* characterized HLCs derived from the umbilical cord by the urea and albumin production, glycogen storage, low-density lipoprotein, and presence of some hepatic markers [47, 55]. However, the metabolic activity of the HLCs and their capability to maintain the functions throughout the culturing time was not studied [47]. Reports from Zhang *et al.* and Zhou *et al.* described HLCs with a less mature phenotype than the one found by Campard *et al.*, having presented a fibroblast morphology [47, 56, 57]. Even though hepatocytes derived from SCs present great advantages, they still exhibit an incomplete phenotype and reduced hepatic functions in comparison with the hpHep [46]. Nevertheless, Cipriano *et al.* described an optimized protocol to generate mature HLCs through hnMSCs-UCM with a phenotype closer to the hpHeps than HepG2, by transcriptomic analysis evaluation [47]. In this protocol, epigenetic modifiers were included, which have helped to improve the cell's phenotype [47]. Besides, Cipriano *et al.* reported that HLCs could be successfully maintained in culture up to 34 days without losing hepatic functions [47].

I.3.1. Deriving hepatocyte-like cells (HLCs) through hnMSCs-UCM

Differentiation strategies to derive HLCs from SCs aim at mimicking liver embryogenesis. During embryo formation, the zygote is first created and then three main germ layers are formed: the ectoderm, the endoderm, and the mesoderm [58]. The liver is derived from the endoderm layer [58]. The endoderm forms a gut tube that originates the foregut, the midgut, and the hindgut [58]. During liver development, hepatocytes are raised in the anterior portion of the hepatic diverticulum that is formed in the foregut [58]. Then, the hepatoblasts, which are the hepatic endoderm cells, give origin to the liver bud [58]. Those cells are bipotent, meaning that the ones sitting next to the portal veins differentiate into cholangiocytes, while the others residing in the parenchyma will undergo hepatocyte differentiation [58].

To induce the embryogenesis *in vitro*, several cytokines, growth factors, and small molecules are included in the culture medium during the procedure in a sequential manner to provide the correct environment to mimic embryogenesis [48]. The protocol to derive HLCs from hnMSCs-UCM can, thus, be divided into four main steps according to the embryo development stage. The first step is the endoderm commitment and foregut induction. The second, the induction of hepatoblasts and the formation of the

liver bud. Then, the hepatoblasts differentiate into hepatocytes. And, finally, the fourth step is the maturation of the HLC phenotype.

Particularly, the endoderm commitment and foregut induction step are mimicked by introducing a fibroblast growth factor (FGF) and an epidermal growth factor (EGF), which were demonstrated to induce the expression of the HHEX gene, a marker of the foregut formation [47, 58]. EGF also stimulates the proliferation of the MSCs by binding to its specific receptor, and the FGF has an important role in the endodermal patterning [48]. For deriving hepatoblasts and, consequently, form the liver bud, it is added to the medium a hepatocyte growth factor (HGF), insulin-transferrin-selenium (ITS), and nicotinamide (NTA) [47]. HGF has the role of inducing cell differentiation into hepatoblast, ITS and NTA are involved in the proliferation and survival of the primary hepatocytes [48]. Next, the hepatoblast differentiation into HLCs is performed by adding Oncostatin M (OSM) and dexamethasone (Dexa) [47]. The cytokine OSM is important for the development and maturation of the hepatic cells, and Dexa triggers the expression of transcription factors that are required for hepatocyte differentiation [48]. Nevertheless, a hepatic differentiation protocol employing soluble molecules that allows generating a fully mature hepatocyte has not been found yet. As such, other strategies to improve the hepatic phenotype are being explored, namely the use of chromatin remodeling agents, such as epigenetic modifiers as histone deacetylase inhibitors and DNA methyltransferase inhibitors [47].

I.4. Microfluidic devices

Microfluidics is a field of study that has been rapidly growing, providing an increasing number of applications in biomedical research [59, 60]. It is defined as being the science and technology behind systems that are built to manipulate or process fluids (usually in the orders of 10^{-9} to 10^{-8} liters) on the microscale level [59, 61]. These systems are often characterized as microfluidic devices with critical dimensions and constituted by channels between ten to hundreds of micrometers [59, 61]. Microfluidic devices can provide applications in several areas, as they can be used as sensors, microreactors, combinatorial arrays, microelectromechanical systems (MEMS), microanalytical systems, and micro-optical systems [62]. More recently, microfluidic devices have been used to do cell cultures for disease modeling and drug testing [63].

The physic of fluids tells us that the ratio between inertial and viscous forces is given by the Reynolds number (Re), which is shown below [60]:

$$Re = \frac{\rho v L}{\mu} \tag{1}$$

Where ρ is the fluid density, v is its velocity, L the linear dimension of the system, and μ is the dynamic viscosity [60]. The dimensions of the system are in the order of microns, therefore, L is reduced. In that way, through **Eqn. 1**, is possible to verify that the Reynold's number acquires lower values as well [60]. This fact reveals that these systems follow a laminar flow regime, which reflects many advantages in comparison with the turbulent flow regime (**Figure 5**) [60].

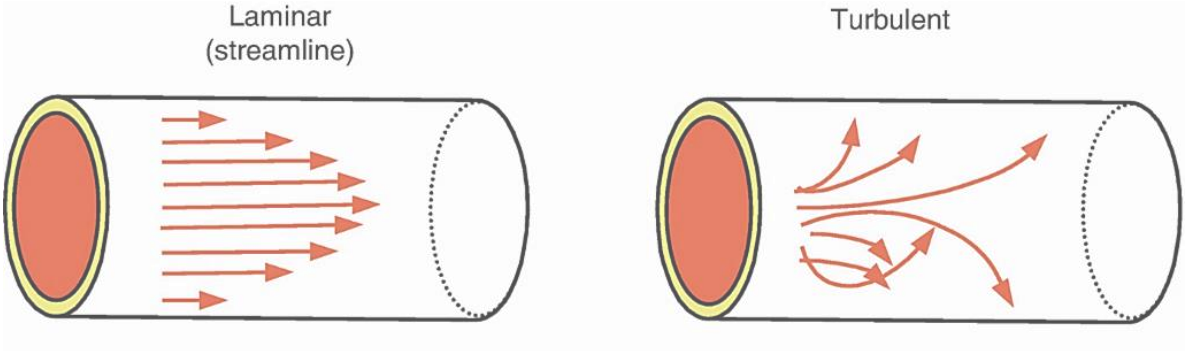

Figure 5- Laminar flow regime versus turbulent flow regime. In the laminar regime, the streamlines are unidirectional whilst, the turbulent regime is characterized by an irregular flow movement. Adapted from Westerhof *et al*., 2019 [64].

The first benefit of the laminar regime that must be highlighted is the fact that is a predictable flow, which means that this type of system is easier to modulate mathematically [60]. In the laminar flow, it only occurs diffusion (no convection observed), which allows tight kinetics control [60]. Besides, inertia has a neglected effect, making the flow manipulation simpler [65].

The fluid dynamics and transport inside a microfluidic system can be studied theoretically by obtaining an analytical solution or by using computational methods [10]. This shows, one more time, that with microfluidics systems it is possible to have excellent control of the circulating fluids and, therefore, of the transported substances. To achieve that, it is required to solve and analyze the analogous equation of Newton's second law, the Navier-Stokes equation for incompressible fluids [10]. That formula is shown in **Eqn. 2**, where p is the fluid's pressure [10].

$$\rho \frac{\partial \vec{v}}{\partial t} = -\rho \vec{v} \nabla \vec{v} - \nabla p + \mu \nabla^2 \vec{v} \quad (2)$$

At the microscale, the capillary forces dominate the gravitational forces, meaning that the fluid will preferentially travel within a porous material or a narrow channel, which is an ability that the macroscale cannot offer [60]. Besides, the reaction times in the microfluidic devices are shorter because of their small dimensions, allowing a reduced diffusion time for any molecule [60]. Other important advantages of the microfluidic systems over the conventional macroscale systems are their portability, improved temperature control, and analytical sensitivity [66]. They have the possibility of being easily actuated by valves and pumps integrated inside them and manipulated through the use of syringes and pumps outside [66]. Moreover, they can also be embedded in other systems, and are designed according to the goal of the study (fit-for-purpose) [66].

The first microfluidic systems were manufactured using silicon and glass. But silicon was shown to be expensive, not permeable to gases, and opaque to visible light, which impaired it as a good material to be used with conventional microscopes and undergo experiences with living cells [60]. On other hand, glass, even though transparent and compatible with living cells, is also not permeable to gases and, because of that, cannot be used for long-term cell culture [67]. Besides, the fabrication of glass devices is highly expensive [67]. Over the years, new materials have been used to build microfluidic devices including

ceramics, elastomers, thermoplastics, hydrogels, composites, and even paper [67]. Nowadays, the microfluidic device's fabrication is mostly carried out by polydimethylsiloxane (PDMS), which is a cheap elastomer, optically transparent, soft, and compatible with cell culturing [60]. Its capability to support widely used components of the microsystems, such as valves, pumps, and mixers, makes it a great material for microfluidic research [60]. Microfluidic devices made of PDMS are easy to be fabricated using soft lithography techniques and they are cheaper because do not require costly equipment or robust cleanroom facilities [60, 66].

I.5. Microtechnology in biological applications

Microtechnology has been brought to the cell and tissue engineering research field, through the form of microfluidic devices, often called chips [68]. Due to its capability of being constructed in a manner that allows the mimicking of human biological functions, these devices are becoming a powerful strategy to create physiologically accurate cell culture models [68].

The small size of the microfluidic devices plays an important role, especially when it comes to the manipulation of living tissues and cells [10, 61]. Indeed, mammalian cells have, approximately, 8 to 30 micrometers in size, and the diameters of the microcapillaries have 10 to 500 micrometers [10]. These measures fit with the already mentioned ranges used for these devices, making the experimental costs, reagent volumes, and cell number needed small, thus, enabling precise microenvironment control and high-throughput experiments [8].

Microfluidic devices bring tremendous advantages when compared with animal models and traditional macroscopic cell culture techniques [68, 69]. Animal models fail to mimic human physiology and present several ethical issues [68, 69]. In macroscopic culture models, it is hard to monitor target cell stimuli and control the communication between cells due to the coexistence of diffusion and convection [68, 69]. In microfluidic devices, only exists diffusion, like in the natural cell's environment, where the transport of substances occurs through diffusion from or to the capillaries, or between neighbor cells [9]. Physiological levels are easier to achieve in microfluidic systems, since medium-to-cell ratios inside the device are closer to the optimal ones, therefore, avoiding the dilution and ineffectiveness of several molecules and metabolites secreted by the cells, as it happens in culture plates [8, 69]. These devices have also the advantage of being properly designed in order to have the features and geometries that better simulate the desired biological environment [9]. In this way, by having the perfect dimension, the shear stresses of the fluid in the microchannels acquire biological values [9]. They have the possibility of being operated by perfusion or recirculation and the flow can be unidirectional or bidirectional, which can be acquired to enable a better approximation of the desired system. Hence, it is possible to say that microtechnology provides more controlled cultures that better mimic cell growth environments [10]. Furthermore, by being a better option for culturing cells, microfluidic devices are seen as an important achievement towards the need of reducing the animals used in experiments by allowing their replacement [8, 70]. Thus, they constitute a method that minimizes animal suffering in scientific research [70].

This technology has, thus, the potential to model biological systems that can be used in pharmacological studies. Indeed, placing different cell types in communication with each other, creating several tissue

structures, and establishing boundaries among them, is a reality in the microfluidic panorama [10]. This had allowed researchers to build organ-on-a-chip (OoC) devices, which are systems that can simulate realistic interactions between the different cells that compose an organ, and to investigate how to achieve the next level of complexity, body-on-a-chip devices [8, 10]. OoCs, according to ORCHID (Organ-on-chip In Development) are defined as '*a fit-for-purpose microfluidic device, containing living engineered organ substructures in a controlled microenvironment, that recapitulates one or more aspects of the organ's dynamics, functionality and (patho)physiological response* in vivo *under real-time monitoring'* [71]. By being fit-for-purpose, OoC devices allow the mimicking of the human organ architecture. They also enable the culturing of different cell types (multi-cell culture) within different chambers but inside the same system, allowing their interaction through paracrine or endocrine signals [8, 63]. Hence, they show the potential to improve drug development and to provide personalized disease treatment solutions [10].

Microfluidic devices are, thus, a novel technology that presents a high impact in the pharmaceutical and medical fields [10]. They are a promising tool for recreating human physiology and pathology and undergo drug discovery studies [71]. Through these devices, it is possible to recapitulate the functions and structures of the human organs in a controlled environment, which is remarkable to modulate diseases without animal use [71].

I.6. Hepatic cell-chips

The liver is a high cellular density tissue with a strong vascularization to provide oxygen and nutrients to hepatocytes and a bile canaliculi system that actively removes the waste products [72]. In this way, it is a challenge to develop a hepatic human model suitable for disease modeling studies and drug testing [72]. By making use of microfluidic devices, it is possible to develop hepatic systems that are shown to be more advantageous in comparison to other models used in pharmaceutical research to recreate the human liver.

Monolayer hepatic models (2D cultures), the simplest and most popular way of culturing cells, do not go together with the *in vivo* environment [9]. Indeed, in these models, the cells are placed on flat surfaces, while in the *in vivo* the cells are placed in a network of special and chemical interactions [9]. This changes the morphology, physiology (lose specific functions), and gene expression of the hepatocytes, which makes them not adequate to replicate the liver environment [9]. Plus, these types of models may make hepatocytes lose their differentiation markers [8]. 3D liver models, like spheroid and scaffold cultures, improve weaknesses found in 2D cultures. They provide a phenotype very close to the one observed in human hepatocytes and enhance biotransformation in HLCs derived from SCs [8]. However, in the case of static 3D models, accumulation of metabolites is elicited, which may be toxic for cells [8]. In comparison with microfluidic devices, 3D cultures do not provide a controlled fluidic flow and medium gradients [8].

Microfluidic devices, on contrary, allow the generation of flow-based systems, meaning that the culture medium is circulating within the cells continually, eliminating all metabolites and supplying the cells with nutrients [8]. In fact, it was previously demonstrated that the imposition of culture medium flow in direction and rate have a great impact on the hepatocyte's phenotype since it simulates blood capillaries [8]. In

particular, this exerts an influence on the spatial arrangement of the hepatocytes by enabling the maintenance of cell's polarity and tissue-specific activity, features that cannot be achieved in macroscopic hepatic cultures [8]. Furthermore, it was observed that culturing high-density hepatocytes in a low volume system increase the accumulation of cytokines, increased albumin production, stimulates the formation of bile canaliculi, and the expression of genes involved in the metabolic functions, which approximates these systems to the physiological pattern (improved phenotype) [8]. In microfluidic devices, hepatocytes can be tightly packed (confluent), which allows a stronger cell-to-cell contact, a continuous nutrient exchange, the establishment of a defined tissue and fluid transport regions [8]. Microfluidic devices are, thus, strong instruments to produce interactive, controlled, and reliable *in vitro* human liver models that can be employed in many applications, such as disease modeling, toxicity testing, biotransformation, and drug discovery (**Figure 6**) [73]. Moreover, microtechnology provides the tools to integrate different systems within a unique platform in a way that resembles human physiology and structure [74].

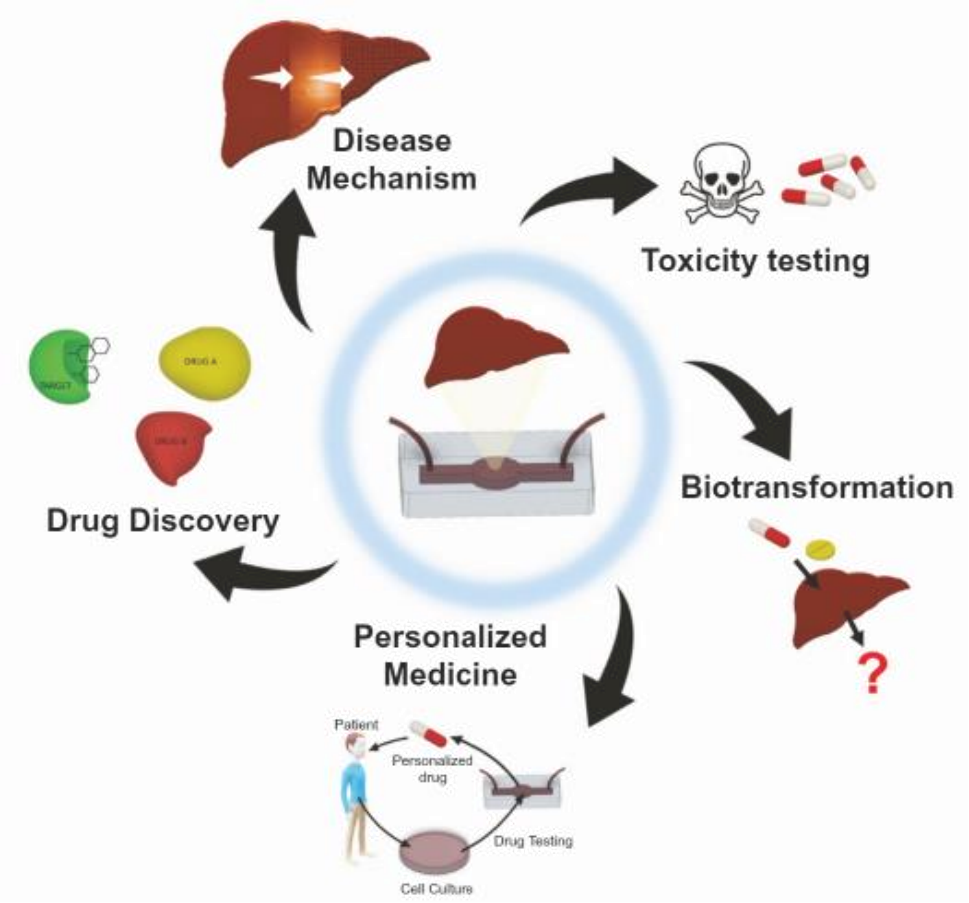

Figure 6- Liver-on-a-chip devices applications. From all the applications of these chips, it can be highlighted their use to test the toxicity of new drugs, study their biotransformation, develop models for personalized medicine, discover novel drugs to treat a given condition and evaluate metabolic mechanisms of diseases. Adapted from Hassan *et al*, 2020 [73].

In literature, it has been described some microfluidic devices designed to *in vitro* model hepatic pathologies, in particular the NAFLD which is one of the main consequences of IR and the most frequent

form of chronic liver disease [6]. For instance, Gori *et al.* created a perfused device where HepG2 cells were seeded [75]. To generate NAFLD, the hepatocytes were supplemented with free fatty acids (FFAs), namely palmitic and oleic acid, because they are the most abundant FFAs in the western diet and liver triglycerides in normal subjects and patients with NAFLD [75]. The goal of the device was to mimic the endothelial-parenchymal interface creating a dynamic culture that continually allows the exchange of nutrients and residues, as it happens in human hepatic physiology [75]. In comparison with 2D models, that device demonstrated higher cell survival, gradual and lower lipid accumulation, and less oxidative stress, proving to better replicate NAFLD [75]. More complex devices to model NAFLD were also created, like the one described in Kostrzewski *et al.* They reported a liver-chip platform where hpHeps were cultured within wells composed of a collagen-coated scaffold which aimed the mimicking of hepatic capillaries [76, 77]. That microfluidic platform is designed in a format of a multi-well plate, each containing small bioreactors with an embedded pneumatic pump system to control the culture medium flow [77]. The continuous medium perfusion allows the vertical disposition of the cells on the scaffold and the formation of 3D microtissue within the well [76, 77]. Furthermore, Bulutoglu *et al.* also created an interesting microfluidic device that consisted of a gradient generator connected to a culture chamber where hpHeps were submitted to FFAs and oxygen gradient to study the role of the oxygen in the generation of steatosis and NAFLD progression [78].

Moreover, were also reported microfluidic devices to study NAFLD that included the culturing of multiple cells. For instance, Lee *et al.* aimed to evaluate the connection of NAFLD with the intestine cells [73, 79]. That device consisted of two chambers, one with intestine cells (Caco-2) and the other seeded with HepG2 cells, divided by a porous membrane [73]. In this way, this chip not only allowed the mimicking of the hepatic metabolism but also of the gut absorption, providing a more complete simulation of human body behavior [79]. Both types of cells were perfused with a culture medium containing FFAs [73]. The results showed that, in comparison with monolayer cultures, steatosis was increased in the chip due to TNF-α (tumor necrosis factor) stimulation by affecting the intestine cells, demonstrating the role of this cytokine in the progression of NAFLD and the potential of multi-organ's devices [73]. Another successful liver-on-a-chip model was the one created by Lasli *et al.* They reported a device system constituted by an array of interconnected microwells where HepG2 and umbilical vein endothelial cells (HUVECs), which simulates the sinusoidal endothelial cells, were co-cultured in spheroids [6]. The chip was shown to be a helpful tool to monitor cells' functionality and proved that the co-culturing of hepatocytes with non-parenchymal cells improved both their physiological phenotype and the mimicking of NAFLD [6]. Indeed, it was demonstrated that the culture of these spheroids into the chip increased the amount of albumin secreted by the hepatocytes, due to the interactions with the HUVECs, and the synthesis of ROS (reactive oxygen species) was verified in the NAFLD spheroids, which is one of the known consequences of this condition [6, 73]. In addition, their chip proved to be great to do the screening of multiple drugs [6].

To the best of knowledge, there are not many developed liver microfluidic devices designed to specifically evaluate the mechanisms leading to hepatic IR. Currently, most of the reported ones aimed to study IR in the peripheral tissues, such as the adipose tissue by the creation of adipocyte microfluidic

models [80]. Only recently, Duan *et al.* reported a liver-kidney microfluidic device that was designed to evaluate the association of hepatic IR and the presence of $PM_{2.5}$ particles in the environment (fine particulate matter present in air pollution) [81]. The liver unit was designed to mimic the hepatic lobule therefore, a hexagonal liver cell chamber was employed [81]. There, L-02 (liver-02 cells) cells were cultured along with HUVECs, to simulate the sinusoid endothelial cells [81]. A kidney-like structure was implemented in this device since it is an important excretory organ [81]. The kidney unit was designed in order to mimic the nephron structure, so three different chambers alternated with a blood vessel chamber were originated (each renal nephron is rich in blood vessels) [81]. There, HK-2 (human kidney-2 cells) cells were cultured with HUVECs as well [81]. It was evaluated two types of culture medium circulation, from the liver to the kidney and the opposite way, to evaluate the impact of the distribution of $PM_{2.5}$ through those two paths in the liver metabolism [81]. However, this device does not allow the study of hepatic IR in terms of its connection with high-fat diets because it would be necessary to study the role of FFAs in hepatocytes and KCs, for instance. Therefore, still needs to be created liver microfluidic models to study the hepatic IR mechanisms associated with obesity and T2DM, and to investigate the next step towards new treatment solutions for this condition.

I.7. Objectives

Microfluidic devices, as previously mentioned, are advantageous platforms to be used for cell culture. They bring huge improvements regarding the creation of reliable *in vitro* hepatic models in comparison with monolayer and 3D cultures. These devices have a huge potential to be used to perform both disease modeling and drug testing studies. HLCs derived from hnMSCs-UCM using the optimized Cipriano *et al.* protocol demonstrated to acquire a phenotype close to the hpHeps than HepG2 (transcriptomic analysis). Moreover, it was demonstrated their capability to maintain the metabolic functions during 34 days in culture, showing HLCs potential to be employed in hepatic models. Nowadays, bad lifestyle habits (sedentarism) and high-fat diets are common problems in our society, which lead to the increase of obese people worldwide. Obesity is the main risk factor for liver diseases, like IR, whose prevalence has been continuously rising. Considering that there is a lack of liver models to study hepatic IR and it is still needed to understand the mechanisms behind hepatocytes and KCs behavior on this disorder, a microfluidic device, that aimed to contain these two hepatic cells, was projected with the objective to *in vitro* create a hepatic IR model (**Figure 7**).

Since the proposed microfluidic device (**Figure 7**) is complex and presupposes the culture of two cell types, it was required to divide its conception into different parts: the hepatocyte culture chamber and its culture medium reservoir (hepatocyte unit), and the Kupffer cell culture chamber and its respective culture medium reservoir (Kupffer unit). This thesis aims to design the hepatocyte unit of this device and adapt HLCs to it, with the view to, hereafter, create an *in vitro* hepatic model to study the IR mechanisms and the effects of the interactions between hepatocytes and Kupffer cells on the disease progression.

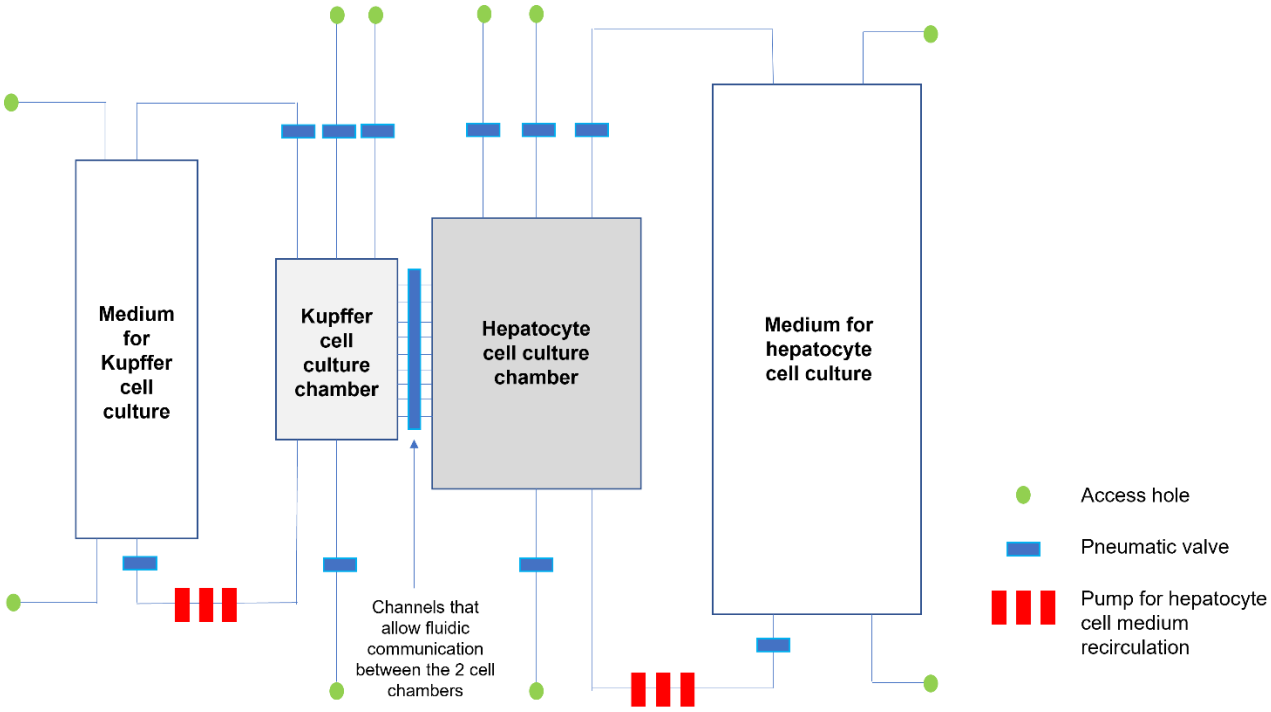

Figure 7- Scheme of the future microfluidic device that will be used to study IR mechanisms regarding the communication of hepatocytes and Kupffer cells. The device is constituted by two chambers, one to culture hepatocytes and the other to culture Kupffer cells, which would be in communication if the valve in between is open. Each culture chamber would have a culture medium reservoir to supply cells. A pneumatic pump would be included to recirculate the culture medium in both cell chambers. Several valves will be used to control the culture medium flow when necessary.

In this way, the first goal was to make use of microtechnology to design and fabricate a functional hepatocyte unit that would be integrated into the future main device. Hereafter, the hepatocyte unit device will be called hepatocyte-chip. To design it, fluid mechanics was considered in order to better scale and predict the flow behavior. In an initial state, the device was thought to be constituted by two different chambers, one to seed hepatocytes, and the other to serve as a culture medium reservoir (**Figure 7**). It was also intended to recirculate the culture medium throughout the hepatocyte's chamber which would ensure a higher concentration of metabolic products in the medium, facilitating their quantification and their future diffusion to the Kupffer chamber. To do the recirculation, it was planned to make use of pneumatically actuated valves. Therefore, the hepatocyte-chip would be composed of two different layers:

- **Fluidic layer**, that can be used independently. It is in this layer where the hepatocytes will be cultured and the culture medium will flow.
- **Control layer**, which will be embedded in the fluidic layer and where the pneumatic valves will be constructed.

The second goal was to adapt HLCs into the designed fluidic layer part of the hepatocyte-chip. In this context, there was the need to optimize not only the dimensions and proposed features of the device, but also the culture surface, the collagen coating, and the cell's insertion into their chamber. In addition, it was aimed to maintain the HLCs cultured within the hepatocyte's chamber for, at least, one week to

demonstrate the suitability of this device. Furthermore, to validate microscale cultures regarding cells' phenotype and functionality, a comparison study between the HLCs seeded within the designed device with the regularly used HLCs in monolayer culture was performed.

The final goal of this work was to prove the workability of the control layer of the hepatocyte-chip. In this way, this layer was combined with the fluidic layer and primary actuation tests were aimed to be performed.

In sum, the objectives of this work are:

1. Design and fabricate the hepatocyte-chip suitable to create an *in vitro* hepatic model that included a chamber reserved for HLCs culture, a culture medium reservoir, and control valves to enable the culture medium recirculation throughout the cell chamber.
2. Adapting the HLCs to the device cell's chamber by optimizing:
    - Device culture surface
    - Collagen coating solution
    - Cell's insertion into the device
    - Features of the designed hepatocyte-chip
3. Perform primary valves actuation tests to demonstrate the potential of having a controlled cell culture model.

II. Materials and Methods

II.1. Hepatocyte-chip fabrication

The techniques used to do the microfabrication of the hepatocyte-chip were based on soft lithography which consists of self-assembly and replica molding methods introduced by Whitesides et al. in 1998 for the first time [62]. The fabrication starts with the design of the desired features. Afterward, the hard mask that will be used to create the master mold giving origin to the PDMS structure is produced. Lastly, the final PDMS structure is sealed against polystyrene (PS) to close the features.

In this work, the device fabricated consisted of two parts: the fluidic layer, which contains the culture medium chamber, hepatocyte's chamber, and the channels that link them, and the control layer, which contains the valves to enable medium flow control and recirculation.

II.1.1. AutoCAD design

Firstly, the design of the device was done using the AutoCAD software (Autodesk Inc., USA) as represented in **Figure 8**. In this step, the requirements of the DWL (Direct Write Lithography System) machine, which will be used in the next step of fabrication, were taken into account. The AutoCAD drawing file (.dwg) was converted to several license files (.lic). Each license file contained information about one different line that composes the drawing, and they are required to enable the proper drawing reading by the DWL. Because, in the future PDMS device, the chambers, channels and valves will have different heights, it was necessary to produce three folders with the license files information correspondent to each in order to give origin to three different hard masks during the next fabrication step.

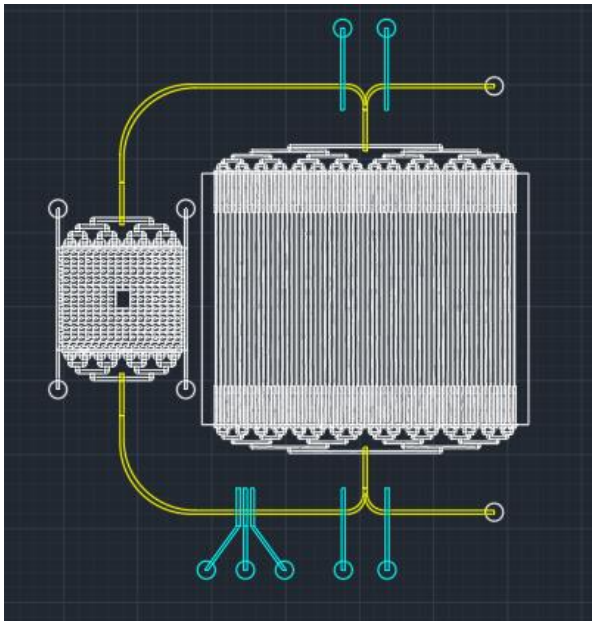

Figure 8- AutoCAD final design of the hepatocyte-chip. The white lines represent the cell's chamber (left) and the culture medium chamber (right), the yellow lines represent the channels, and the blue lines represent the pneumatic valves.

II.1.2. Hard mask fabrication

Following the device design and its respective conversion, three hard masks were fabricated. Therefore, the procedure described below was performed twice to create the fluidic layer device, one for the chambers (**Figure 9a**) and the other for the channels (**Figure 9b**). And was performed another time to create the control layer hard mark that incorporates the valves (**Figure 9c**).

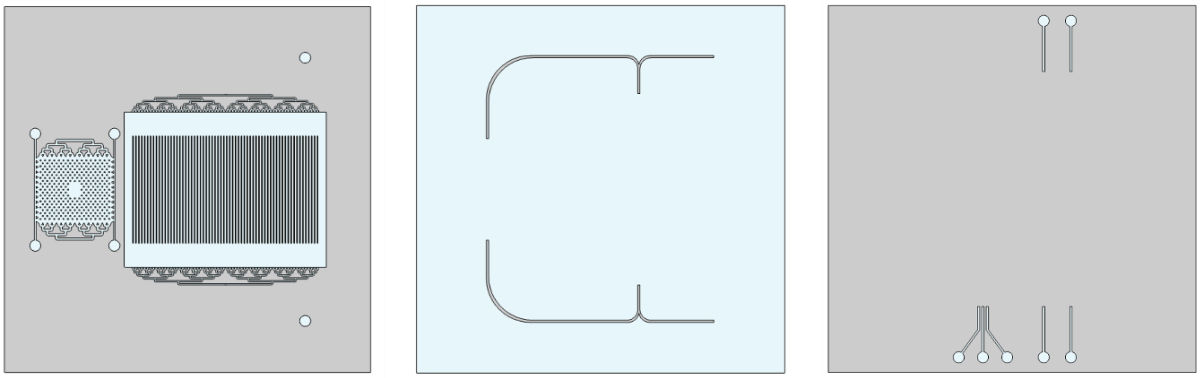

Figure 9- Fluidic layer and control layer hard masks. The fluidic hard masks are constituted by (a) HLCs and culture medium chambers and (b) the channels. The control layer hard mask is constituted by (c) the valves. The glass is being represented in blue and the aluminum is represented in grey. In both hard masks (a) and (c), the features were exposed so they are only composed of glass. In hard mask (b), the surrounding of the features was exposed, therefore, they are composed of Al deposited on glass.

First, a 5x5 cm glass substrate (Coring Inc., USA) was cleaned using isopropanol (IPA), and deionized water (DI water) followed by an ultrasound bath in Alconox (Alconox Inc., USA) for 30 minutes at 65ºC. The glass was rinsed with DI water again and dried with compressed air. All the following procedures were performed within a cleanroom where the environment is strictly controlled so that air particles do not interfere with the protocol.

A 2000 Å of aluminum (Al) was deposited on top of the glass surface using the Nordiko 7000 Magnetron Sputterer system (Nordiko Technical Services Ltd, UK), giving origin to an Al substrate. The Al substrate was taped on a silicon wafer and the deposition of PFR7790G positive photoresist (JSR, USA) was done on a swivel plate at 2000 rpm for 1 minute (SVG resist coater Silicon Valley Group Inc., USA), achieving a thickness of 1.5 µm. Next, the wafer was poured on a hot plate at 85ºC for 1 minute to evaporate the photoresist's solvent.

The wafer was placed inside the DWL (Heidelberg Instruments, DE) and the alignment of the Al substrate edge with the machine's origin of coordinates was performed. Then, the DWL reads the folder containing the information about the drawing lines. The laser travels through the substrate in the y axis direction and only falls in the zones where there is a correspondent line in the folder. In those zones, the laser exposes the positive photoresist which leads to its detachment. When it reaches the end of the y axis, the beam advances in the x-axis and jumps to the top part of the substrate exposing the next strip, and so on until the entire substrate is traversed.

Afterward, the development step was taken (developer track, Silicon Valley Group Inc., USA). The substrate was heated at 110ºC for 1 minute. After cooling down for 30 seconds, it was washed with a regulator and water, to take off the photoresist exposed, while the wafer was spinning on a swivel plate. At this stage, it was possible to visualize the features appearing. After that, on the wet bench, the aluminum non-covered by the photoresist (exposed part) was removed using an Al etchant (TechniEtch A180, Microchemicals, DE). Finally, the remaining positive photoresist was washed with acetone, IPA, and DI water and dried using an air gun.

It is important to notice that, as shown in **Figure 9**, both chambers and valve's hard masks only had glass in the features part, but the surroundings were still covered by aluminum. Therefore, in these hard masks, the features were the exposed part. In the channel's hard mark was the opposite, the surrounding was exposed. These hard masks characteristics will be crucial for the correct master mold fabrications.

II.1.3. Master mold fabrication

In this step, a total of two master molds were fabricated, one corresponding to the fluidic layer (**Figure 10a**) and the other to the control layer (**Figure 10b**). First, a 5x5 cm silicon (Si) substrate (Silicon water with 150 mm diameter and 675 um thickness, University Wafer, USA) was cleaned with IPA and DI water. Then, was dived in Alconox solution inside a Petri dish and placed in a bath with ultrasounds for 15 minutes at 65ºC. After that, the Si substrate was rinsed with DI water and dried with compressed air. Then, it was poured into the UVO Cleaner for 20 minutes, to ensure that it was fully cleaned. Lastly, it was rinsed again with DI water and dried with compressed air. Because it was needed two Si substrates, one for each mold, the steps described before were done twice. The next procedures were performed inside a laminar flow hood.

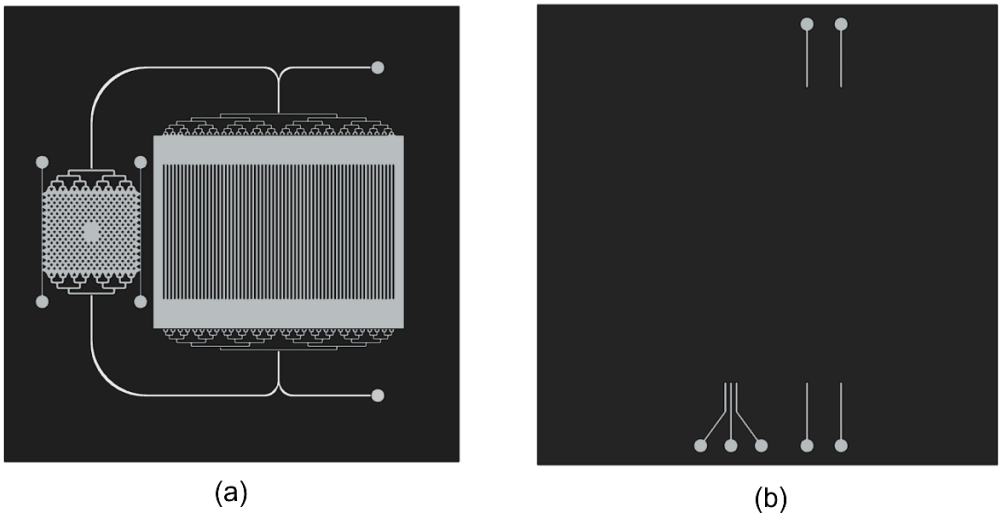

Figure 10 - Fluidic layer and control layer master molds. The fluidic layer master mold (a) is constituted by the chambers, 100 µm height, and the channels, 35 µm height. The control layer master mold (b) is constituted by the valves with 50 µm of height. The silicon is represented in black, the SU8-50 in grey, and the AZ40XT-11D in white.

Fluidic Layer Mold:

To fabricate the chambers of 100 µm of height that are included in the fluidic layer, the negative photoresist SU-8 50 (Microchem Corp., USA) was placed on top of the Si substrate in the spinner (Spin Coater, Laurel Corp., USA) to perform the spin-coating. Two steps were executed for the photoresist to acquire a thickness of 100 µm on the substrate (**Table 1**). Next, a pre-exposure bake was done on a hot plate at 65ºC for 11.5 minutes. Then, without removing the substrate from the hot plate, the temperature was increased to 95ºC. When the 95ºC were reached, 34 minutes were counted. Afterward, the substrate with the photoresist on top was cooled down for 1 minute. The chamber hard mask fabricated lately was placed on top of the SU-8 50 with the aluminum surface facing down. Then, it was poured inside the UV-KUB 2 (Kloé SA, France), and exposed to UV light for 62 seconds with only 30% of the maximum lamp power. In this case, since the photoresist is negative, the UV light will solidify the SU-8 50 exposed. A post-exposure bake took place on a hot plate at 65ºC for 1 minute. Then, another heating ramp was done by increasing the temperature to 95ºC without removing the substrate from the hot plate, and 11.5 minutes were counted after the 95ºC were reached. The substrate was cooled down for 2 minutes. The substrate was submerged in a PGMEA solution (Sigma-Aldrich, USA) for 10 minutes with manual agitation until the non-exposed photoresist was entirely removed. Next, it was cleaned with IPA and dried with compressed air. The last step of this procedure was the hard bake on a hot plate at 150ºC for 15 minutes followed by a slow cool down until it reaches 50ºC.

Table 1- Steps followed during the spin-coating of the SU-8 50 photoresist to achieve a thickness of 100 µm.

Step	Spin Speed (rpm)	Acceleration (rpm/s)	Time (s)
1	500	100	10
2	300	978	30

To finalize the fluidic layer mold, channels of 35 µm of height were done to link the chambers. Here, it was used the positive photoresist AZ40XT-11D (Merck Performance Materials GmbH, Germany) which has the capability to create round-shaped channels, a thing that will be advantageous during the valve's actuation. Firstly, the photoresist was poured on top of the Si substrate with the SU8-50 features. If air bubbles were formed in the zones where the channels will be placed, the substrate is poured inside the desiccator until they disappear. Next, the photoresist was spin-coated following the steps of **Table 2**. The pre-exposure bake was done by placing the substrate on a hot plate at 100ºC, then, ramping up to 125ºC, and baking for 5 minutes when the latter had been reached. After cooling down for 3 minutes, the channel's hard mask was poured on top of the Si substrate and the exposure was done for 10 seconds with 100% of the maximum power of the UV-KUB 2 lamp. In this case, since the photoresist is positive, the non-exposed zones remained in the Si substrate. The substrate was cooled down for 3 minutes and it was developed for 5 minutes using a TMAH based developer solution (ma-D 533 S, micro resist technology GmbH, Germany) with manual agitation. Then, it was washed with DI water and dried with compressed air. Finally, the hard bake was performed by placing the substrate on a hot plate for 5

minutes at 80ºC, followed by 5 minutes at 100ºC, 15 minutes at 115ºC, and 5 minutes at 125ºC with temperature ramping.

Table 2- Steps followed during the spin-coating of the AZ40XT-11D photoresist to achieve a thickness of 35 µm.

Step	Spin Speed (rpm)	Acceleration (rpm/s)	Time (s)
1	500	100	10
2	2000	1000	21

Control Layer Mold:

The control layer mold (valves) was fabricated using the negative photoresist SU-8 50. The photoresist was firstly spin-coated in order to achieve a height of 50 µm following the steps described in **Table 3**. The pre-exposure bake was done on a hot plate for 6.6 minutes at 65ºC. Without removing the substrate, the temperature was ramped to 95ºC, and the substrate was left at that temperature for 20 minutes. After cooling down for 1 minute, the hard mask corresponding to the valves was placed above the Si substrate and the exposition was made for 39 seconds with 30% of the maximum power of the UV-KUB 2 lamp. The post-exposure bake was performed at 65ºC for 1 minute. Then, the temperature was increased to 95ºC, and the substrate was left for 5.8 minutes. After cooling down for 2 minutes, the substrate was developed with a PGMEA solution for 7 minutes with manual agitation. Then, the substrate was cleaned with IPA and dried with compressed air. Finally, the hard bake was done in the same way as it was for the 100 µm fluidic layer chambers.

Table 3- Steps followed during the spin-coating of the SU-8 50 photoresist to achieve a thickness of 50 µm.

Step	Spin Speed (rpm)	Acceleration (rpm/s)	Time (s)
1	500	100	10
2	2066	300	30

II.1.4. PDMS structure fabrication and sealing

Having the master molds fabricated, it was possible to do the PDMS structure. Firstly, the PDMS was fabricated by mixing curing agent and base in a ratio of 1:10 in a plastic cup (Sylgard 184 PDMS and curing agent KIT, Dow Corning, USA). The cup was covered (not totally) by an aluminum foil and placed inside the desiccator for 45 minutes so that the air bubbles of the PDMS, that were created during the mixing, disappear. In this work, PDMS structures that only contained the fluidic layer, to perform perfusion experiments, and others containing both layers, to enable valves actuation, were fabricated.

Perfusion hepatocyte-chip structure:

The PDMS was poured on top of the fluidic mold previously taped on a PMMA frame. The air bubbles that appear after the deposition were removed using a scalpel. Next, a PMMA plate was placed on top of the frame, and springs were poured on the sides to increase the junction. The baking of the PDMS

on its mold was done for 1 hour and 30 minutes at a temperature of, approximately, 70ºC. Then, the PDMS structure was removed from the mold, and it was possible to visualize the features printed on it (**Figure 11a**).

The structure was drilled using an 18 ga syringe tip (Instech Laboratories Inc., USA) in the places designed for the hepatocyte's chamber access holes. Since it was only needed the hepatocyte's chamber part of the device for the chip operation in perfusion, additionally, a top inlet was drilled in a zone above the top dispenser to allow the entry of culture medium flow into the chamber. Similarly, an outlet, through where the culture medium flow will exit from the chamber, was drilled in the zone below the bottom dispenser. Plus, it was necessary to interrupt the communication to the culture medium chamber, therefore, were drilled two holes above the top inlet and below the bottom outlet to be maintained closed while perfusing the hepatocyte's chamber with medium (**Figure 11b**).

The last step to obtain the fully functional device was sealing. In this work, the structures were sealed against the polystyrene (PS) of Petri dishes (**Figure 11c**). Since the PDMS is hydrophilic, the sealing was done using an oxygen plasma bonding. The Petri dishes were placed inside the Plasma Cleaner (Oxygen Plasma Cleaner PDC-002-CE, Harrick Plasm, USA) without the lid. The instructions of the machine were followed, and 5 minutes of high voltage was performed. After that, a solution of 3-Aminopropyltriethoxysilane (APTS; AcroSeal, Thermo Fisher Scientific, USA) with water was spilled inside the Petri dishes and it was left for 20 minutes. After that time, the Petri dishes were rinsed with DI water and dried with compressed air. The PDMS structures were washed with IPA followed by DI water and dried with compressed air. Then, they were placed inside the Plasma Cleaner with the features part facing up. High voltage for 5 minutes was done. After that, the structures were sealed against the Petri dishes. This procedure had to be done as fast as possible since the hydrophilicity of both, PDMS structures and PS, decays during the time. The PDMS structures were poured on top of the PS that received the plasma bonding treatment (part facing up inside the Plasma Cleaner) and, with the help of a tweezer, it was applied enough pressure to ensure the sealing. The recently sealed structures were left to rest to ensure that they do not collapse.

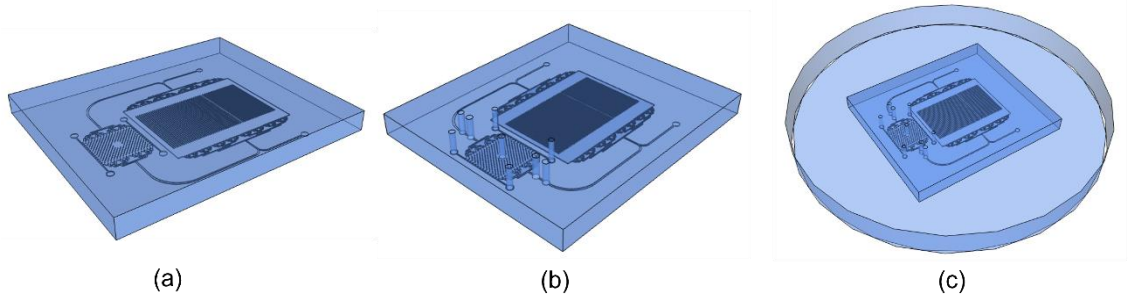

Figure 11- Final steps to create the hepatocyte-chip structure for perfusion experiments. (a) represents the fluidic layer PDMS after being removed from the mold. (b) shows the structure after being drilled. In this device, it was added two more access holes, one above the top dispenser (inlet) and, the other, below the bottom dispenser (outlet). Additionally, another two holes were drilled above/below the new ones to ensure the independence of the cell's chamber. And (c) shows the structure sealed against the PS of a Petri dish.

Recirculation hepatocyte-ship structure:

To create the complete structure, the control mold was taped to a Petri dish and PDMS was poured on the top of it in order to cover the entire mold. The Petri dish was placed in the oven for 1 hour and 30 minutes at a temperature of 70ºC. After baking, the PDMS was cut with a scalpel upon the mold's edges and the structure was taken of the Petri dish. Then, the holes were drilled using a 20 ga syringe (Instech Laboratories Inc., USA). In parallel, the fluidic mold was taped to a PMMA plate. A PMMA frame of 6.2 x 6.2 cm was poured on top and, about 3 mL of PDMS was spilled on it in order to cover the fluidic mold and the spaces between the mold and the frame. Then, the wafer was placed inside the oven and the PDMS was baked for 1 hour at 70ºC. Then, the PMMA frame was taken away from the plate.

Afterward, the control and fluidic PDMS structures were sealed against each other. Therefore, after being washed with IPA and DI water and dried with compressed air, both structures were poured into the Plasma Cleaner. The control layer PDMS was placed inside with the features facing up and the fluidic layer PDMS was poured yet on its mold. High voltage for 1 minute was applied. After taking the structures of the machine, the valves were aligned with the channels, and the control layer was sealed on top of the fluidic layer creating a PDMS stack (**Figure 12a**). The already sealed structure was peeled off the fluidic mold, and the access holes of the fluidic layer PDMS were drilled using an 18 ga syringe (**Figure 12b**). Then, the complete structures were sealed against Petri dishes by following the same protocol used for the hepatocyte-chip perfusion structure (**Figure 12c**).

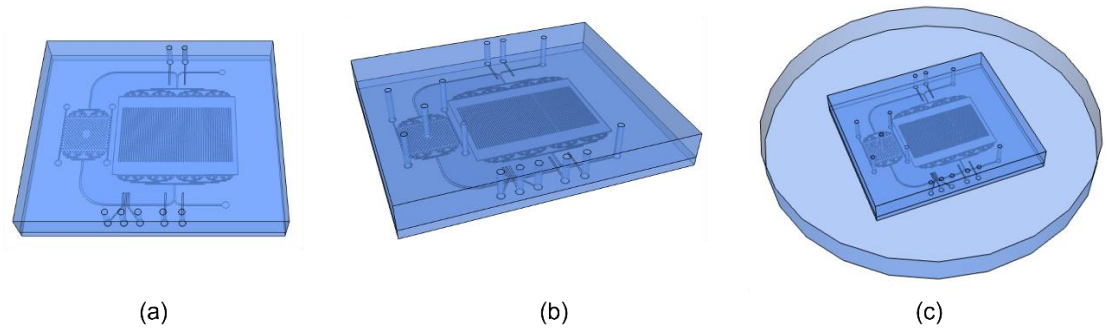

Figure 12- Final steps to create the hepatocyte-chip structure for recirculation experiments. In (a) it is represented the drilled control layer PDMS sealed against the fluidic layer PDMS, (b) shows the structure after the fluidic layer be drilled, and (c) shows the final structure after the sealing against the Petri dish's PS.

II.2. Microfluidic device set-up

The fluidic layer of the hepatocyte-chip (**Figure 13a**) is constituted by a cell's chamber where the HLCs will be seeded, a culture medium chamber to supply the cells, and channels that connect the two previous chambers. It is important to notice that the chip is always presented with the HLCs chamber on the left side and the culture medium chamber on the right side.

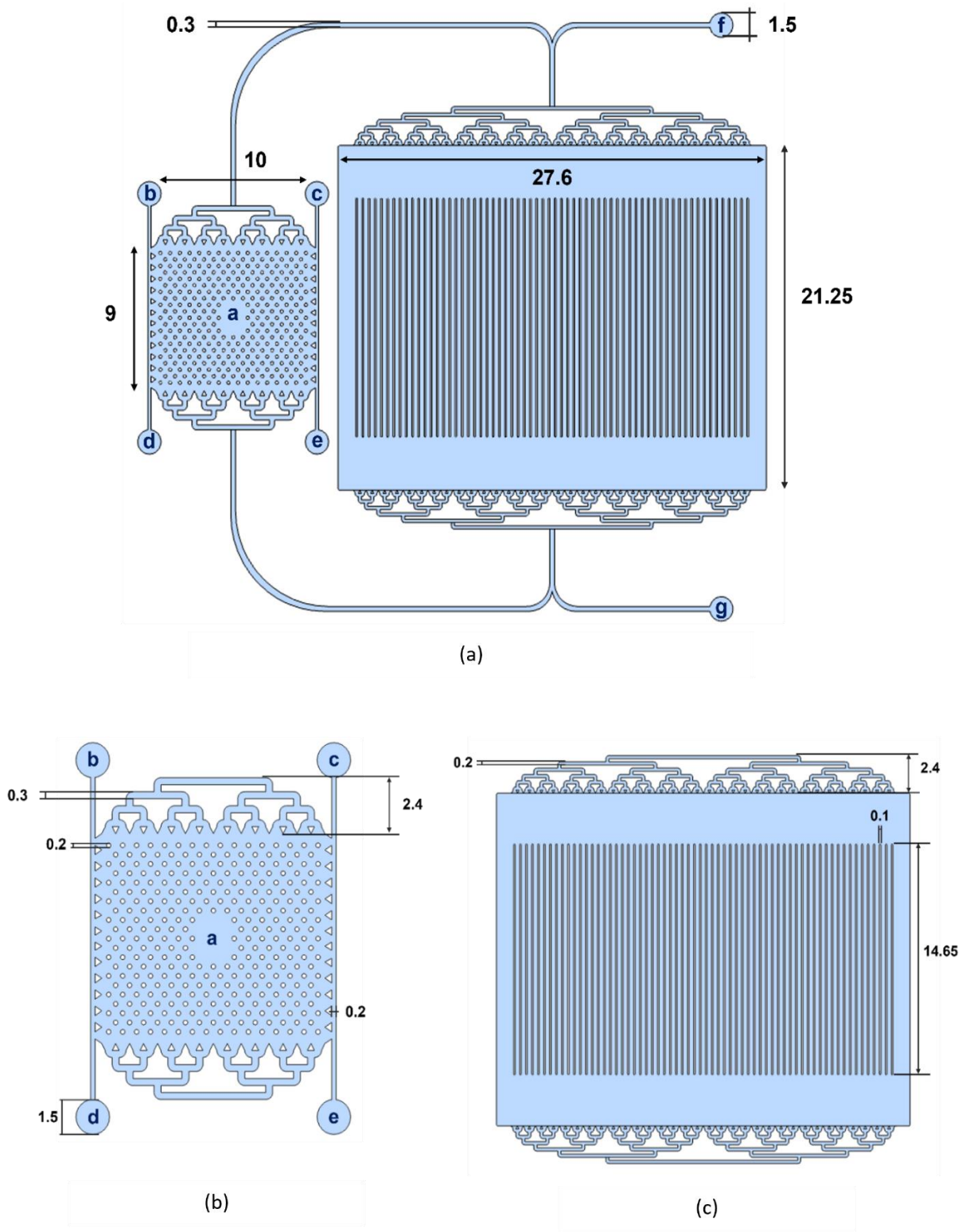

Figure 13- Fluidic layer dimensions of the final hepatocyte-chip in millimeters (mm). In image (a) it is being represented an overview of the main dimensions of the fluidic part of the device. In (b) it is possible to visualize a detailed representation of the cell's chamber including some particular dimensions and the given access hole's nomenclature. Image (c) represents specific dimensions of the culture medium chamber.

The HLC's chamber (**Figure 13b**) has a height of 0.1 mm, a culture surface of 10 x 9 mm, and is composed of several micropillars, to ensure that the chamber does not collapse, with 0.2 mm diameter, except in the middle to allow the drilling of a center access hole (**Figure 13b**, inlet **a**). Two dispensers were built on the top and bottom of the chamber having 2.4 mm of height and being composed of 0.3 mm wide channels for allowing the culture medium entry and exit, respectively. On the right and left sides of the HLC's chamber, one 0.2 mm wide channel is connected to allow better dispersion of the cells into these zones. Two corner inlets at each end of the two side channels were designed (**Figure 13b**, inlets **b**, **c**, **d**, and **e**). Both the dispensers and the side channels connections were made in a way that covers all chamber edges to allow a better culture medium dispersion.

The culture medium chamber (**Figure 13c**) has a height of 0.1 mm, a surface of 27.6 x 21.25 mm, and it has also in its composition 14.65 mm long and 0.1 mm wide pillars. Two 2.4 mm high dispensers were created on the top and bottom of the chamber which are constituted by 0.2 mm wide channels. Similar to the cell's chamber, these dispensers also cover all the entire top and bottom edges of the culture medium chamber.

Finally, the channels are round-shaped and have a width of 0.3 mm. At their very end, a medium inlet (**Figure 13c**, inlet **f**) and a medium outlet (**Figure 13c**, inlet **g**) were created to place the medium inside and outside the chamber, respectively.

The control layer of the hepatocyte-chip (**Figure 14**) is composed of four valves with a width of 0.3 mm and an inlet at the end. Valves 1 and 2 are located in the top part of the culture medium dispensers, perpendicularly to the channels, while valves 3 and 4 are located in the same position but on the bottom part of the dispensers. They were placed in a way that each valve controls one section of the channels. The pump (**Figure 14b**, 5) is located in the inferior channel and is composed of three valves whose width and space between have 0.3 mm.

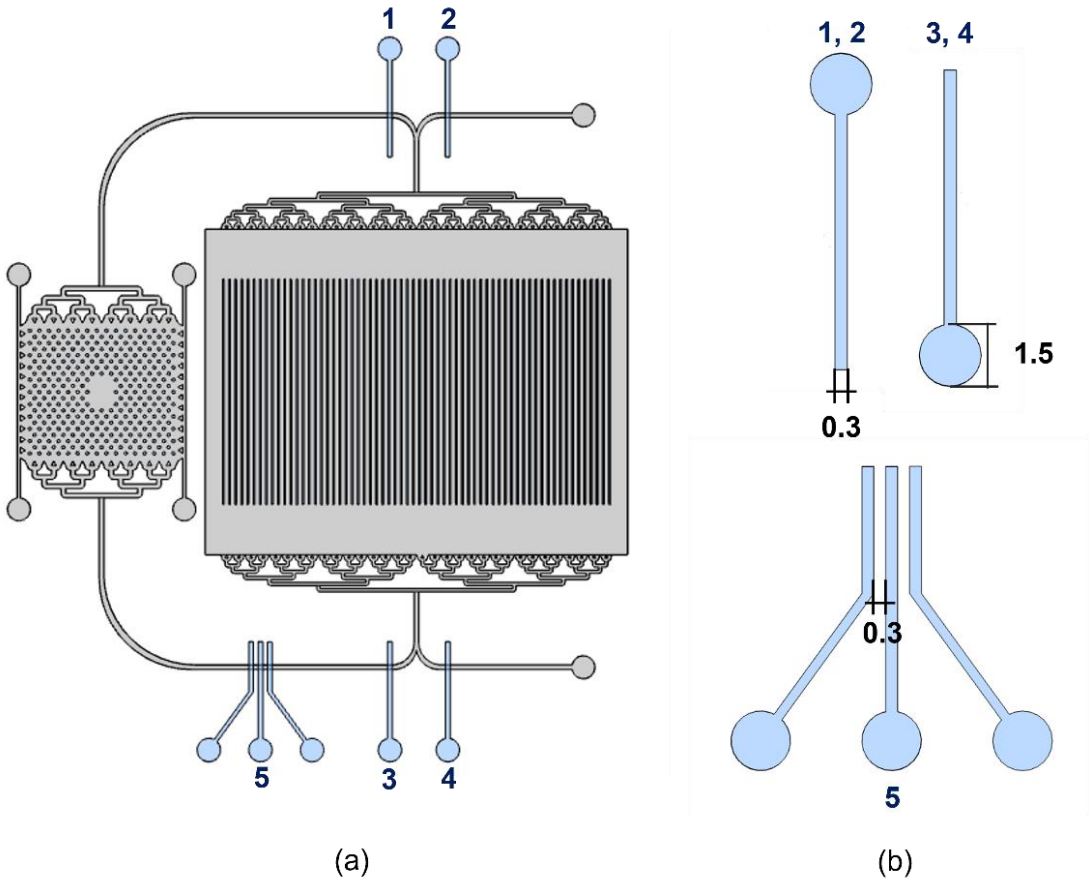

Figure 14- Control layer dimensions of the final hepatocyte-chip in millimeters (mm). In image (a) it is being represented the disposition of the pneumatic valves and pump throughout the fluidic layer design, and the numbers attributed to each. In (b) it is possible to visualize a detailed representation of each valve conformation and pump, as well as some of their dimensions.

II.3. Reagents for cell culture

All culture media and supplements, solvents (all analytical grade), and other chemicals were acquired from Sigma-Aldrich (Spain) unless specified.

II.4. Collagen coating

Rat-tail type I collagen and commercial rat-tail type I collagen (Gibco, UK) were used in this work. The protocol for rat-tail extraction was based on Rajan *et al.* [82]. Briefly, rat tails were washed twice in 70% ethanol prior to skin removal using surgical material. Tendon fibers were pulled out, separated from the bone and cartilaginous tissue, and suspended in PBS. Fibers were then washed three times and immersed for 1h in 70% ethanol before being transferred into 0.1% acetic acid and stirred for 48h at 4°C, for fiber acid digestion. The solution was centrifuged at 16000xg for 90 minutes at 4ºC. The supernatant was collected, lyophilized and the resultant solid was stored at -80°C until further use.

The extracted rat-tail collagen was dissolved in 0.1% acetic acid to a stock concentration of 1 mg/mL. The stock solution was diluted in PBS to 0.2 mg/mL in a volume that assures total culture surface coverage. After 1 hour of incubation at 37 ºC, cell culture surfaces were washed with PBS before inoculation. The differentiation process occurred using this collagen coating until D17 and onwards for cultures in well plates.

Coating with commercial type I collagen was used for the microfluidic devices. Commercial collagen at a stock concentration of 3 mg/mL was diluted in PBS to a final concentration of 0.2 mg/mL. After 1h in the incubation at 37 ºC, the devices and the well plates were washed with PBS.

II.5. Cell culture

hnMSCs isolated from human umbilical cord stroma were fully characterized accordingly to Martins *et al.* and expanded in Eagle's minimum essential medium - alpha modification (α-MEM) supplemented with 10% (v/v) of fetal bovine serum (FBS; Gibco, UK) [83, 84]. For generating HLCs, a three-step differentiation protocol (**Figure 15**) was applied to hnMSCs as detailed previously by Cipriano *et al*. [47]. Briefly, hnMSCs were seeded at a density of 1.5×10^5 cells/cm^2 in rat-tail collagen-coated surface plates. At day 17 (D17) of differentiation, cells were trypsinized and reinoculated in Iscove's modified Dulbecco's medium (IMDM) with 8 ng/mL oncostatin M (OSM; Peprotech, USA), 1 µM dexamethasone (Dexa), 1% (v/v) DMSO, 1% (v/v) insulin-transferrin-selenium solution (ITS; Gibco, UK), 20 µM of 5-azacytidine (5-AZA), 5% (v/v) FBS, 1% (v/v) penicillin-streptomycin (Pen-strep) and 0.01% (v/v) amphotericin B (Anfo) into (i) microfluidic devices (**Section II.8.3.**) and (ii) culture plates pre-coated with collagen (2×10^4 cells/cm^2). The medium was changed 24h after inoculation to remove 5-AZA and FBS. From D21 onwards, HLCs were maintained in Physiol, composed of Dulbecco's modified Eagle's medium (DMEM) with 1 nM of insulin, 100 nM of Dexa, and 0.2% BSA. The medium was replaced every 3 days.

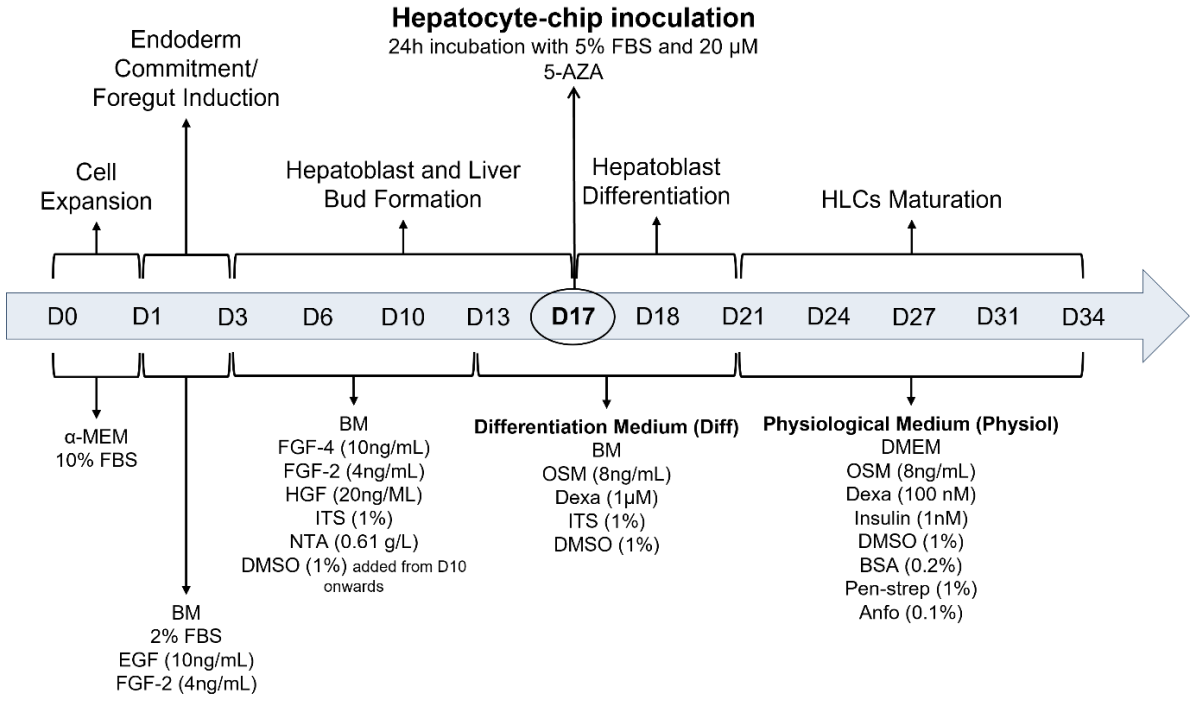

Figure 15- Hepatocyte-like cells differentiation protocol. The HLCs differentiation is constituted by three main steps after cell expansion: endoderm commitment and foregut induction, hepatoblast formation and differentiation and, HLCs maturation. Throughout these steps, the culture medium composition is changed in order to achieve the correct hepatocyte phenotype. BM is composed of IMDM with 1% of Pen-strep and 0.01% of Anfo.
Abbreviations: α-MEM (Minimum essential medium Eagle with alfa modification), BM (basal medium), DMEM (Dulbecco's modified Eagle's medium), FBS (fetal bovine serum), 5-AZA (5-azacytidine), EGF (epidermal growth factor), FGF (fibroblast growth factor), HGF (hepatocyte growth factor), ITS (insulin-transferrin-selenium), NTA (nicotinamide), DMSO (dimethyl sulfoxide), OSM (oncostatin M), Dexa (dexamethasone), BSA (bovine serum albumin), Pen-strep (penicillin-streptomycin), Anfo (amphotericin B), D0-D34 (day 0-34 of the differentiation protocol).

HepG2 cells were cultured in α-MEM supplemented with 10% FBS, 1 mM of sodium pyruvate, and 1% (v/v) of non-essential amino acids (NEAA). Cryopreserved human primary hepatocytes (hpHeps; pool of 10 donors) were purchased from Invitrogen (Carlsbad, USA), thawed on cryopreserved hepatocyte recovery medium (Invitrogen), and manipulated according to manufacturer instructions. Cell cultures of hnMSCs, HepG2 and were maintained at 37 °C in a humidified atmosphere with 5% CO_2 in air. Cell viability was assessed through the trypan blue exclusion method.

II.6. Freezing of HLCs

After trypsinization at day 17 of differentiation, HLCs were resuspended in 90% FBS and 10% DMSO and put in cryovials. The vials were immediately placed in an isopropanol cooling container (Mr. Frosty) which was kept at -80 ºC overnight. The vials were then stored in liquid nitrogen until further use.

II.7. Thawing of cryopreserved HLCs

The thawing procedure was performed rapidly using a 37ºC water bath. The aliquots were resuspended in a culture medium and centrifuged at 200xg for 5 minutes. HLCs were seeded into (i) microfluidic

devices (**Section II.8.3.**) and (ii) culture plates pre-coated with collagen (4×10^4 cells/cm^2) and plated in Diff with 10% FBS and 20 µM of 5-AZA. FBS and 5-AZA were removed after 24 hours.

II.8. Hepatocyte-chip perfusion assays

In the following sections, it will be explained the hepatocyte-chip operation when the culture medium is perfused to the HLC's chamber. In these conditions, the culture medium flowed inside the chamber by making use of a syringe pump (NE-1002C, New Era Pump Systems, Inc., USA) to control the flow rates, syringes (1 mL insulin syringes U-100 Luer-Lock, Codan, DE), 20 ga syringe stubs (Instech Laboratories, Inc., USA), BTPE 60 tube (Instech Laboratories, Inc., USA), and metallic plugs (SC20/15, Instech Laboratories, Inc., USA). In **Figure 16**, it is possible to visualize a resume of the steps that were taken during these experiments.

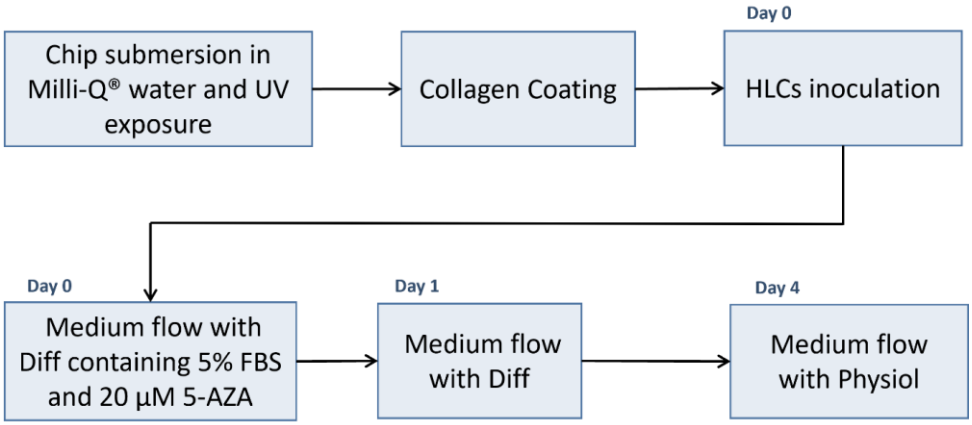

Figure 16- Steps followed during perfusion experiments. Six main steps had to be considered during these assays: device submersion in water and UV exposure, coating with collagen, cell's insertion, and adhesion in the chip, then, on day 0, Diff supplemented with FBS and 5-AZA is flowed, on day 1, the medium is changed to Diff without the FBS and 5-AZA, and, on day 4, the medium is changed Physiol. Abbreviations: Day 0-Day 4 (days of cell's maintenance inside the microfluidic device), HLCs (hepatocyte-like cells), Diff (differentiation medium), FBS (fetal bovine serum), 5-AZA (5-azacytidine), Physiol (physiological medium).

II.8.1. Set-up

Procedures to avoid contaminations and prevent air bubble formation inside the chip during the culturing were required. Accordingly, the device was submerged in Milli-Q® water to remove the air inside and subjected to 2h of UV exposure inside the laminar flow hood as a sterilization procedure.

Next, was prepared the set-up used to proceed with the collagen coating and cell inoculation. Therefore, BTPE 60 tubes were decontaminated with ethanol and then, washed with PBS. Afterward, the tube was connected to a syringe tip, and a metallic plug was inserted in its other extremity. The syringe tip was attached to a syringe and the syringe was poured on a syringe pump. The other tube end was plugged into the device.

II.8.2. Collagen coating

The coating was performed 72h before HLCs inoculation. The collagen solution was flowed inside the device, through inlet **a** (**Figure 13b**), using 50 µL/min for 2 min. After 1h in the incubator at 37ºC to allow polymerization, PBS solution was flowed through the same inlet for 2 minutes at a flow rate of 50 µL/min to wash the device. The device was stored at 4 ºC until the inoculation day to dissolve air bubbles at sharp edges and corners of the fluidic structure. To ensure the polymerization of collagen fibers throughout the chip surface, the coating was repeated on inoculation day.

II.8.3. HLCs inoculation and hepatocyte-chip operation

On D17 of HLCs differentiation, the cells were inoculated in the microfluidic cell's chamber. A concentration of 1 million cells/mL was resuspended in DM with 5% FBS and 20 µM of 5-AZA. Device inoculation was performed by flowing 5 µL/min for 2 minutes through the inlet **a** (**Figure 13b**), then 10 µL/min for 4 minutes through the same inlet, and, finally, 10 µL/min during 1 minute through the inlets **b**, **c**, **d**, and **e** (**Figure 13b**), which gave an inoculum of, approximately, 90000 cells/cm^2. Over the insertion, the concentration and dispersion of the cells inside the chamber were visually inspected under the microscope. After 1 h, when most of the cells were adherent, the medium was flowed at a rate of 0.2 µL/min. Cryopreserved HLCs were inoculated on D20 of differentiation into the hepatocyte's chamber by following a similar protocol as the one described before for the freshly differentiated HLCs.

In the final operation set-up, as it is possible to schematically visualize in **Figure 17**, a syringe filled with culture medium was poured on the syringe pump, the metallic end of the tube plugged in the top inlet of the device. The inlets **a**, **b**, **c**, **d**, and **e** (**Figure 13b**) were plugged with closed metallic plugs to ensure that no leaks occur, as well as the inlets created to close the communication to the culture medium chamber. The outlet was plugged with BTPE 60 tube and an Eppendorf was attached to the other end to collect the cell's supernatant for sampling.

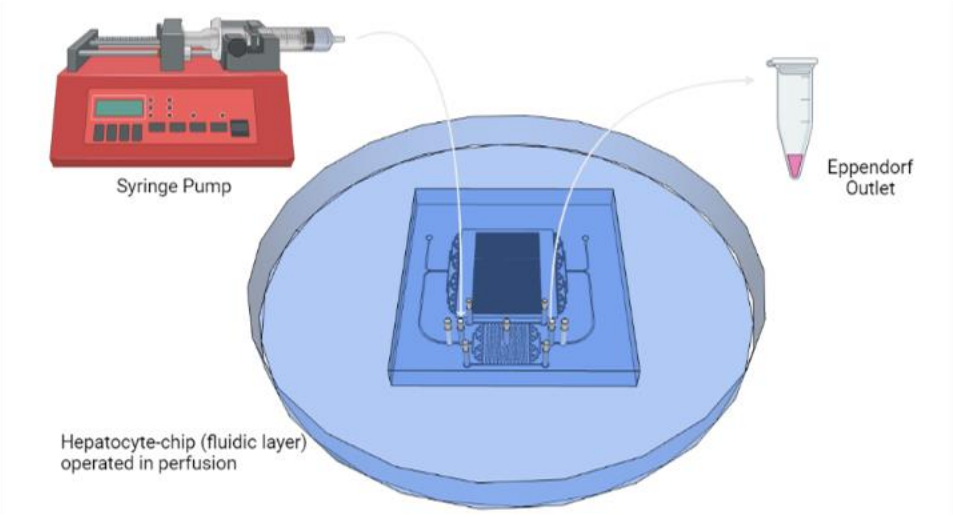

Figure 17- Scheme of the final perfusion set-up. The culture medium was being flowed using a syringe pump with a constant flow rate of 0.2 µL/min, at the same time, the cell's supernatant was being collected through an Eppendorf placed in the far end of the outlet tube. The hepatocyte-chip was inside the incubator to maintenance the typical cell's environment.

II.9. Valves actuation

To control the single valves (**Figure 14a**, valves 1, 2, 3, and 4), a mechanical pressure regulator (maximum pressure of 400 Pa; SMC Precision Regulator IR2010-F02, Orange Coast Pneumatics Inc., Japan) connected to an array of normally closed solenoid valves (SMC SY114-5MZ-Q, Orange Coast Pneumatics Inc., Japan) was used (**Figure 18**). Firstly, to ensure that no air bubbles were created and diffused to the fluidic channel of the chip during the valve operation, filling the valve channel with water was required. Accordingly, a piece of BTPE 60 tube was filled with DI water and plugged into the valve's inlet. In the other extremity, the tube was attached to a tubing coupler (SMC TU0425 polyurethane tubes, Orange Coast Pneumatics Inc., Japan) that was coupled to the solenoid valve. The air pressure regulator was adjusted to 100 Pa until the channel was completely filled with water. To close the fluidic channel, it was necessary to increase the air pressure inside the valve channel, therefore the regulator was adjusted to higher pressures. To open the fluidic channel, the pressure of the regulator was decreased.

The pump (**Figure 14a**, pump 5) control was done using, additionally, a teensy circuit board (Teensy 3.5, 32 Bit Arduino Compatible Microcontroller, PJRC, USA) that was connected to the array of solenoid valves, to allow their control, and to the computer (USB connection), to provide the code (**Section VI.1.**) to enable the three valves functioning as a pump (**Figure 18**). The teensy circuit was supplied by a 24 V power source (HP Hewlett Packard E3612A DC Power Supply, USA).

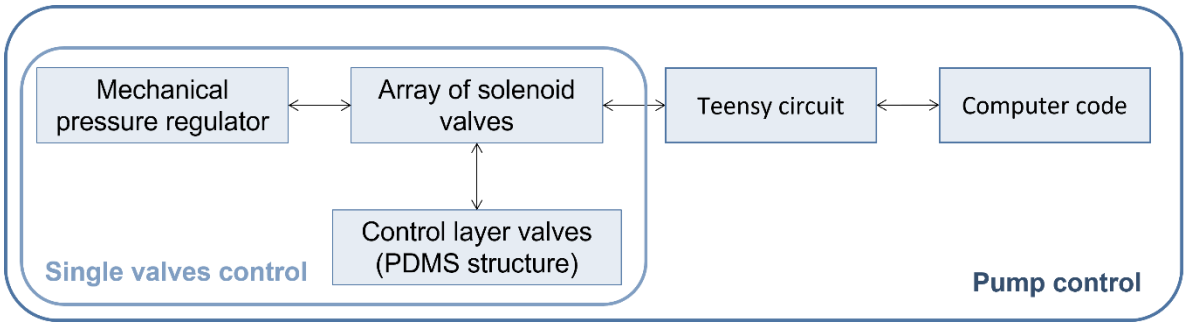

Figure 18- Scheme representing the components used for single valves and pump control.

II.10. Urea quantification

Urea was quantified in cell culture supernatants using a colorimetric urea kit (Urea Assay Kit, Abnova, Hayward, Taiwan). The absorbance was measured at 520 nm in a microplate reader (SPECTROStar Omega, BMG Labtech, Germany), according to the manufacturer's instructions. Data are presented as the rate of production µg/10^6 cells.h.

II.11. Statistical analysis

The results are presented as Average ± SEM unless stated otherwise. The urea and albumin quantifications were analyzed with two-way ANOVA with GraphPad Prism. A threshold of $p < 0.05$ was considered statistically significant.

III. Results and Discussion

The main goal of this work was to design a hepatocyte-chip to obtain a microphysiologically relevant and controlled hepatic *in vitro* model using HLCs derived from human stem cells. In the next sections, the optimizations performed to allow the culture of HLCs in the microfluidic device leading to the final chip design will be described. HLC culture in regular 2D plates was previously characterized and validated. Therefore, plates were considered the control for the HLC culture, and the hepatocyte-chip culture was compared to it in terms of morphology and urea production. Moreover, to test the possibility of having an off-the-shelf microphysiological hepatic *in vitro* model, the culture of previously frozen HLCs in the hepatocyte-chip was also assessed and compared with freshly obtained HLCs. Finally, tests regarding the control part of the chip will be presented to show the potential of the valves concerning the recirculation of the culture medium throughout the cell's culture.

III.1. PS surface improved HLCs maintenance inside microfluidic devices

The first parameter to be optimized was the culture surface. The majority of the microfluidic devices used for cell culture purposes are made with PDMS since this elastomer is easy to manipulate, optically transparent, allowing cell's visualization under the microscope, and it is compatible with cell culture. PDMS can be sealed against different types of materials according to the aim of the study. Herein, the goal of the microfluidic device was to culture HLCs on a PS or a PDMS culture surface. From a biological point of view, it would be preferable to seal the devices against PS since the hepatic differentiation protocol herein pursued is performed normally using PS as a culture surface. Indeed, in the initial 17 days of HLCs differentiation, the cells are cultured within PS flasks previously coated with rat-tail collagen, meaning that this culture surface is already optimized for the culturing of this cell type. Moreover, PS is the most widely used thermoplastic for laboratory cultureware, having provided validated research conclusions regarding cell behavior and function throughout decades [85]. However, from a microfluidic point of view, a PDMS surface would be advantageous because it facilitates microfluidic valve control to allow fluid recirculation. In fact, if the cells could be adapted to PDMS, it would be possible to reproduce the most commonly used process for valve fabrication and actuation, and the one already optimized at INESC-MN. Accordingly, initial tests were made to evaluate the adaptation of the HLCs to PS and PDMS culture surfaces in order to choose the optimum one to seal the device against.

As a first approach, to optimize the culture surface two different experimental microfluidic devices that were designed for cell culturing, devices A and B, were used (**Figure 19**). Device A has a height of 0.1 mm and a culture surface of 10 x 10 mm that is constituted by several micropillars with a diameter of 0.1 mm. Three dispensers are built on every side of the chamber and, each one leads to an access hole, being used to perfuse the culture medium. It was also drilled an access hole in the middle of the chamber for coating and cell insertion. Device B has also a height of 0.1 mm and is constituted by two chambers in a diamond-like shape with a culture surface of, approximately, 12 x 4 mm. Each chamber is connected by 1 mm channels and is composed of 0.1 mm micropillars as well. In this device, two

access holes in the middle of each chamber were drilled for the coating and cell's insertion, and two top and bottom holes to perfuse the medium.

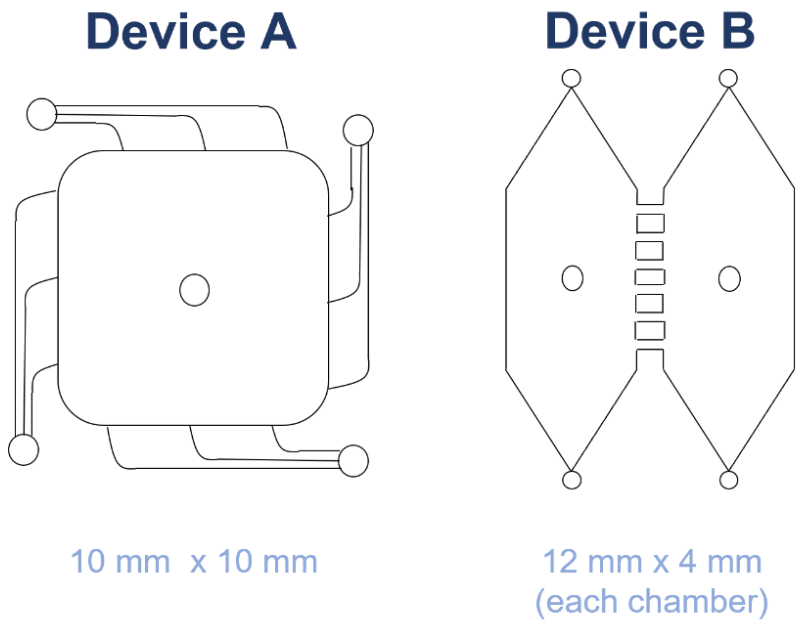

Figure 19- Simplified scheme of devices A and B used to optimize the culture surface. Device A has a culture surface area of 10 mm x 10 mm and device B has a surface of, approximately, 12 mm x 4 mm in a diamond-like shape. The middle chamber access holes were used to insert the coating and the HLCs, two of the others were used to perfuse the culture medium, the rest was closed with metallic plugs.

In this experiment, devices were sealed against PS or PDMS. A coating of commercial collagen type I diluted with acetic acid was used since it was previously demonstrated to produce better results regarding the HLCs culturing inside commercially available microfluidic devices sealed against glass. HLCs were inoculated inside devices A and B on their D17 of differentiation. After cell adherence to the culture surface, the medium was then perfused into each device after choosing two opposite side access holes to serve as an inlet and an outlet, in order to introduce a unidirectional flow throughout the chamber. The other access holes were closed with metallic plugs. Although the coating and inoculation protocol were not yet optimized in the devices, it was possible to evaluate the behavior of the cells when seeded on each surface. The results show that, even though the cell's adhesion was not fully achieved in neither of the surfaces, the cells demonstrated a better adaptation in the device sealed against polystyrene (MD 1) since they were maintained in the chip longer than the cells from the chips sealed against PDMS (MD 2) (**Figure 20**). As it is possible to visualize, on the day after the inoculation (day 1), the cells from MD 2 detached from the PDMS (**Figure 20d**). While, on the same day, the cells from MD 1 were still adherent to the PS (**Figure 20c**). However, three days after inoculation, the HLCs from the PS surface device started to detach (**Figure 20e**), which was believed to be due to the not yet optimized collagen coating and inoculum.

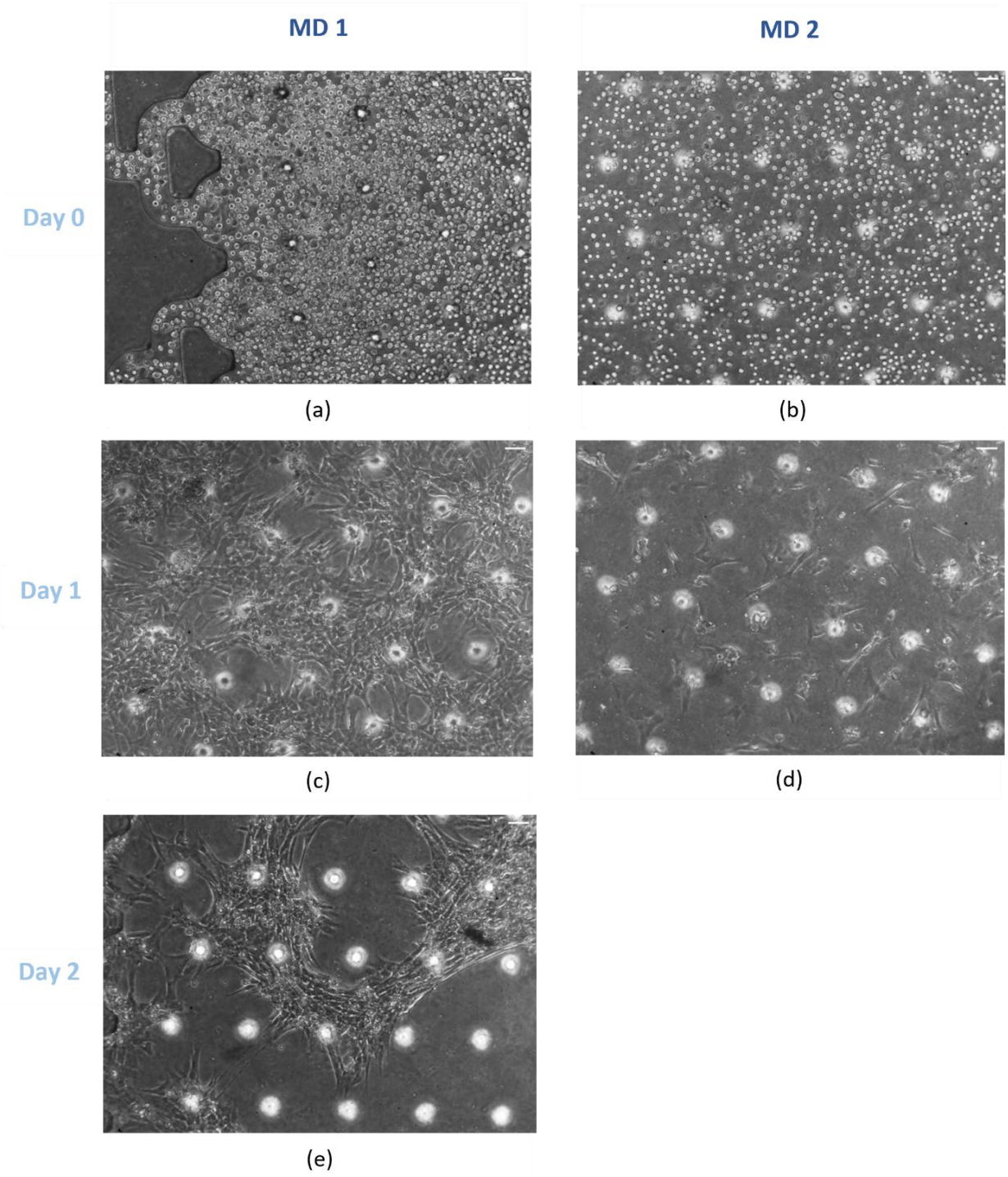

Figure 20- Cell's aspect, from day 0 to day 2, when cultured on PS (MD 1) and PDMS (MD 2) surfaces inside microfluidic devices. (a) and (b) show the cell's dispersion after being inoculated in the devices (day 0). (c) and (d) show cell adhesion in PS and PDMS, respectively, one day after the cell's insertion (day 1). (e) shows HLCs on their second day (day 2) in the device sealed against PS. Scale bar = 100 µm.
Abbreviations: Day 0-Day 2 (days of cell's culture in the microfluidic device), MD 1, and MD 2 (microfluidic device 1 and 2).

To understand if HLC adhesion to PDMS could be improved with higher cell inoculum, or with a different type of coating, a second assay was made. Therefore, a 24-well plate was prepared with, approximately, 500 µL of PDMS in each well. In the hepatic differentiation protocol, the surface's coating is performed using rat-tail type I collagen, which is one of the most abundant ECM proteins that exist within our body [86]. Herein, two different types of collagen type I were tested to coat the PDMS: rat-tail type I collagen and commercial type I collagen. The rat-tail collagen made in the laboratory does not have the same purity as the commercial collagen, that was fabricated at an industrial scale. Thus, commercial collagen provides a better culture definition and enables the achievement of standard methods for *in vitro* cell culturing. The solvent used to dilute the collagen has an impact on the thickness of the coating solution, which is due to their pH and composition [86]. Indeed, the type I collagen conformation is pH-dependent, meaning that, at an acidic pH, the collagen form long thin fibers, while when the pH is raised achieving a value close to the physiological levels, collagen is polymerized creating thick aggregates [86]. Accordingly, we tested two types of solvents with different pH to conclude which one could be better for cell adhesion to PDMS. Namely, acetic acid and PBS as collagen solvents were used. Because acetic acid has a more acidic pH, it makes the collagen fibers thinner than PBS. Indeed, collagen is more soluble and flexible in acidic conditions, that is why acid acetic is used to conserve collagen [86]. PBS has a pH closer to the physiological levels, therefore with this solvent the collagen molecules tend to polymerize, self-assembly, and form bundles of fibers, which contributes to a thicker coating layer [86]. In sum, four different types of coatings were tested, namely, rat-tail collagen diluted with PBS, rat-tail collagen with acetic acid, commercial collagen diluted with PBS, and, lastly, commercial collagen diluted with acetic acid. Additionally, two inoculum conditions were tested, specifically, the regularly used 20 000 cells/cm^2, and 30 000 cells/cm^2. The results show that none of the conditions provided the correct environment for HLCs adhesion and preservation (data not shown) resulting in cell detachment on every coating surface tested. Therefore, it was possible to conclude that PDMS is not a good surface for HLCs culture in these conditions. Consequently, to proceed with the sealing of the microfluidic devices it was chosen to seal them against PS as it was the surface that had better results to undertake HLCs culturing.

III.2. Commercial collagen diluted with PBS provided better HLCs attachment to the PS culture surface of microfluidic devices

To enable a better attachment of the HLCs in the microfluidic devices sealed against PS, the coating was optimized. The coating is a treatment made on the culture surface to increase cell adhesion and is performed using proteins or peptides to mimic the human body environment. Commercial type I collagen was demonstrated to provide better coating results in commercially available microfluidic devices sealed against glass. The previous results (**Section III.1.**) also show the potential of using commercial collagen in the PS coating. Furthermore, as mentioned, the commercial collagen is purer and enables the development of standard coating methods in comparison with rat-tail collagen produced in the laboratory. Accordingly, only commercial collagen was chosen to test two different coating solutions, namely, commercial type I collagen diluted in acetic acid, and commercial type I collagen diluted in PBS. In general, PBS, as a collagen solvent, enables a better cell attachment to PS culture surfaces since it forms a more robust coating (PBS is normally used to coat PS plates). However, because PBS is more viscous than the acetic acid, may form clogs inside the microfluidic device once it solidifies, which may obstruct the chamber. Therefore, comparing these two coating solvents on PS culture surfaces were required.

To test the two different coating conditions, devices A and B, previously described (**Figure 19**), were used. In both types of devices, the collagen solution was inserted through the center access holes, for 2 min at 10 µL/min, to ensure that it was distributed equally throughout the chips. A concentration of 0.2 mg/mL in the two different collagen solutions was used, as it had already been optimized in the protocol. **Figure 21** shows the cell's images on inoculation day (day 0) and the next day (day 1) in MD 1, coated with collagen diluted with PBS, and MD 2, coated with collagen diluted with acetic acid. It can be noticed in **Figure 21a** that a higher concentration of cells was inserted in MD 1 in comparison with MD 2 (**Figure 21b**). That happened since MD 1 was the first device to be inoculated and cell distribution into different Eppendorf for each device was not being done at this stage. Even considering this fact, it is still possible to notice a significant distinction in HLCs' adhesion on the two coatings. Indeed, one day after inoculation (day 1), the cells from MD 1 were confluent, adherent, and showed a polygonal shape, which constitutes the usual HLCs morphology (**Figure 21c**). On contrary, the cells from MD 2 were still rounded and detached from the coating surface (**Figure 21d**). Hence, the results indicate that HLCs had a better attachment in the chip coated with collagen diluted with PBS (**Figure 21c**) than in the device coated with collagen diluted with acetic acid (**Figure 21d**). Consequently, type I collagen diluted in PBS was chosen as the coating solution for the microfluidic devices.

Even though MD 1 fulfills the chosen condition, in this chip, the HLCs start to detach from the surface and lose their polygonal shape during the culturing (data not shown). This could be because not enough coating solution flowed through the device. Indeed, even though the volume of coating solution (20 µL) was higher than the effective device volume (device A, 10 µL), it could not have been enough to guarantee the formation of collagen fibers on the entire culture surface. Another explanation was that a larger volume of PBS (30 µL) than the actual volume of coating solution inserted (20 µL) was used to

wash the non-adherent collagen, ending up removing the adherent one as well. Therefore, to avoid these problems, it was decided to perform the coating twice before cell inoculation to ensure cells' adhesion and morphology throughout the culture period, and perform the PBS washing using the same protocol (flow rate and time) as the used to flow the coating solution.

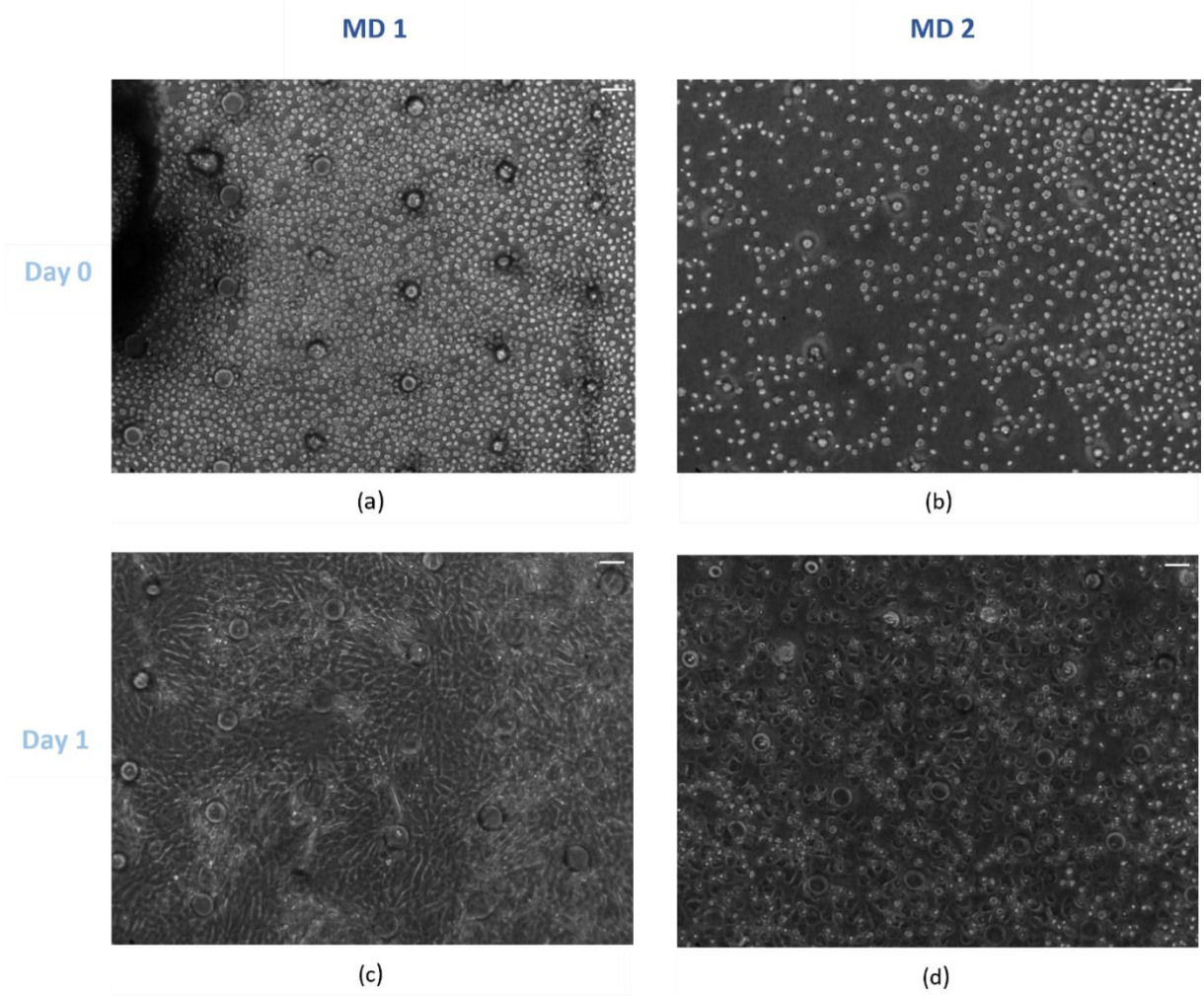

Figure 21- Cell's behavior when seeded on a PS culture surface coated with type I collage diluted with PBS (MD 1) and with acetic acid (MD 2). (a) and (b) show the cell's dispersion after being inoculated in the devices (day 0). HLCs, after one day of inoculation (day 1), on a surface coated using PBS (c) and acetic acid (d) are also presented. Scale bar = 100 µm.
Abbreviations: Day 0-Day 1 (days of cell's maintenance inside the microfluidic device), MD 1, and MD 2 (microfluidic device 1 and 2).

The next step was to evaluate how much time was needed for the whole coating solution to cover the entire cell's chamber of the hepatocyte-chip once establishing a constant flow rate. It was concluded that 2 minutes at a flow rate of 50 µL/min was sufficient to fill the hepatocyte's chamber. In **Figure 22**, it is possible to observe collagen fibers in several parts of the chamber, proving the validity of the performed coating optimizations.

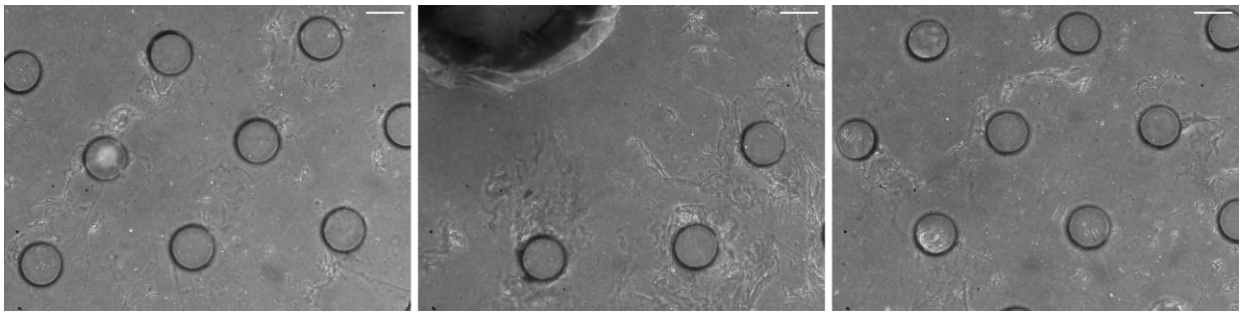

Figure 22- Collagen fibers throughout the final hepatocyte's chamber. In the images, it is shown three different parts of the final chamber where it can be distinguished several collagen fibers after performing the two coatings. Scale bar = 200 µm.

III.3. Right and left channels on the hepatocyte's chamber allowed better cell distribution into the sides

The next parameter to be optimized was the chip design, in particular, the hepatocyte's chamber. The aim was to create a microfluidic device that was constituted by two different chambers: one for HLCs culturing, and the other to serve as a culture medium reservoir to supply the cells through recirculation. Accordingly, to recirculate the medium through the HLC's chamber, the device should be actuated by pneumatic valves. In addition, the existence of valves may provide the automatization of the cell culturing process, which would change the way of doing cell research by improving culture reproducibility, facilitating technology exchange to other laboratories, and lowering time spent on repetitive manual work by the researchers [87].

To successfully maintain HLCs in culture it is required to achieve 100% confluency on the culture surface [88]. From the devices used in the culture surface and coating optimization that were previously designed for cell culture purposes, it was verified that device A, in comparison with each chamber of device B, demonstrated to have an architecture that was able to homogeneously disperse the cells throughout the chamber, providing better cell confluency and arrangement. This happened mostly because device A has a square shape, meaning that, when inserting the HLCs through the center, the cells spread equally in all directions, ensuring a homogeneous and confluent surface. This is adequate since the cells enter the chamber in a radial direction. On the other hand, each chamber of device B has a high length-to-width ratio. Therefore, when inoculating the cells through the center inlet, there was a higher cell concentration in the right and left sides than in the top and bottom of the chamber. Inoculation through the top and bottom inlets was also attempted. However, in this case, fewer cells were dispersed to the center part of the chamber while in the triangular parts, near the top and bottom inlets, high cell accumulation was verified. Moreover, another advantage verified in device A was the presence of dispensers, which ensured that the culture medium is equally flowed throughout the culture area. Therefore, considering all these aspects, the cell's chamber of the hepatocyte-chip was firstly designed to have a square shape with similar culture surface dimensions to device A (10 x 9 mm) and also to have two dispensers, one on the top and the other on the bottom to guarantee the unidirectional flow. The height of the device was the same as devices A and B since it was shown to be appropriate for

HLCs culturing. In addition, several micropillars to ensure that the chamber does not collapse were distributed throughout the surface, except in the middle where the space necessary for an inlet to perform both the surface coating and HLCs' inoculation was created.

To evaluate how the culture medium and coating solution would behave when flowed throughout the designed cell's chamber, trypan blue solution was perfused to it through the top inlet and center inlet, respectively (**Figure 23**). This solution was chosen to mimic the behavior that the culture medium and coating solution would have when inserted in the chamber in order to observe the flow evolution by naked-eye. In this manner, while the trypan blue solution flowed at a constant flow rate, it could be seen that it was being propagated uniformly all over the chamber, both when inserted in the center and top inlet. Therefore, it can be concluded that the dispersers promoted an equal distribution of the fluid to all parts of the chamber when flowing the solution through the top inlet. Moreover, it was also possible to state that the micropillars do not insert perturbations to the flow direction. Therefore, it was expected that the culture medium would be able to distribute nutrients to all seeded cells and the coating solution uniformly distributed to the whole chamber.

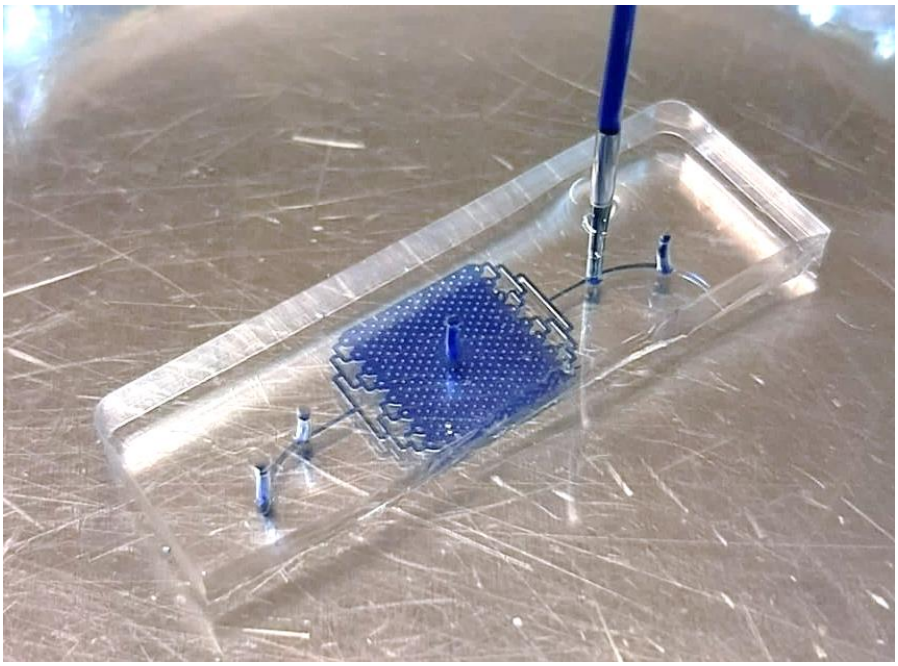

Figure 23- Hepatocyte's chamber filled with trypan blue solution. Trypan blue solution was inserted through the top inlet (above the top dispenser), as shown in the image, but also through the center inlet.

Cell insertion was tested to evaluate the efficacy of the designed hepatocyte chamber regarding cell distribution and seeding. It was verified that the cells were not homogeneously dispersed throughout the designed chamber represented in **Figure 24a**, as was expected. After inoculation, HLCs were well dispersed throughout the dispensers and in the central part of the chamber, but, as it is possible to visualize in **Figure 24b**, near the right and left sides there are only a few cells. This happened because, when inserting the cells through the center inlet, they will tend to circulate towards the top and bottom inlets, as they are the only connection to the outside and, therefore, the paths that offer less resistance to the flow. Due to this, the confluency was not reached and cells started to detach gradually from the

surface because there was not enough cell-to-cell contact. To solve this problem, two side channels, as demonstrated in **Figure 24c**, were added. At each end of both channels, an access hole was placed to diminish the flow resistance to these parts of the cell's chamber. **Figure 24d** demonstrates that the addition of the side channels considerably improved the dispersion of the cells towards these specific zones, proving the importance of the addition of this feature.

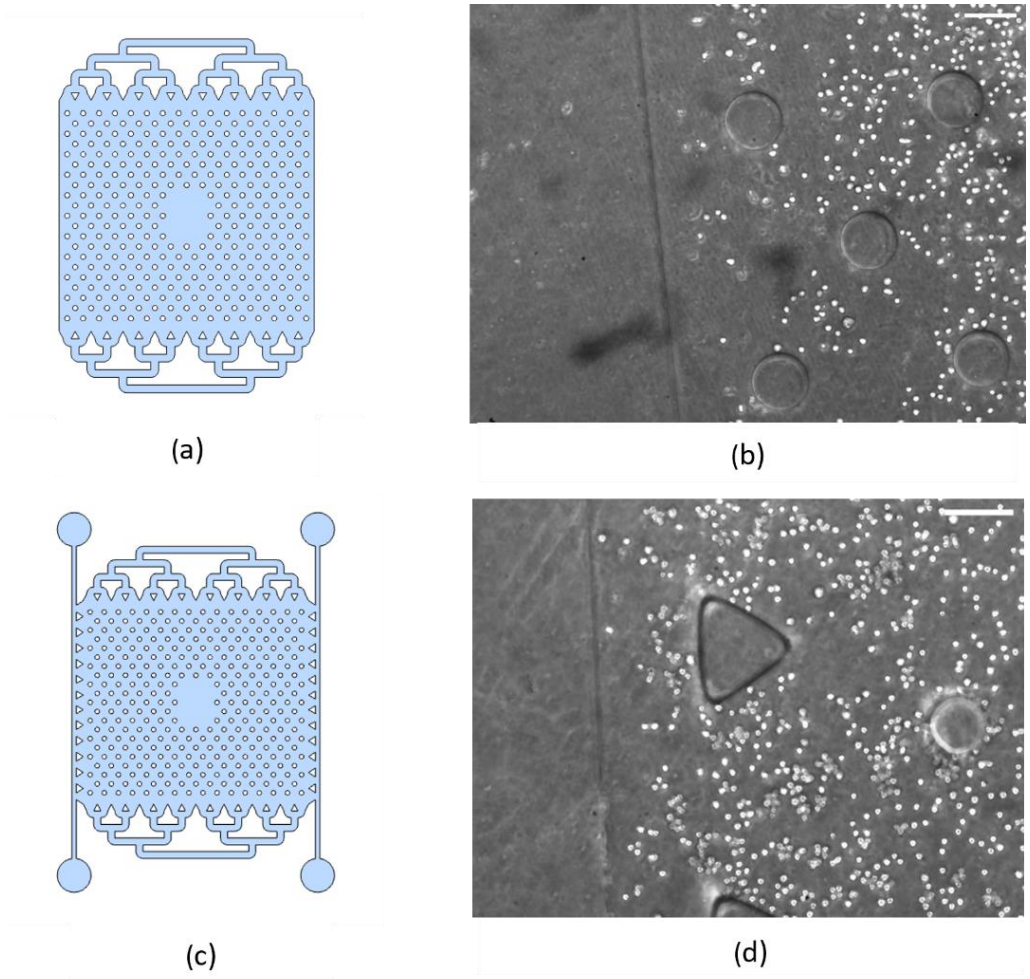

Figure 24- Comparison between cell dispersion in the chambers without (a) and with (c) the addition of the side channels. (b) and (d) represent the cell's disposition in one of the sides of the designed chambers (a) and (c), respectively. Scale bar = 200 µm.

Regarding the culture medium chamber, the top and bottom dispensers were built to facilitate the medium entry and exit, and long pillars were made to conduct the flow only in a vertical direction and to guarantee that the chamber do not collapse. The design of the culture medium chamber was also done by having into consideration the effective medium volume that the chamber is able to hold. The volume of the culture medium should be high enough to not create a toxic environment due to the accumulation of toxic metabolites (e.g.: ammonia). On the other hand, we wanted the volume of medium to be as reduced as possible, so that the metabolites, cytokines, and growth factors produced by the cells were not diluted, low cells-to-medium ratio. By having these metabolites less diluted in the culture medium, the quantification of, for instance, urea to assess HLCs phenotype is more easily performed. This is very

important to achieve since the hepatocyte-chip has the capacity to seed lower cell amounts when compared to other culture systems such as plates. In fact, this is an advantage of this type of culturing because it better mimics the environment that hepatocytes present in the liver. Therefore, a culture medium chamber with a volume of, approximately, 50 µL was designed since it was thought that it could ensure the equilibrium between concentration and dilution of metabolic products in the designed 90 mm^2 cell's culture area. However, since experiments using recirculation were not performed, only perfusion was evaluated, the culture medium chamber was not accessed. Consequently, in the future, it will be necessary to test the culturing of HLCs with medium recirculation using the culture medium chamber to investigate if its capacity fulfills the requirements.

The type of valves to be used was also an important aspect to be thought about. For this work, two different types of valves were considered, namely, the push-down and push-up valves, since only PDMS is required to fabricate them and all the equipment for their actuation was available in our laboratory. In the push-down valve's conformation (**Figure 25a**), the control layer is placed above the fluidic layer which makes the PDMS membrane deflect downwards once the valves are actuated, closing the fluidic channel [89]. On contrary, the push-up valves (**Figure 25b**) are constructed with the control layer under the fluidic layer and the membrane deflects upwards when pressure is applied [89]. In both types of valves, it is required the fluidic channels to be fabricated with a rounded profile to enable their complete closure during the valve's actuation, which was essential, mainly, for the correct pump functionalization [90]. One important advantage of the push-up valves is that the membrane presents uniform thickness and is not dependent on the fluidic layer features height (the membrane is independent) [90]. This makes push-up valves easier to be designed and fabricated, and requires lower actuation pressures to operate, which higher their probability to completely close the fluidic channel and provide an optimum actuation [90]. However, push-down valves have the great benefit of allowing the sealing of the fluidic layer against any desired substrate, while in the push-up valves the fluidic layer has obligatorily to be sealed against the control layer PDMS [89]. In this case, as it was verified that the hepatocytes require a PS culture surface, push-down valves were chosen for the hepatocyte-chip control.

To ensure the functioning of the push-down valves, it was important to take into account the relative dimensions of the valve and fluidic channels. Therefore, to enable their correct operation, each valve needed to have a bigger height (50 µm) than the fluidic channel (35 µm). Additionally, it was required the thickness of the PDMS membrane, placed between them, to be the minimum possible. Indeed, the membrane constitutes the critical component of the operation of this type of pneumatic valve because, if it is too thin, only the central part of the fluidic channel is deflected and the channel does not close on the edges. However, if the membrane is too thick, the valve's actuation pressure needs to be very high to enable the fluidic channel closure, which can lead to device failure (e.g.: unsealing of the two layers). Furthermore, the ratio between width versus height was required to be lower than 10:1, regarding the valves and fluidic channels [90]. Consequently, it was chosen to build both with a width of 300 µm because this value was suitable for the two channel's height, considering the 10:1 ratio, making the valve's actuation area be 0.09 mm^2 (300 µm by 300 µm).

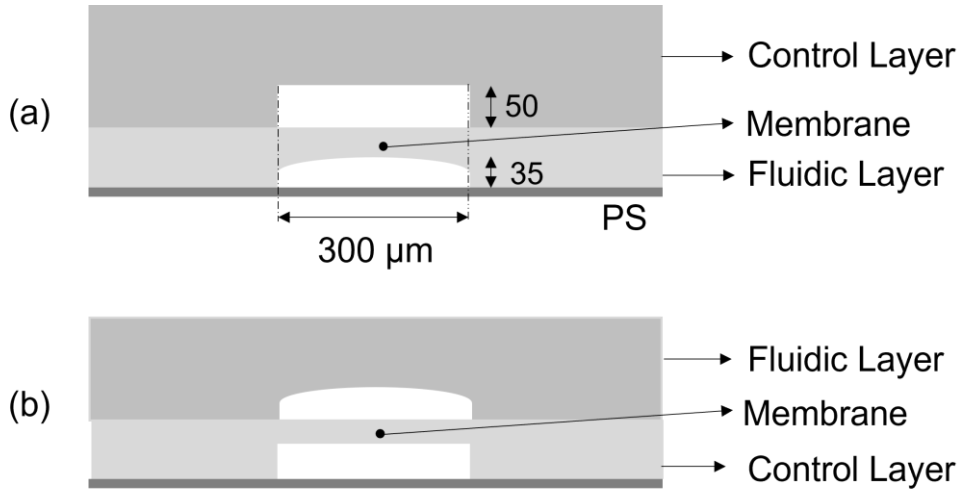

Figure 25- Push-down valve with the dimensions used in the final Hepatocyte-chip (a) and Push-up valve (b). In each type is represented the three main valve components: control layer, fluidic layer, and the membrane in between. In the final hepatocyte-chip, the control layer valve has a width of 300 µm and a height of 35 µm, and the fluidic channel has the same width as the valve and a height of 50 µm.

A total of seven valves in the control layer part of the hepatocyte-chip were fabricated (**Figure 14a**). Three of them would give origin to a pump (**Figure 14a**, 5) by being pneumatically actuated through a sequential pattern (teensy code) that closes and opens the valves. The continuous actuation of these three valves will ensure the recirculation of the culture medium, placed inside the reservoir, through the cell's chamber. The other four valves (**Figure 14a**, 1, 2, 3, and 4) were thought to be used to restrict the medium flow whenever is wanted. As such, when the culture medium is being flowed through inlet **f** (**Figure 13a**), valve 1 would be actuated (fluidic channel closed) to guarantee that the flow only enters the medium chamber and does not follow the channel path toward the cell's chamber. Similarly, when the culture medium is being collected for sampling, valve 3 would be actuated to ensure the medium exit through inlet **g** (**Figure 13a**). Valves 2 and 4 (**Figure 14a**) would be actuated only when the recirculation is being done to inhibit medium leaks through the access holes **f** and **g** (**Figure 13b**).

III.4. HLCs could be homogeneously distributed into the hepatocyte's chamber

On the first differentiations performed inside the hepatocyte's chamber, the HLCs were inoculated through the center inlet (**Figure 13b**, inlet **a**), on their D17 of differentiation, following observation of the cells entering and spreading throughout the chamber under the microscope. We wanted to understand which combination of flow rates and flowing times were required to obtain a homogeneous cell distribution and confluency of 100% on the culture surface. Furthermore, it was necessary to make the cell's inoculation more automatized to decrease the time spent in this procedure.

Inserting HLCs from a solution with 1 million cells/mL provided a good distribution and concentration of cells throughout the culture surface. Starting cell inoculation with a flow rate of 5 µL/min for 2 minutes allowed a slow radial cell's entrance, ensuring a controlled diffusion (**Figure 26a**). In the second step,

the flow rate was increased to 10 µL/min for 2 minutes while the tube was being rotated in intervals of 30 seconds to the sides of the chamber (**Figure 26b**). By elevating the flow rate, the cells already inside the device were pushed to furthest chamber zones, particularly to the side parts. The third step included more 10 µL/min flow rate for 2 minutes with the tube being rotated towards the chamber corners in intervals of 30 seconds (**Figure 26c**). This was required to increase the concentration of cells in the corners. Although ensuring a homogeneous HLCs dispersion, confluency was not being achieved through this protocol, especially on the right and left sides. Since, in the context of maintaining hepatocytes in culture, it is very important to ensure high cell-to-cell contact to reach optimum confluency, it was necessary to add another step to the inoculation protocol [88]. Therefore, this step consisted in inserting the cells through the outer inlets (**Figure 13b**, inlets **b**, **c**, **d**, and **e**) for 1 minute each (**Figure 26d**).

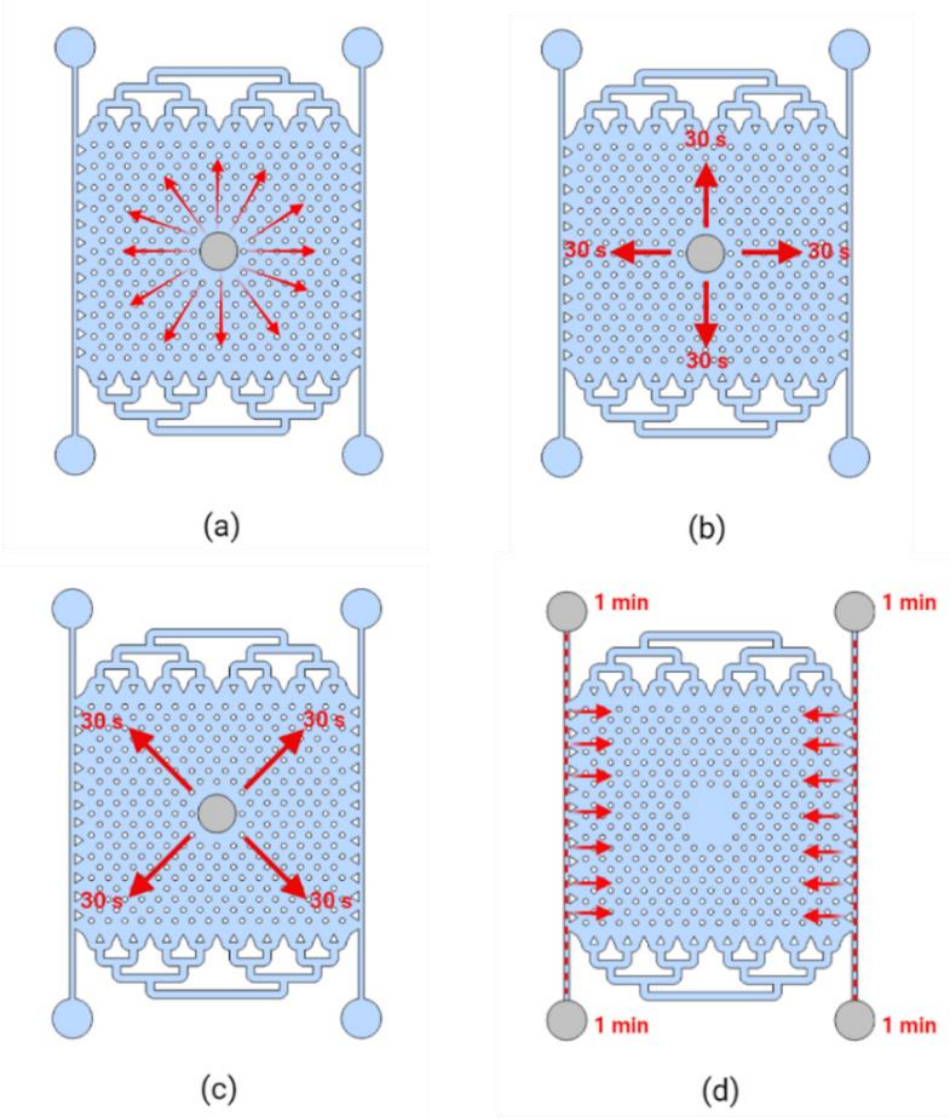

Figure 26- Optimized inoculation steps. Cell's insertion in the chamber is constituted by four steps: (a) radially dispersion of cells through inlet **a** with a flow rate of 5 µm/min during 2 min; (b) side's dispersion through inlet **a** with a flow rate of 10 µm/min during 2 min; (c) dispersion through inlet **a** towards the chamber corners with a flow rate of 10 µm/min during 2 min; (d) cell's insertion through inlets **b**, **c**, **d**, and **e** with a flow rate of 10 µm/min during 1 min in each.

In **Figure 27**, it is possible to visualize the differences in cell confluency in the chamber after including this last inoculation step. As shown, the cell's confluency substantially increases with the addition of this fourth step, which improves their morphology after adherence.

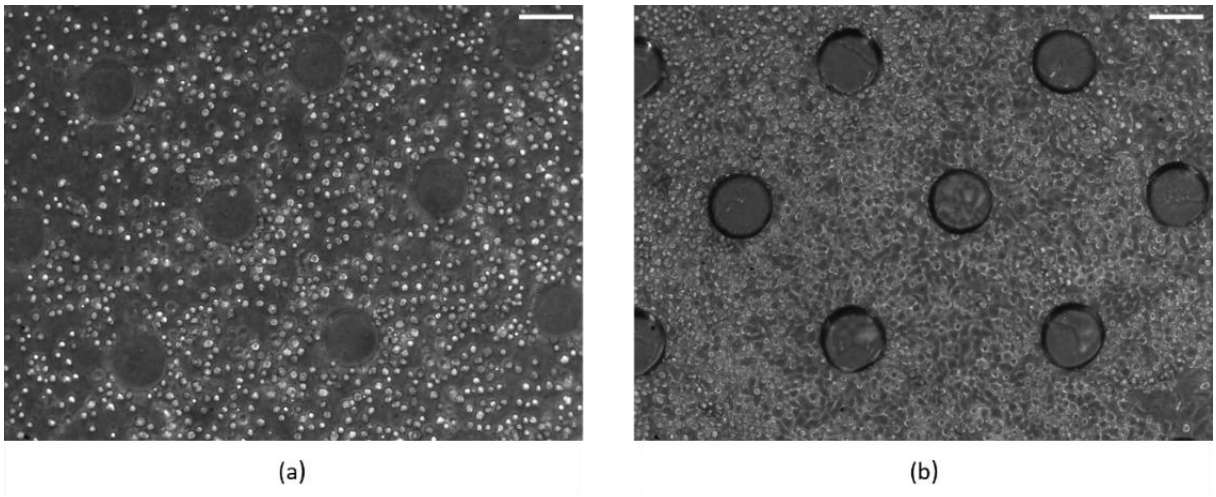

Figure 27- Differences in cell confluency in a device where the last inoculation step was not included (a) and in one where that step was performed (b). The images show the cells on their day 0 (day of cell's insertion) right after spending 1 hour in the incubator to promote adhesion. Scale bar = 200 µm.

III.5. HLCs could be maintained in perfusion for more than one week in the designed hepatocyte's chamber

After optimizations regarding the culture surface, coating, hepatocyte's chamber, and HLCs inoculation, characterization of HLCs in the hepatocyte's culture chamber was performed. Herein, only the hepatocyte's chamber of the chip was used and worked under perfusion to lower the complexity of the operation (perfusion hepatocyte-chip structure). Through those perfusion experiments, it was verified that it was possible to maintain in culture the HLCs into the device for 17 days by starting the inoculation on their D17 (day 0 in the MD) of differentiation and ending on D34 (day 17 in the MD). **Figure 28** is showing the cell's images during some of the differentiation days. It is possible to visualize that, after inoculation (day 0), the HLCs looked well dispersed through the entire chamber. It is also possible to verify that after 1h in the incubator the cells were adherent. Moreover, throughout the culturing days, HLCs present a tissue-like aspect, exhibiting their typical polygonal shape, throughout the whole chamber including the dispensers and side channels (as shown in **Figure 28** on days 1, 4, 7, and 10). This confirms the efficacy of the side channels and demonstrates that the coating is being well performed as it is reaching these furthest chamber zones. HLC morphology was maintained throughout the whole culture. Additionally, it was possible to verify that the cultured HLCs were oriented accordingly with the medium flow which is something that can also be noticed in liver architecture since the hepatocytes follow the bloodstream orientation.

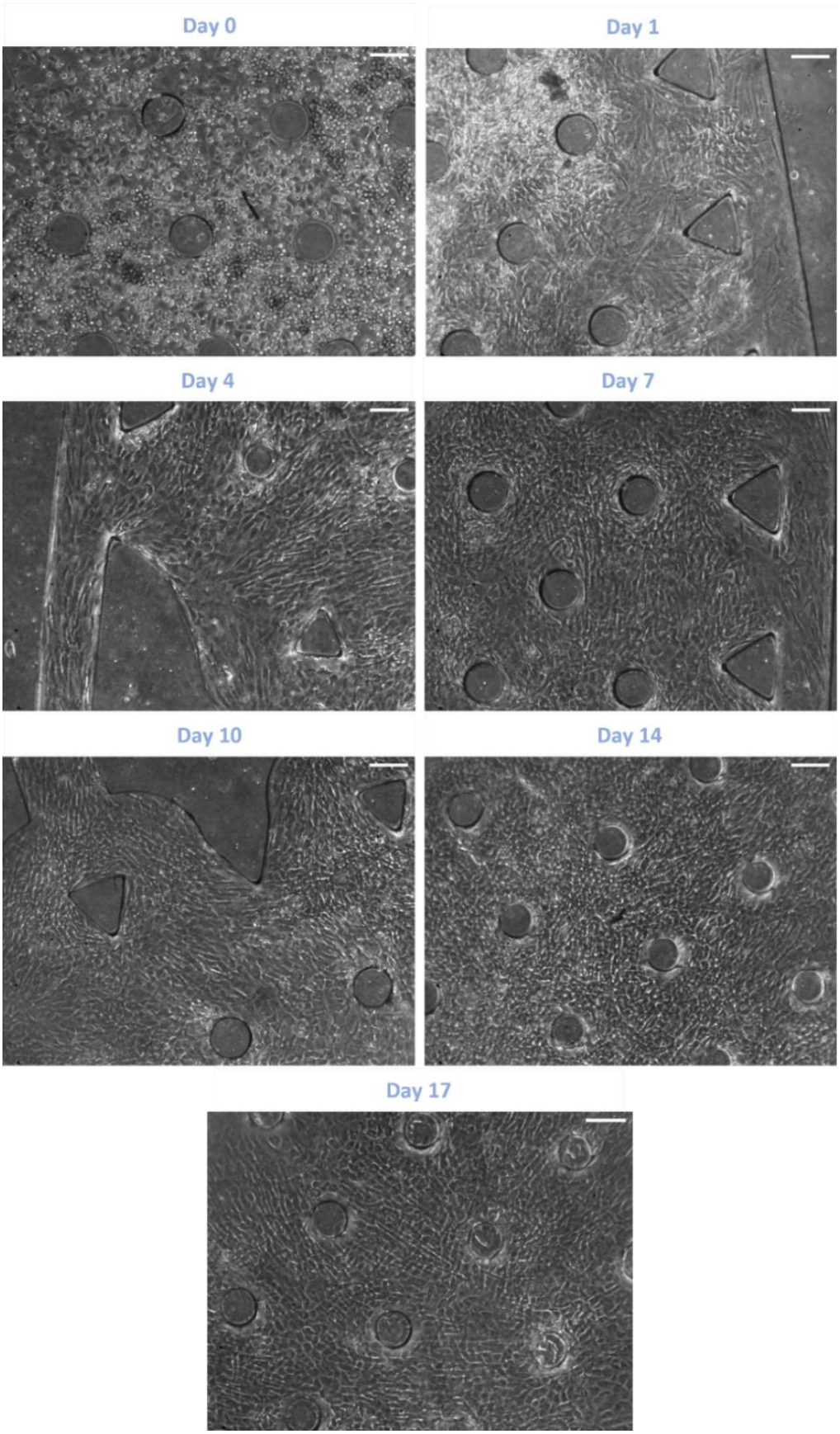

Figure 28- Maintenance of HLCs inside the designed cell chamber for 17 days. In each image, it is represented the cell's aspect in different zones of the chamber in some days (0, 1, 4, 7, 10, 14, and 17) after inoculation. Scale bar = 200 µm.

Hepatocytes are involved in the urea metabolism, being responsible for ammonia detoxification. Urea is, thus, one of the most important metabolites secreted by the hepatocytes. Therefore, to evaluate the HLCs phenotype throughout the culture time inside the microfluidic device, urea production was accessed from the cell's supernatant. Accordingly, the urea was measured in HLCs maintained for 4 and 7 days in the device. Urea production from HLCs in microfluidic devices was compared with the one produced by HLCs in 2D plates, undifferentiated hnMSCs, HepG2, a regularly used hepatic cell line, and hpHep, the gold standard cell source for hepatic *in vitro* models. In **Figure 29**, we can observe that after 7 days in culture, urea production by HLCs in the chip is similar to that of HepG2 and higher than HLCs in plates (p <0.001). It is also noticeable that from day 4 to day 7, urea production increases in the microfluidic device, meaning that cells improve their phenotype and metabolic functions during the culture time inside the chip. In fact, on day 7, the HLCs are no longer placed in the Diff culture medium (as in day 4), but in a Physiol medium, that better approximates the human liver physiological levels of glucose and insulin, improving cell's functions. Indeed, besides ammonia detoxification, it was previously demonstrated in the laboratory that a Physiol culture medium improves other hepatocyte's functions, such as biotransformation activity.

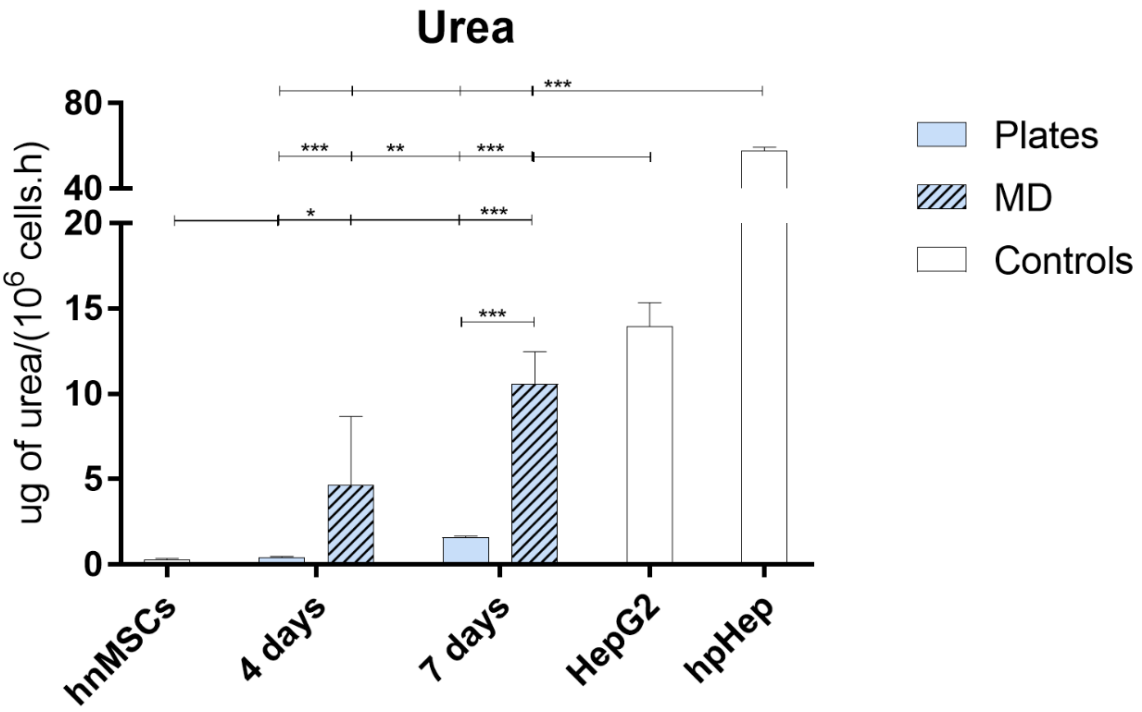

Figure 29- Urea production 4 and 7 days after the inoculation of HLCs into the microfluidic device and plates. Undifferentiated hnMSCs are the negative control. HepG2 and hpHep are positive controls. *, **, *** Significantly differs among the controls with $p < 0.05$, $p < 0.01$ and $p < 0.001$, respectively. Abbreviations: hnMSCs (human neonatal mesenchymal stem cells), hpHep (human primary hepatocytes), MD (microfluidic device).

Cryopreserved HLC culture was also tested in the hepatocyte-chip and plates, and the amount of urea secreted was also accessed. Those cells are HLCs that were cryopreserved on their D17 of differentiation. After being unfrozen, they were seeded on 24-well plates until D20, because it was

previously demonstrated that improve their phenotype. On D20, their inoculation on the hepatocyte's chamber and other culture plates was performed. Morphologically, cryopreserved HLCs also present a polygonal shape, which is characteristic of hepatocytes, but they can show decreased confluency in culture since a high number of cells do not survive after the cryopreservation. Nevertheless, cryopreserved cells have a great advantage in comparison to freshly differentiated HLCs, they are ready-to-use cells since they already acquire some maturation level before being preserved. Therefore, cryopreserved HLCs are rapidly available because it is not required to wait 3 or 4 weeks for them to achieve a complete differentiation state, as is needed in the case of freshly differentiated HLCs. However, the cryopreserved cell's phenotype is still poor. Indeed, the techniques used to thaw are aggressive for cells and may cause loss of functions [91]. Studies demonstrate that biliary metabolism is not affected by HLCs thawing, although glucose and glycogen synthesis, and albumin and urea production are shown to be reduced [91].

In **Figure 30** it is possible to observe the results regarding the urea production of cryopreserved HLCs achieved in microfluidic and plate cultures. In comparison with freshly differentiated HLCs cultured in devices, the cryopreserved HLCs in devices were able to produce less urea. Nevertheless, the urea secreted in cryopreserved HLCs seeded in devices is higher than the one present in the plate's supernatant, showing, once again, the potential of microscale cultures in comparison to the typical monolayer cultures in improving hepatic functions.

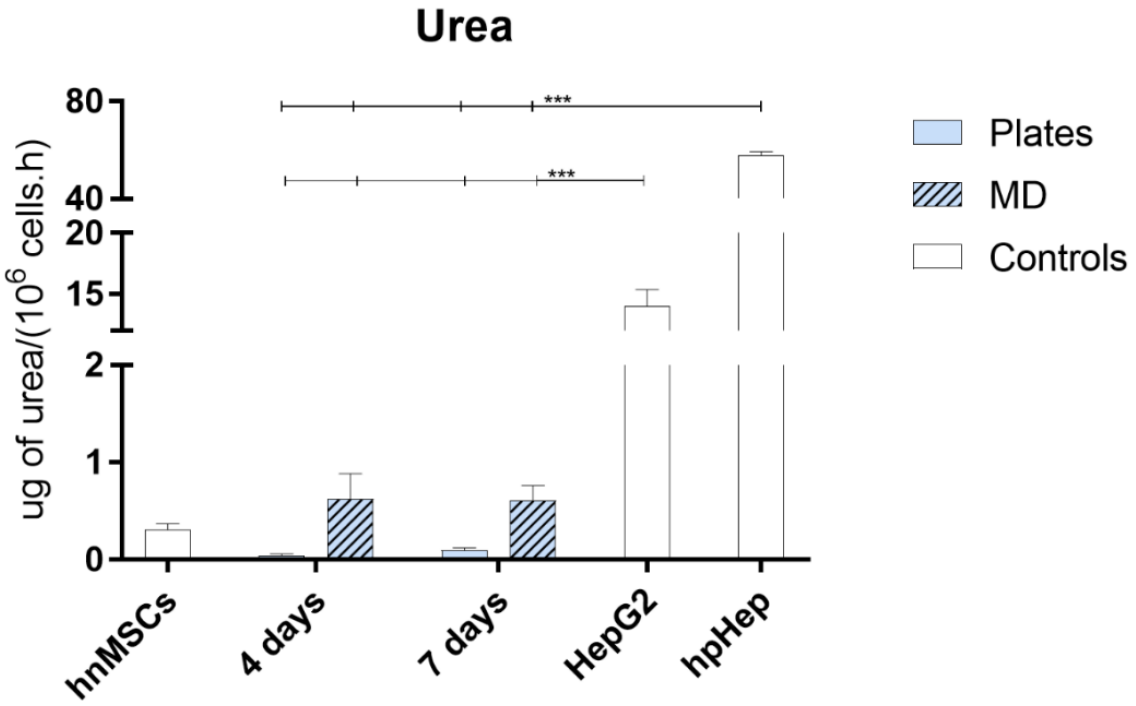

Figure 30- Urea production 4 and 7 days after inoculation of cryopreserved HLCs into the microfluidic device and plates. Undifferentiated hnMSCs are the negative control. HepG2 and hpHep are positive controls. *, **, *** Significantly differs among the controls with $p < 0.05$, $p < 0.01$ and $p < 0.001$, respectively. Abbreviations: hnMSCs (human neonatal mesenchymal stem cells), hpHep (human primary hepatocytes), MD (microfluidic device).

Morphology of freshly obtained HLCs and cryopreserved HLCs maintained in the hepatocyte-chip and on plate cultures was compared in **Figure 31**. Overall, it can be observed that the HLCs (fresh and thawed) acquire better morphology in the microfluidic device than in plates. As it can be verified by **Figures 31b** and **31d**, cells acquire higher confluency and, consequently, higher cell-to-cell contact which better mimics the liver environment. This may promote the formation of ECM, thus enabling tissue-like formation. In comparison, in the plates, HLCs even though having also the typical polygonal morphology, cells look more stretched and randomly orientated (**Figures 31a** and **31c**).

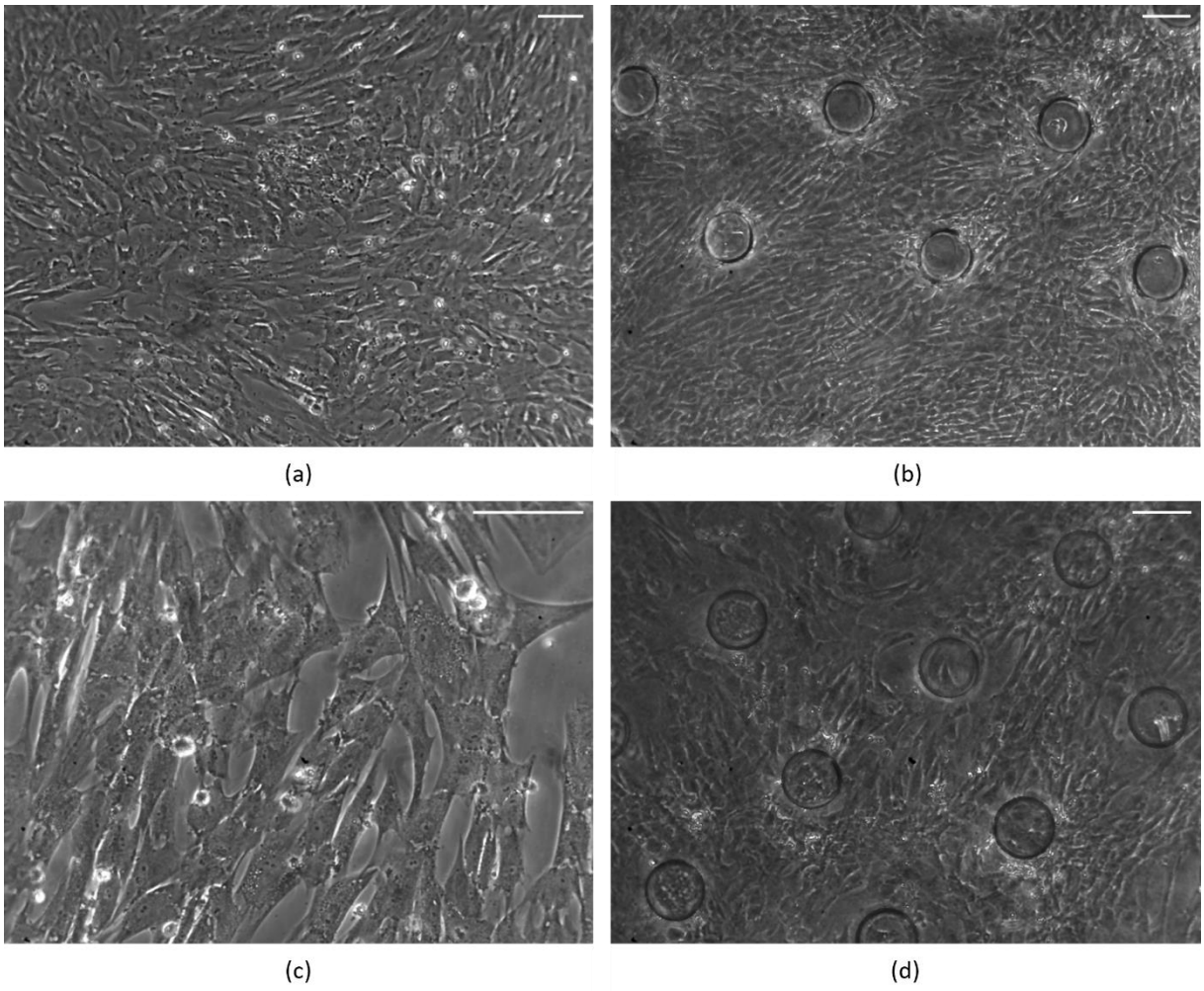

Figure 31- Comparison between freshly differentiated and thawed HLCs on plate and microfluidic device cultures. (a) and (b) are freshly differentiated HLCs cultures on plate and device, respectively. (c) and (d) are thawed HLCs cultures on plate and device, respectively. Scale bar = 100 µm (a and c), 200 µm (b and d).

III.6. Pneumatic valves allow complete fluidic channel closure

Culture medium recirculation was aimed for the conception of the final device to evaluate IR (**Figure 7**), for both the Kupffer culture chamber and hepatocyte culture chamber. In this context, supplying cells with the medium through recirculation increases the concentration of cytokines and metabolic products (e.g.: urea, albumin) in circulation, providing the delivery of a higher amount to signaling molecules by

diffusion to and from each cell, which may impact their cellular response. In this case, the delivery of cytokines from Kupffer cells to the HLCs is crucial to modulate IR in hepatocytes since it is thought to influence its pathological phenotype. In perfusion, these secreted molecules are washed out and do not accumulate in the supernatant, which inhibits their effect in the stimulation of the cell's pathological phenotype. Moreover, it is known that there are drugs that need to achieve a threshold concentration to be transformed into active metabolites and, therefore, to produce the desired effect on the target organ [92]. Through perfusion, that drugs can remain undetected, leading to deviated conclusions. Consequently, microfluidic recirculation also exerts a great advantage regarding drug testing. Accordingly, with the view to use the control layer valves in the culturing of HLCs in the designed chip to provide medium recirculation, the control and fluidic layers of the hepatocyte-chip were combined (recirculation hepatocyte-chip structure) and tests were done to investigate if the dimensions of the valves, fluidic channel, and PDMS membrane placed in between were suited for the complete fluidic channel closure, and therefore, for the correct pneumatic control.

First, all the single valves (**Figure 14a**, valves 1, 2, 3, or 4) actuation was individually tested. A dye solution was flowed through the fluidic channel that was underneath the valve to be tested, to simulate the culture medium. A dye solution was chosen to allow naked-eye inspection of valve actuation towards the fluidic channel. Air pressure was continuously applied to the valve channel by adjusting the regulator until the complete fluidic channel closure was visualized and checked under the microscope. When that happened, in the fluidic channel zone corresponding to the valve active area, it was no longer possible to see the dye solution because it was compressed and spread along the fluidic channel. **Figure 32** shows the valve and fluidic channel aspect at different stages of the actuation, while the valve was being continuously pressurized. **Figure 32c** demonstrates that the valve can completely close the underneath channel, validating the pneumatic valve's operation. However, that was only possible if high pressures were applied, between 350 Pa and 400 Pa, which, besides fulfilling the purpose, can lead to the unsealing of the layers if long periods (not tested) of actuation are done.

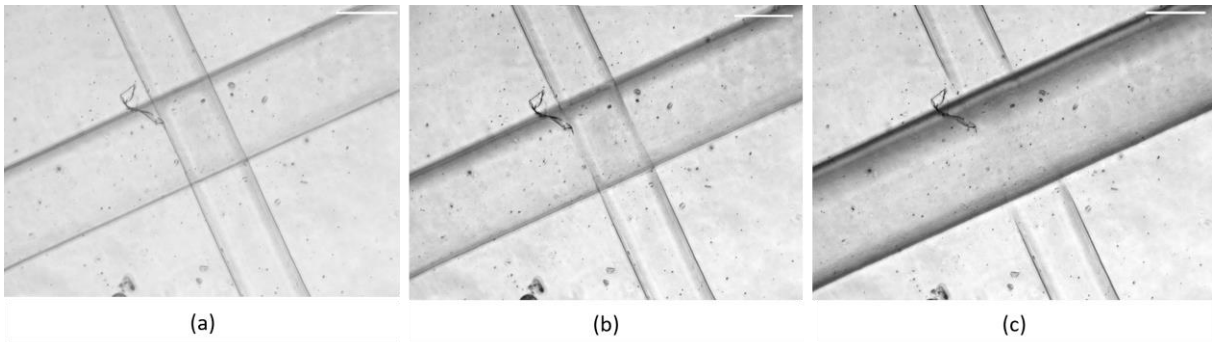

Figure 32- Valve operation with the increase of air pressure. The valve channel is above and the fluidic layer channel is underneath. The air pressure inside the valve channel is increasing from (a) to (c). In (a) the valve is not being actuated. In (c) the valve is being actuated with 400 Pa (maximum regulator pressure) and the fluidic channel is completely closed. And, in (b) the valve is being actuated by an intermediate pressure. Scale bar = 300 µm.

Having the confirmation that the single valves can be operated, the next step was to test the pump (**Figure 14a**, 5) in order to verify if fluid recirculation throughout the hepatocyte's chamber was possible. Firstly, a dye solution was flowed to the culture medium chamber using a constant flow rate of 50 µL/min until the whole chamber volume was filled. Then, after air bubble removal from the valves channels, the teensy circuit was connected to the computer which enabled the functioning of the valves as a pump by being pressurized (actuated, 1) and depressurized (non-actuated, 0) following a sequential pattern constituted of a six-step loop (**Figure 33**) [93].

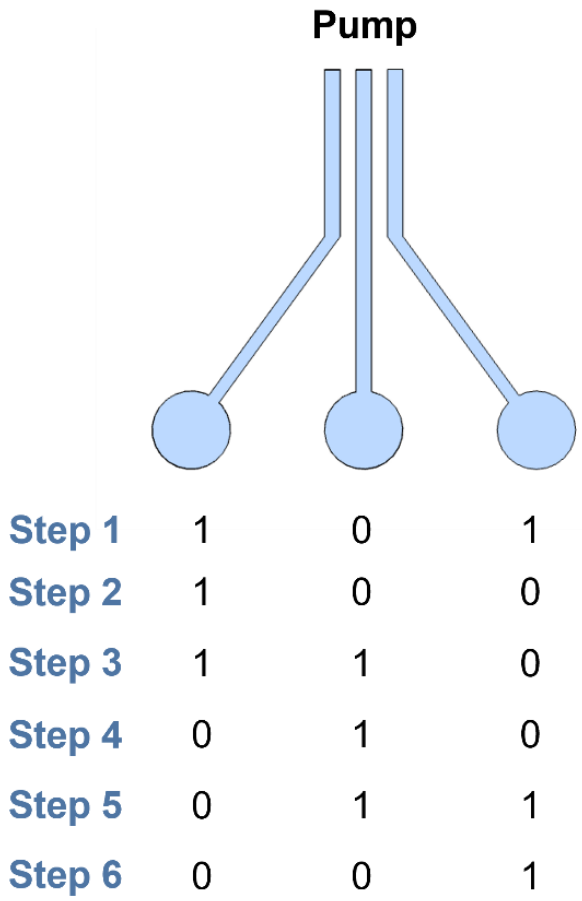

Figure 33- Sequence of steps used to operate the pneumatic pump. This sequence was done in loop. A time interval divided each step. Abbreviations: 1 (valve actuated; fluidic channel closed), 0 (valve non-actuated; fluidic channel open).

When increasing the air pressure regulator close to 400 Pa, each valve was able to close (valve actuated) and open (valve non-actuated) the fluidic channel while the teensy code was being employed, allowing the pump operation. However, as expected, the unsealing of the fluidic and control layers occurred minutes after the starting of the pump operation. Indeed, the consecutive application of high pressures to each valve channel and the sudden depressurization led to rapid device failure. Consequently, in the future, optimizing the fluid's recirculation throughout the cell's chamber will be required by, for instance, adequate pump dimensions to be suited for lower actuation pressures.

IV. Conclusions and Future Perspectives

With the goal to create an *in vitro* hepatic model to be used in pharmaceutical research to model liver pathologies, namely IR, in this work, a fit-for-purpose microfluidic device was designed and fabricated and HLCs were adapted to it.

The hepatocyte-chip was designed and fabricated having in mind its future integration on the microfluidic device projected to evaluate IR (**Figure 7**). Accordingly, to fulfill the requests of the hepatocyte unit, the hepatocyte-chip was constituted by a hepatocyte culture chamber, a culture medium chamber, and a control layer to provide medium recirculation throughout the cell culture. Perfusion experiments using the HLCs chamber were tested with the aim to adapt the cell culture into the chip. The culture surface, the collagen coating, the design of the chamber, and the cell's insertion were optimized. It was concluded that a PS surface provided better HLCs attachment, therefore it was decided to seal the chip against PS. A collagen type I diluted in PBS demonstrated better results regarding HLCs adhesion and maintenance, in comparison with collagen type I diluted in acetic acid which did not allow HLCs adherence. The firstly designed hepatocyte's chamber did not provide optimum cell dispersion and confluency, especially in the sides of the chamber, since it was creating resistance to the cell's flow. Consequently, a new chamber was designed and fabricated including side channels. It was concluded that this addition allowed an improved and homogeneous cells dispersion. Afterward, the cells' inoculation was optimized by achieving an automatized protocol that not only ensured 100% cell confluency but also lowered the time spent in this procedure. HLCs were, then, successfully maintained inside the chip during at least one week in perfusion, having demonstrated a polygonal morphology and an improved tissue-like aspect compared with plate's cultures throughout the culturing. HLC urea production was assessed and compared with the urea produced by HLCs cultured in the regular used 2D plates. It was shown that HLCs cultured in the device produce more urea than HLCs in plates and that this production increased after 7 days in culture because the chip provided HLCs maturation. Because cryopreserved HLCs provide an off-the-shelf and ready-to-use source of cells, their potential was also assessed in the designed hepatocyte chamber. From that, it was verified that these cells produce less urea than the freshly differentiated HLCs. However, in comparison with cryopreserved HLCs cultured in plates, the ones seeded in the chip also demonstrated superior urea production, which corroborates, once again, the potential of microscale cultures.

In this thesis, embedding pneumatic valves into the HLCs culture with the view to automatize the culture process by including culture medium recirculation was also attempted, which constitutes a key feature to allow the quantification of metabolites to evaluate cell's phenotype. From the performed valve tests, it can be concluded that the valves were capable of closing the fluidic channel through high actuation pressures, which led to the unsealing of the layers when the pump was operating. Therefore, further optimization regarding valves control needs to be done in order to achieve culture medium recirculation.

Despite the successful results in terms of adapting and maintaining the HLCs in the device, it was also detected that, in some zones of the chamber, cells often start to detach during the culturing. The detachment happens predominantly in the cells placed near the center inlet and in the ones close to the

micropillars, where there is cell-to-PDMS contact which is more fragile than the cell-to-cell contact. This can be one of the problems of the microscale culture. In fact, in flasks cultures, they also detach near the border zones, where the cells lack cell-to-cell contact. However, this does not influence the cell's morphology and maintenance since the flask's culture surface area is large. In microfluidic cultures, the culture surface area is much lower, meaning that the cell's detachment has a higher impact on their maintenance. Another problem frequently verified during microscale culturing is the existence of air bubbles inside the device. Even though the total closure of the access holes with metallic plugs diminishes bubble formation, air bubbles end up being created, possibly, due to the humid environment of the incubator, an event that does not affect macroscale cultures. Air bubbles can be problematic in devices because they change the medium flow direction, meaning that there will be cells without contact with new nutrients, causing their death. However, it was also verified that the ones still receiving culture medium did not have alterations in their aspect. Another disadvantage of microscale cultures within chips is the fact that these procedures require a higher number of manipulations, therefore more care is needed to provide and maintain a sterilized environment. Furthermore, in comparison with macroscale cultures, to maintain microscale cultures it is needed to invest more time because every step, namely cell's inoculation and medium changes, takes longer, which is due to the use of other laboratory materials, such as syringe pump and tubes, that require more manipulation. All these issues associated with microscale cultures are challenges that need to be addressed in the future, namely through the automatization of processes, in order to improve their use in the laboratory context.

Furthermore, studies regarding oxygen and nutrient gradients through the hepatocyte's chamber would be interesting to be performed in the future. Indeed, the culture medium enters the chamber through the top inlet and exits through the outlet placed in the other chamber extremity. Consequently, it is thought that the seeded HLCs may acquire distinct phenotypes depending on their location in the chamber due to the establishment of different environments triggered by different oxygen and nutrient concentrations, which can recapitulate the hepatic acinus microenvironment, namely the PP and the PV zones. The HLCs placed near the medium entry can develop a phenotype similar to the liver PP hepatocytes with higher oxygen and nutrients concentrations, while the ones placed close to the medium exit can acquire a PV phenotype, with less oxygen and nutrients concentrations. In this context, this potential characteristic of the hepatocyte's chamber would be of great importance since it would increase the similarity to the physiological microenvironment in the *in vitro* IR model. Moreover, since the number of cells cultured in the chip is much lower compared with macroscale cultures, some traditional laboratory protocols cannot be employed, such as qPCR and western blot. Accordingly, adapting these protocols to the microfluidic device could be done in the future using, for instance, imaging-based assays, such as immunofluorescence.

The use of microfluidic devices to provide *in vitro* human models is currently in vogue, however, there is still a lack of experience in the use of these chips in biological applications because it is required expertise in both cell culturing and microfluidic design and fabrication. In fact, cell and tissue researchers are usually not familiarized with microtechnology, and microfluidic researchers are not familiarized with cell culturing. Therefore, it is often required the cooperation of different teams to be well succeeded in

the conception of physiologically relevant models. This work provides both, a biological and a microtechnological perspective regarding the conception of a hepatic model for *in vitro* research, which helps to close the gap between these two fields of study. Furthermore, because microfluidics' cell cultures are yet a novel method, there are not so many studies of hepatic models in chips, which makes these a trial-and-error approach, as we proceed in this work. Here, it was presented a set of optimizations that are thought to be useful for future researchers of this field of study.

V. References

1. Asrani, S. K., Devarbhavi, H., Eaton, J. & Kamath, P. S. Burden of liver diseases in the world. *J. Hepatol.* **70**, 151–171 (2019).
2. Obesity (Accessed: 22/05/2021). https://www.who.int/health-topics/obesity#tab=tab_2.
3. Diabetes (Accessed: 22/05/2021). https://www.who.int/health-topics/diabetes#tab=tab_1.
4. Wilcox, G. Insulin and Insulin Resistance. *Clin. Biochem. Rev.* **26**, 19 (2005).
5. Santoleri, D. & Titchenell, P. M. Resolving the Paradox of Hepatic Insulin Resistance. *Cmgh* **7**, 447–456 (2019).
6. S, L. *et al.* A Human Liver-on-a-Chip Platform for Modeling Nonalcoholic Fatty Liver Disease. *Adv. Biosyst.* **3**, 1900104 (2019).
7. Jager, J., Aparicio-Vergara, M. & Aouadi, M. Liver innate immune cells and insulin resistance: the multiple facets of Kupffer cells. *J. Intern. Med.* **280**, 209–220 (2016).
8. Serras, A. S. *et al.* A Critical Perspective on 3D Liver Models for Drug Metabolism and Toxicology Studies. *Front. Cell Dev. Biol.* **9**, 1–30 (2021).
9. Ziółkowska, K., Kwapiszewski, R. & Brzózka, Z. Microfluidic devices as tools for mimicking the in vivo environment. *New J. Chem.* **35**, 979–990 (2011).
10. Sung, J. H. *et al.* Microfabricated mammalian organ systems and their integration into models of whole animals and humans. *Lab Chip* **13**, 1201–1212 (2013).
11. Liver: Anatomy and Functions | Johns Hopkins Medicine (Accessed: 29/03/2021). https://www.hopkinsmedicine.org/health/conditions-and-diseases/liver-anatomy-and-functions.
12. Liver (Anatomy): Picture, Function, Conditions, Tests, Treatments (Accessed: 29/03/2021). https://www.webmd.com/digestive-disorders/picture-of-the-liver.
13. Fígado: características gerais, funções e doenças - Mundo Educação (Accessed: 29/03/2021). https://mundoeducacao.uol.com.br/biologia/figado.htm.
14. Kalra, A. & Tuma, F. *Physiology, Liver*. *StatPearls* (StatPearls Publishing, 2018).
15. The Liver - Lobes - Ligaments - Vasculature - TeachMeAnatomy (Accessed: 29/03/2021). https://teachmeanatomy.info/abdomen/viscera/liver/.
16. The Liver | Boundless Anatomy and Physiology (Accessed: 29/03/2021). https://courses.lumenlearning.com/boundless-ap/chapter/the-liver/.
17. Vekemans, K. & Braet, F. Structural and functional aspects of the liver and liver sinusoidal cells in relation to colon carcinoma metastasis. *World J Gastroenterol* **11**, 5095–5102 (2005).
18. 23.6 Accessory Organs in Digestion: The Liver, Pancreas, and Gallbladder - Anatomy and Physiology | OpenStax (Accessed: 09/10/2021). https://openstax.org/books/anatomy-and-physiology/pages/23-6-accessory-organs-in-digestion-the-liver-pancreas-and-gallbladder?query=hepatic lobule&target=%7B%22type%22%3A%22search%22%2C%22index%22%3A0%7D#fs-id1257384.
19. Wang, L. & Boyer, J. L. The Maintenance and Generation of Membrane Polarity in Hepatocytes. *Hepatology* vol. 39 892–899 (2004).
20. T, P.-S. & SP, M. Blood-Bile Barrier: Morphology, Regulation, and Pathophysiology. *Gene Expr.* **19**, 69–87 (2019).
21. Tabibian, J. H., Masyuk, A. I., Masyuk, T. V., O'Hara, S. P. & LaRusso, N. F. Physiology of Cholangiocytes. *Compr. Physiol.* **3**, 541–565 (2013).

22. Wilkinson, A. L., Qurashi, M. & Shetty, S. The Role of Sinusoidal Endothelial Cells in the Axis of Inflammation and Cancer Within the Liver. *Front. Physiol.* **0**, 990 (2020).

23. Nguyen-Lefebvre, A. T. & Horuzsko, A. Kupffer Cell Metabolism and Function. *J. Enzymol. Metab.* **1**, 1-101 (2015).

24. Kuntz, E. & Kuntz, H.-D. *Hepatology Textbook and Atlas*. *Hepatology Textbook and Atlas* (2008).

25. Yin, C., Evason, K. J., Asahina, K. & Stainier, D. Y. R. Review series Hepatic stellate cells in liver development, regeneration, and cancer. *J. Clin. Invest.* **123**, 1092- 1910 (2013).

26. Chiang, J. *Liver Physiology: MetaboLism and Detoxification*. *Pathobiology of Human Disease: A Dynamic Encyclopedia of Disease Mechanisms* (Elsevier Inc., 2014).

27. Rui, L. Energy metabolism in the liver. *Comprehensive Physiology* vol. 4, 177–197 (2014).

28. Trefts, E., Gannon, M. & Wasserman, D. H. The liver. *Curr. Biol.* **27**, R1147 (2017).

29. The Liver as Filter - Viral Hepatitis and Liver Disease (Accessed: 14/09/2021). https://www.hepatitis.va.gov/basics/liver-as-filter.asp.

30. Hfiussinger, D. *Klinische Wochen-schrift Organization of Hepatic Nitrogen Metabolism and Its Relation to Acid-Base Homeostasis*. *Klin Wochenschr* vol. **68** (1990).

31. Aronoff, S. L., Berkowitz, K., Shreiner, B. & Want, L. Glucose Metabolism and Regulation: Beyond Insulin and Glucagon. *Diabetes Spectr.* **17**, 183–190 (2004).

32. Mergenthaler, P., Lindauer, U., Dienel, G. A. & Meisel, A. Sugar for the brain: the role of glucose in physiological and pathological brain function. *Trends Neurosci* **36**, 587–597 (2013).

33. B, D., L, M. & W, W. Transcriptional regulation of metabolism. *Physiol. Rev.* **86**, 465–514 (2006).

34. Vargas, E. & Carrillo Sepulveda, M. A. *Biochemistry, Insulin, Metabolic Effects*. *StatPearls* (StatPearls Publishing, 2018).

35. E, B., AJ, M. & G, M. Insulin resistance: a metabolic pathway to chronic liver disease. *Hepatology* **42**, 987–1000 (2005).

36. Leclercq, I. A., Da Silva Morais, A., Schroyen, B., Van Hul, N. & Geerts, A. Insulin resistance in hepatocytes and sinusoidal liver cells: Mechanisms and consequences. *J. Hepatol.* **47**, 142–156 (2007).

37. Rakhra, V., Galappaththy, S. L., Bulchandani, S. & Cabandugama, P. K. Obesity and the Western Diet: How We Got Here. *Mo. Med.* **117**, 536 (2020).

38. Al-Goblan, A. S., Al-Alfi, M. A. & Khan, M. Z. Mechanism linking diabetes mellitus and obesity. *Diabetes, Metab. Syndr. Obes. Targets Ther.* **7**, 587–591 (2014).

39. Hotamisligil, G. S. Inflammation and metabolic disorders. *Nat. 2006 4447121* **444**, 860–867 (2006).

40. Guzmán, M. & Castro, J. Zonation of fatty acid metabolism in rat liver. *Biochem. J.* **264**, 107–113 (1989).

41. Quistorff, B. Gluconeogenesis in periportal and perivenous hepatocytes of rat liver, isolated by a new high-yield digitonin/collagenase perfusion technique. *Biochem. J.* **229**, 221–226 (1985).

42. Kitade, H., Chen, G., Ni, Y. & Ota, T. Nonalcoholic Fatty Liver Disease and Insulin Resistance: New Insights and Potential New Treatments. *Nutrients* **9**, 387 (2017).

43. DM, T. *et al.* The Intricate Relationship between Type 2 Diabetes Mellitus (T2DM), Insulin Resistance (IR), and Nonalcoholic Fatty Liver Disease (NAFLD). *J. Diabetes Res.* **2020**, 3920196 (2020).

44. Primary Hepatocytes versus Hepatic Cell Lines | Lonza (Accessed: 07/06/2021).

https://bioscience.lonza.com/lonza_bs/PT/en/hepatocytes-versus-hepatic-cell-lines.

45. Hepatocytes - an overview | ScienceDirect Topics (Accessed: 07/06/2021). https://www.sciencedirect.com/topics/agricultural-and-biological-sciences/hepatocytes.

46. Zeilinger, K., Freyer, N., Damm, G., Seehofer, D. & Knöspel, F. Cell sources for in vitro human liver cell culture models. *Exp. Biol. Med.* **241**, 1684 (2016).

47. Cipriano, M. *et al.* The role of epigenetic modifiers in extended cultures of functional hepatocyte-like cells derived from human neonatal mesenchymal stem cells. *Arch. Toxicol.* **91**, 2469–2489 (2017).

48. Afshari, A., Shamdani, S., Uzan, G., Naserian, S. & Azarpira, N. Different approaches for transformation of mesenchymal stem cells into hepatocyte-like cells. *Stem Cell Res. Ther.* **11**, 1–14 (2020).

49. Kalra, K. & Tomar, P. Stem Cell: Basics, Classification and Applications. *Am. J. Phytomedicine Clin. Ther.* **4**, 2321–2748 (2014).

50. Nanjwade, B. K., Sudulaguntla, A., Gurung, S. & Tamang, J. K. A Review: Stem Cells and Classification of Stem Cells Based on Their Origin. *Sudulaguntla al. World J. Pharm. Pharm. Sci.* **5**, 534 (2016).

51. Types of Stem Cell | Stem Cells | University of Nebraska Medical Center (Accessed: 08/06/2021). https://www.unmc.edu/stemcells/educational-resources/types.html.

52. Omole, A. E. & Fakoya, A. O. J. Ten years of progress and promise of induced pluripotent stem cells: historical origins, characteristics, mechanisms, limitations, and potential applications. *PeerJ* **6**, 4370 (2018).

53. Hass, R., Kasper, C., Böhm, S. & Jacobs, R. Different populations and sources of human mesenchymal stem cells (MSC): A comparison of adult and neonatal tissue-derived MSC. *Cell Commun. Signal.* **9**, 12 (2011).

54. Iwatani, S. *et al.* Isolation and characterization of human umbilical cord-derived mesenchymal stem cells from preterm and term infants. *J. Vis. Exp.* **2019**, e58806 (2019).

55. Campard, D., Lysy, P. A., Najimi, M. & Sokal, E. M. Native Umbilical Cord Matrix Stem Cells Express Hepatic Markers and Differentiate Into Hepatocyte-like Cells. *Gastroenterology* **134**, 833–848 (2008).

56. Zhou, R. *et al.* Human umbilical cord mesenchymal stem cells and derived hepatocyte-like cells exhibit similar therapeutic effects on an acute liver failure mouse model. *PLoS One* **9**, 1–14 (2014).

57. Zhang, Y. N., Lie, P. C. & Wei, X. Differentiation of mesenchymal stromal cells derived from umbilical cord Wharton's jelly into hepatocyte-like cells. *Cytotherapy* **11**, 548–558 (2009).

58. Liver development | StemBook (Accessed: 02/11/2021). https://www.stembook.org/node/512.

59. Gale, B. K. *et al.* A review of current methods in microfluidic device fabrication and future commercialization prospects. *Inventions* **3**, 60 (2018).

60. Convery, N. & Gadegaard, N. 30 Years of Microfluidics. *Micro Nano Eng.* **2**, 76–91 (2019).

61. Whitesides, G. M. The origins and the future of microfluidics. *Nature* **442**, 368–373 (2006).

62. Xia, Y. & Whitesides, G. M. Soft lithography. *Angew. Chemie - Int. Ed.* **37**, 550–575 (1998).

63. Aryasomayajula, A., Bayat, P., Rezai, P. & Selvaganapathy, P. R. Microfluidic Devices and Their Applications. in *Springer Handbook of Nanotechnology* (ed. Bhushan, B.) 487–536 (Springer Berlin Heidelberg, 2017).

64. Westerhof, N., Stergiopulos, N., Noble, M. I. M. & Westerhof, B. E. Turbulence. in *Snapshots of Hemodynamics: An Aid for Clinical Research and Graduate Education* 23–25 (Springer International Publishing, 2019).

65. Infeld, E., Karczewska, A., Rowlands, G. & Rozmej, P. Exact cnoidal solutions of the extended KdV equation. *Acta Phys. Pol. A* **133**, 1191–1199 (2018).

66. Microfluidics: A general overview of microfluidics - Elveflow (Accessed: 15/06/2021). https://www.elveflow.com/microfluidic-reviews/general-microfluidics/a-general-overview-of-microfluidics/.

67. Materials for microfluidic chips fabrication : a review 2017 - Elveflow (Accessed: 15/06/2021). https://www.elveflow.com/microfluidic-reviews/general-microfluidics/materials-for-microfluidic-chips-fabrication-a-review-2017/.

68. Sei, Y., Justus, K., Leduc, P. & Kim, Y. Engineering living systems on chips: From cells to human on chips. *Microfluid. Nanofluidics* **16**, 907–920 (2014).

69. Fernandes, J. T. S., Chutna, O., Chu, V., Conde, J. P. & Outeiro, T. F. A novel microfluidic cell co-culture platform for the study of the molecular mechanisms of Parkinson's disease and other synucleinopathies. *Front. Neurosci.* **10**, 1–11 (2016).

70. The 3Rs | NC3Rs (Accessed: 26/03/2021). https://www.nc3rs.org.uk/the-3rs.

71. Mastrangeli, M., Millet, S. & van den Eijnden-Van Raaij, J. Organ-on-chip in development: Towards a roadmap for organs-on-chip. *ALTEX* **36**, 650–668 (2019).

72. Burkhardt, B., Martinez-Sanchez, J. J., Bachmann, A., Ladurner, R. & Nüssler, A. K. Long-term culture of primary hepatocytes: New matrices and microfluidic devices. *Hepatol. Int.* **8**, 14–22 (2014).

73. Hassan, S. *et al.* Liver-on-a-Chip Models of Fatty Liver Disease. *Hepatology* **71**, 733 (2020).

74. Yoon No, D., Lee, K. H., Lee, J. & Lee, S. H. 3D liver models on a microplatform: well-defined culture, engineering of liver tissue and liver-on-a-chip. *Lab Chip* **15**, 3822–3837 (2015).

75. Gori, M. *et al.* Investigating nonalcoholic fatty liver disease in a liver-on-a-chip microfluidic device. *PLoS ONE* vol. **11**, e0159729 (2016).

76. Kostrzewski, T. *et al.* Three-dimensional perfused human in vitro model of non-alcoholic fatty liver disease. *World J. Gastroenterol.* **23**, 204 (2017).

77. Vivares, A. *et al.* Morphological behaviour and metabolic capacity of cryopreserved human primary hepatocytes cultivated in a perfused multiwell device. *Xenobiotica* **45**, 29–44 (2015).

78. Bulutoglu, B. *et al.* A microfluidic patterned model of non-alcoholic fatty liver disease: Applications to disease progression and zonation. *Lab on a Chip* vol. **19** 3022–3031 (2019).

79. SY, L. & JH, S. Gut-liver on a chip toward an in vitro model of hepatic steatosis. *Biotechnol. Bioeng.* **115**, 2817–2827 (2018).

80. Tanataweethum, N. *et al.* Towards an Insulin Resistant Adipose Model on a Chip. *Cell. Mol. Bioeng. 2020 141* **14**, 89–99 (2020).

81. Duan, X. *et al.* Association of PM2.5 with Insulin Resistance Signaling Pathways on a Microfluidic Liver–Kidney Microphysiological System (LK-MPS) Device. *Anal. Chem.* **93**, 9835–9844 (2021).

82. Rajan, N., Habermehl, J., Coté, M. F., Doillon, C. J. & Mantovani, D. Preparation of ready-to-use, storable and reconstituted type I collagen from rat tail tendon for tissue engineering applications. *Nat. Protoc.* **1**, 2753–2758 (2007).

83. Martins, J. P. *et al.* Towards an advanced therapy medicinal product based on mesenchymal stromal cells isolated from the umbilical cord tissue: Quality and safety data. *Stem Cell Res. Ther.* **5**, 1–15 (2014).

84. Santos, J. M. *et al.* Three-dimensional spheroid cell culture of umbilical cord tissue-derived mesenchymal stromal cells leads to enhanced paracrine induction of wound healing. *Stem Cell*

Res. Ther. **6**, 1–19 (2015).

85. E, B., EW, Y. & D, B. Engineers are from PDMS-land, Biologists are from Polystyrenia. *Lab Chip* **12**, 1224–1237 (2012).

86. Stanton, A. E., Tong, X. & Yang, F. Varying solvent type modulates collagen coating and stem cell mechanotransduction on hydrogel substrates. *APL Bioeng.* **3**, 036108 (2019).

87. Kempner, M. E. & Felder, R. A. A Review of Cell Culture Automation. *JALA J. Assoc. Lab. Autom.* **7**, 56–62 (2002).

88. Ben-Ze'ev, A., Robinson, G. S., Bucher, N. L. & Farmer, S. R. Cell-cell and cell-matrix interactions differentially regulate the expression of hepatic and cytoskeletal genes in primary cultures of rat hepatocytes. *Proc. Natl. Acad. Sci. U. S. A.* **85**, 2161 (1988).

89. Studer, V. *et al.* Scaling properties of a low-actuation pressure microfluidic valve. *J. Appl. Phys.* **95**, 393–398 (2004).

90. Melin, J. & Quake, S. R. Microfluidic large-scale integration: The evolution of design rules for biological automation. *Annu. Rev. Biophys. Biomol. Struct.* **36**, 213–231 (2007).

91. Stéphenne, X., Najimi, M. & Sokal, E. M. Hepatocyte cryopreservation: Is it time to change the strategy? *World J. Gastroenterol.* **16**, 1 (2010).

92. Lohasz, C. *et al.* Predicting Metabolism-Related Drug–Drug Interactions Using a Microphysiological Multitissue System. *Adv. Biosyst.* **4**, 2000079 (2020).

93. Unger, M. A., Chou, H. P., Thorsen, T., Scherer, A. & Quake, S. R. Monolithic microfabricated valves and pumps by multilayer soft lithography. *Science (80-.).* **288**, 113–116 (2000).

VI. Appendix

VI.1. Teensy code used to test recirculation (pump functioning)

```
// To set the pin number:
int Pin1 = 37;
int Pin2 = 36;
int Pin3 = 35;

void setup() {
  // To set the digital pin as output:
  pinMode(Pin1,OUTPUT);
  pinMode(Pin2,OUTPUT);
  pinMode(Pin3,OUTPUT);
}

void loop() {
  // Recirculation loop (pump operation):
  digitalWrite(Pin1, LOW);
  digitalWrite(Pin2, HIGH);
  digitalWrite(Pin3, LOW);
  delay(500);
  digitalWrite(Pin1, LOW);
  digitalWrite(Pin2, HIGH);
  digitalWrite(Pin3, HIGH);
  delay(500);
  digitalWrite(Pin1, LOW);
  digitalWrite(Pin2, LOW);
  digitalWrite(Pin3, HIGH);
  delay(500);
  digitalWrite(Pin1, HIGH);
  digitalWrite(Pin2, LOW);
  digitalWrite(Pin3, HIGH);
  delay(500);
  digitalWrite(Pin1, HIGH);
  digitalWrite(Pin2, LOW);
  digitalWrite(Pin3, LOW);
  delay(500);
  digitalWrite(Pin1, HIGH);
  digitalWrite(Pin2, HIGH);
  digitalWrite(Pin3, LOW);
  delay(500);
}
```